Universidade de São Paulo
Instituto de Física

Teoria da produção de entropia de Wehrl para sistemas quânticos fora do equilíbrio

Bruno Ortega Goes

Orientador: Prof. Dr. Gabriel Teixeira Landi

Dissertação de mestrado apresentada ao Instituto de Física da Universidade de São Paulo, como requisito parcial para a obtenção do título de Mestre em Ciências.

Banca Examinadora:
Prof. Dr. Gabriel Teixeira Landi - Instituto de Física da Universidade de São Paulo
Prof. Dr. Daniel Mendonça Valente - Universidade Federal de Mato Grosso
Prof. Dr. Saulo Vicente Moreira - Universidade Federal do ABC

São Paulo
2020

FICHA CATALOGRÁFICA
Preparada pelo Serviço de Biblioteca e Informação
do Instituto de Física da Universidade de São Paulo

Goes, Bruno Ortega

Teoria da produção de entropia de Wehrl para sistemas quânticos fora do equilíbrio. São Paulo, 2020.

Dissertação (Mestrado) – Universidade de São Paulo. Instituto de Física. Departamento Física dos Materiais e Mecânica

Orientador: Prof. Dr. Gabriel Teixeira Landi

Área de Concentração: Física

Unitermos: 1. Informação quântica.; 2. Termodinâmica quântica.; 3. Mecânica estatística quântica; 4. Mecânica quântica; 5. Fenômenos críticos.

USP/IF/SBI-041/2020

University of São Paulo
Physics Institute

Wehrl entropy production theory for non-equilibrium quantum systems

Bruno Ortega Goes

Supervisor: Prof. Dr. Gabriel Teixeira Landi

Dissertation submitted to the Physics Institute of the University of São Paulo in partial fulfillment of the requirements for the degree of Master of Science.

Examining Committee:
Prof. Dr. Gabriel Teixeira Landi - Physics Institute of the University of São Paulo
Prof. Dr. Daniel Mendonça Valente - Federal University of Mato Grosso
Prof. Dr. Saulo Vicente Moreira - Federal University of ABC

São Paulo
2020

To my grandmothers: Diomar and Zenaide (in memoriam).

Acknowledgments

Inicio agradecendo ao meu orientador, Gabriel Landi, por toda a sua paciência, disponibilidade para discutir física, e principalmente por todo incentivo e suporte dado ao longo deste últimos três anos. Sua orientação foi impecável!

Agradeço à minha querida avó Diomar, por seu apoio e suporte incondicional ao longo de toda minha vida. Agradeço também ao meu pai Roberto, que sempre me apoiou e me incentivou para que eu me dedicasse à física.

Agradeço muito à minha companheira Tainá Roberta, ela esteve sempre pacientemente ao meu lado, dando apoio, conselhos, carinho e comemorando cada conquista nos últimos anos.

I thank Lucas Céleri, Mikel Sanz and Enrique Solano and all the members of the QUTIS group for hosting me at the University of Basque Country. That was a very nice and productive period, full of stimulating discussions.

Agradeço aos amigos que fiz durante a graduação e o pessoal do grupo QT2 com os quais tive o prazer de compartilhar o caminho até aqui e que foram responsáveis por torná-lo agradável. Em especial, agradeço ao André Fantin que durante a escrita da dissertação se disponibilizou para ler algumas partes manuscrito e deu algumas boas sugestões. Agradeço também aos meus amigos da vida com os quais sempre posso contar.

Agradeço aos funcionários da CPg pela prontidão em tirar minhas dúvidas e pela ajuda fornecida durante e, principalmente, na fase final do mestrado.

Por fim, sou grato ao CNPq, por ter possibilitado a realização deste trabalho com o

auxílio financeiro fornecido ao longo destes 2 anos.

"The saddest aspect of life right now is that science gathers knowledge faster than society gathers wisdom."

- Isaac Asimov

Abstract

The physics of systems out of equilibrium is a topic of great interest, mainly due to the possibility of exploring phenomena that can not be observed in equilibrium systems. Driven-dissipative phase transitions open the opportunity of studying phases with no classical counterparts, and these can be experimentally realized in quantum optical platforms. Since these transitions occur in systems kept out of equilibrium, they are characterized by a finite entropy production rate. However, due to technical difficulties regarding the zero temperature limit and the non-gaussianity of such models, very little is known about how entropy production behaves around criticality. Using a quantum phase-space method, based on the Husimi Q-function, we put forth a framework that allows for the complete characterization of the entropy production in driven-dissipative transitions. This new theoretical framework is tailored specifically to describe photon loss dissipation, which is effectively a zero temperature process for which the standard theory of entropy production breaks down. It makes no assumptions about Gaussianity about the model or the state. It works for both, steady-states as well as the dynamics and as an application, we study both situations in the paradigmatic driven-dissipative Kerr model, which presents a discontinuous phase transition. For general driven-dissipative critical systems, where one can define a thermodynamic limit, we find that the entropy production rate and flux naturally split into two contributions: an extensive one and a contribution due to quantum fluctuations only. Moreover, we identify a contribution to the entropy production due to unitary dynamics, and we find that the behavior of this contribution at the non-equilibrium steady-state (NESS) matches the behavior of entropy production rate observed in classical systems. The quantum contributions are found to diverge at the critical point.

Keywords: Quantum thermodynamics; Quantum phase transitions; Open quantum systems; Entropy production; Critical phenomena; Quantum master equation.

Resumo

A física de sistemas fora do equilíbrio é um tópico muito interessante, principalmente devido à possibilidade de explorar fenômenos que não podem ser observados em sistemas de equilíbrio. Transições de fase forçada-dissipativas (*driven-dissipative phase transitions*) possibilitam o estudo de fases da matéria que não possuem análogos clássicos, e estas podem ser realizadas experimentalmente em plataformas de óptica quântica. Uma vez que estas transições ocorrem em sistemas mantidos fora do equilíbrio, elas são caracterizadas por uma taxa de produção de entropia finita. Entretanto, devido a dificuldades técnicas relacionadas ao limite de temperatura nula e à não gaussianidade de tais modelos, muito pouco se sabe sobre o comportamento da produção de entropia próximo à criticalidade. Utilizando um método de espaço de fase quântico, baseado na função Q de Husimi, apresentamos uma estrutura teórica que permite a caracterização completa da produção de entropia para tais transições. Esta nova estrutura é adequada para descrever especificamente a dissipação devido a perda de fótons, que é um processo que ocorre efetivamente a temperatura nula, para o qual a teoria usual da produção de entropia não se aplica. Ele também não impõe nenhuma restrição sobre a gaussianidade do modelo ou do estado. Ele funciona tanto para estados estacionários quanto para a evolução temporal e como uma aplicação, estuda-se ambas as situações para o modelo paradigmático de Kerr, o qual apresenta uma transição de fase descontínua. Para sistemas forçado-dissipativos gerais apresentando criticalidade, onde se pode definir um limite termodinâmico, encontra-se que a taxa de produção/fluxo de entropia dividem-se em duas contribuições: uma extensiva e outra devido somente à flutuações quânticas. Além disso, identifica-se uma contribuição para a taxa de produção de entropia devido à dinâmica unitária, e encontra-se que o comportamento desta contribuição no estado estacionário de não equilíbrio assemelha-se àquele observado em sistemas clásicos. As contribuições quânticas por sua vez divergem no ponto crítico.

Palavras-chave: Termodinâmica quântica; Transições de fase quânticas; Sistemas quânticos abertos; Produção de entropia; Fenômenos críticos; Equação mestra quântica.

Contents

List of Figures

Introduction

Thermodynamics is an old and robust physical theory [4, 5]. It played a major role during the Industrial Revolution and since then had a simple objective: to answer how to exploit as much as possible of the available resources to accomplish a given task.

The *Laws of thermodynamics* are experimentally based postulates, which cannot be violated by any classical system. The zeroth law provides the concept of thermodynamic equilibrium, the first law is related to energy conservation and finally, the Second Law is the one that contains the most interesting and important physical content: it dictates which processes are allowed by nature, what are their consequences, and imposes restrictions on their efficiency. It introduces the concept of entropy production, which measures the irreversibility of a process.

Moreover, after the acceptance of the atomic theory, it became possible to understand thermal phenomena from a more fundamental level. The macroscopic quantities that were used in thermodynamics, such as pressure and temperature could be understood as a consequence of the random motion of microscopic entities. Statistical mechanics has become the bridge between the microscopic world and the emergent phenomena observed. All the concepts and laws of thermodynamics can be put into this new theoretical framework, including phase transitions [5–7].

Equilibrium phase transitions are abrupt structural changes on a system between two equilibrium states which occur as a consequence of the *competition* between different energetic and entropic contributions. Phase transitions have been one of the topics of great interest by the physics community as they extend from particle physics, through condensed matter and even cosmology. Historically, the first types of phase transitions studied were related to the solid, liquid and gaseous phases. But this concept was extended to other phases of matter, such as ferromagnetism and paramagnetism in magnetic systems [7, 8].

The pinnacle of the theoretical description of such phase transitions occurred with the establishment of Landau's theory [9], and the notions of an order parameter and symmetry breaking.

A better understanding and description of microscopic phenomena was provided by quantum mechanics [10–12]. It made possible the development of several new, quantum-based technologies and the exploration of the microscopic realm. Quantum mechanics is robust both theoretically and experimentally and it encompasses highly counter-intuitive physical properties, such as coherence and entanglement. Much can be inferred by considering the quantum system completely isolated, since it may be a good approximation in many cases, but it does not represent reality. For a more precise description, it is necessary to consider the interplay between the system and its surroundings. The theory that deals with this scenario is called *open quantum systems*, which has an intrinsic non-equilibrium nature [13, 14].

For a long time, it was believed that it did not make sense to apply thermodynamics, a macroscopic theory, to quantum systems. However, with the advent of stochastic thermodynamics [15], which enabled the thermodynamic description of systems of arbitrary sizes, the conception that genuinely quantum properties (such as entanglement and coherence) could be used as resources plus the miniaturization of electronic components to a size where quantum fluctuations appear, led to the development of *quantum thermodynamics* [16–19].

Open quantum systems describe processes out-of-equilibrium that are of great interest since they are more commonly found in nature than their equilibrium counterparts. While the later is very well established theoretically, the former imposes great difficulty for a theoretical description and much can still be developed for them. Systems that are continuously pushed out of equilibrium may reach a steady-state, in this case, it is called a non-equilibrium steady state (NESS). They are observed in both quantum and classical systems. The main feature that distinguishes a NESS from an equilibrium state is the *flux* of some physical quantity such as charge, energy, mass, etc. For instance, we can think about a classical case, the RL circuit. When we turn on the circuit the battery will generate a steady electric current, i.e. a steady flux of charges. We can also consider the effect of dissipation due to the Joule effect. The wires will heat the air surrounding them, which generates a heat flux from the system to the environment. Hence, the circuit will tend to a

NESS, with a constant flux of charges and heat, as long as the battery is charged.

In the classical context, there are non-equilibrium phase transitions. For these types of transitions, it becomes interesting to look at the behavior of the entropy production due to the information it provides about the non-equilibrium nature of the process. Several studies in this context [20–24] indicates that the entropy production is always finite across a non-equilibrium transition, presenting either a kink or a discontinuity. Indeed, this behavior was shown to be universal for systems described by classical Pauli master equations and breaking a Z_2 symmetry in Ref. [2].

In the last decades, it was discovered the existence of phase transitions at zero temperature, called quantum phase transitions [25]. They occur due to the existence of competing terms in the Hamiltonian. The quantum analog of classical non-equilibrium phase transitions are *driven-dissipative phase transitions*, that occur due to the competition between the coherent and dissipative evolution of the quantum state.

There is an experimental indication that the mentioned classical behavior of entropy production across a dissipative phase transition does not hold. We can refer to the driven-dissipative Dicke model, in which it was experimentally found that the contribution of quantum fluctuations to the entropy production diverges at the critical point [26]. However, important questions such as if this divergence is universal or not and what are the ingredients required for it to happen were not addressed so far due to two technical problems.

First, dissipative phase transitions occur at zero temperature, where the usual theory of entropy production, based on the von Neumann formalism, breaks down; secondly, the models and state are, in general, not gaussian, what makes it not possible to use a theory recently developed in our group of the Wigner entropy production rate (this one applies only for gaussian systems). This dissertation aims to fill this gap. Based on Ref. [27] we formulate a theory that is suited for describing non-equilibrium quantum systems in general and specializes for driven-dissipative transitions.

This dissertation is organized as follows:

- Chapter 1 is devoted to reviewing important concepts of quantum mechanics and open quantum systems. The latter is exemplified with two simple textbook systems. We list some properties of coherent states and introduce the Husimi Q-function, the

phase space method we use to develop our theory of entropy production rate;

- In chapter 2, we introduce and review the concept of entropy production in classical thermodynamics, thus introducing the concept of irreversibility. We also review the entropy production based on the von Neumann entropy, which is the usual definition one uses for quantum mechanical systems and comment why it breaks down for zero temperature;

- In chapter 3, we briefly review the concept of phase transitions highlighting some important properties both in the classical and quantum context. As an example, we make a detailed discussion of the Lipkin-Meshkov-Glick (LMG) model quantum phase transition. Moreover, we make some comments on how entropy production has helped to characterize classical non-equilibrium phase transitions in recent works. Finally, at the end of this chapter, we introduce and discuss the concept of driven-dissipative phase transitions. This is the last review chapter;

- In chapter 4, we put forth the main contribution of this dissertation, the theory of *Wehrl entropy production rate*. We apply it to an example of a driven-dissipative system at zero temperature (already encountered in chapter 1). Then, we specialize it to critical driven-dissipative systems and find the contributions solely due to quantum fluctuations for this type of systems;

- In chapter 5, we introduce the paradigmatic Kerr bistability model (KBM), which presents a discontinuous phase transition, discuss it in detail and apply the theory developed in the previous chapter for the NESS of this system. We mention that the results of these two last chapters were the content of a recently published paper [28], which can be found attached to this dissertation;

- In chapter 6, we apply our formalism to the dynamics of the KBM model under quantum quenches. We study the gaussianity of the state during the dynamics and the Wehrl entropy rate components.

- Finally, in chapter 7 we draw our conclusions and give perspectives of future research.

Chapter 1

The theoretical framework of quantum mechanics

Historically, quantum mechanics (QM) was developed from the necessity of explaining experimental data that could not be understood within the theoretical framework provided by classical physics. Planck proposed that energy was *quantized* to fit data of the black body radiation spectrum and in 1905, Einstein used the same assumption so that he could explain the photoelectric effect. These two events were the milestone of what would become modern quantum theory.

One could say that the scope of QM is the description of the dynamics of objects at the a small scale. This way of defining QM is not wrong at all, but one must have in mind that nowadays experimentalists are able to create and control mesoscopic objects that display quantum behavior, for instance Bose-Einstein condensates and optomechanical systems [26, 29–32].

In modern terms, the mathematical framework of quantum theory is linear algebra [10–12]. To every physical quantum system there is an associated Hilbert space, denoted by $\mathscr{H}$, which is a particular normed vector space. The dimension of $\mathscr{H}$ can be either finite or infinite. If we have N quantum systems, say $S_1, S_2, ..., S_N$, each one have with its own Hilbert space, then the Hilbert space of the composite system will be constructed by the Kronecker product of the individual Hilbert spaces, $\mathscr{H} = \mathscr{H}_1 \otimes \mathscr{H}_2 \otimes ... \otimes \mathscr{H}_N$.

The elements of the Hilbert space are represented by kets such as $|\phi\rangle$, these are the pure states of the system. We can chose a orthogonal *basis* $\{|i\rangle\}$, i.e. a set of linearly

independent vectors $|i\rangle$, such that $\langle j|i\rangle = \delta_{ij}$, where δ_{ij} is the Kronecker delta. This way we can write,

$$|\phi\rangle = \sum_i c_i |i\rangle \tag{1.1}$$

where c_i are complex coefficients. A pure state is normalized $\langle\phi|\phi\rangle = 1$, it leads to $\sum_i |c_i|^2 = 1$, this gives us the concept of *quantum probability*, which is given by $|c_i|^2$ and stands for the probability of a system to be in the state $|i\rangle$.

For each ket there is a dual correspondence $\langle\xi|$ in the dual space of $\mathscr{H}$, so that the inner product between two vectors $|\phi\rangle$, $|\xi\rangle$ is given by $\langle\xi|\phi\rangle$ (a bracket). It is also possible to define an *outer product*, $|\phi\rangle\langle\xi|$, which represents a linear operator and not a scalar.

Modern quantum mechanics for isolated systems can be summarized by four postulates, which are the subject of next section.

1.1 The postulates of quantum mechanics

The state is an object that carries all the information one can obtain about a physical system. The most general quantum state has to take into account both quantum and classical probabilities, so

Postulate 1 (about the state): The state of a physical quantum system is completely characterized by a density matrix ρ. The properties of a density matrix are:

i) It is normalized $\mathrm{tr}\{\rho\} = 1$;

ii) It is hermitian, $\rho = \rho^\dagger$ and

iii) It is positive semi-definite, $\rho \geq 0$.

One can always diagonalize ρ as ,

$$\rho = \sum_i p_i |\psi_i\rangle\langle\psi_i| \tag{1.2}$$

where $p_i \in [0, 1]$ represents classical probabilities and $|\psi_i\rangle$ are pure states encoding quantum probabilities. The average of an operator $\mathscr{O}$ can be written as $\langle\mathscr{O}\rangle = \mathrm{tr}\{\mathscr{O}\rho\}$. Another important concept is the purity of the state defined as $\mathscr{P} = \mathrm{tr}\{\rho^2\} \leq 1$; the state

is said to be pure if the equality holds and mixed otherwise. If we chose a basis where ρ is not diagonal, then the off-diagonal terms represent the *coherence*.

When dealing with a physical system we are often interested in quantities which can be measured in a laboratory, these are called observables and are associated to special set of operators,

Postulate 2 (about observables): Physical observables, i.e. quantities that can be measured in a laboratory, are represented by *hermitian operators*, $\mathscr{O} = \mathscr{O}^\dagger$, which are defined in a Hilbert space.

Observables are associated with hermitian operators because they have the important property that all its eigenvalues are real.

The third postulate is related to measurements. To obtain information about a quantum system one must perform a measurement on it and this concept is formalized as follows:

Postulate 3 (about measurements): Any quantum measurement is specified by a set of Kraus operators $\{M_i\}$, satisfying $\sum_i M_i^\dagger M_i = 1$. The probability of obtaining the outcome i is $p_i = \mathrm{tr}\Big\{M_i \rho M_i^\dagger\Big\}$ and, if the outcome is i then the state after the measurement is updated to,

$$\rho_0 \to \rho_i = \frac{M_i \rho_0 M_i^\dagger}{p_i}, \tag{1.3}$$

this is the most general way of formalizing the concept of a measurement. Projective measurements are a particular case.

Finally, the time evolution of a quantum state must take an initial physical state, where all three properties specified in postulate 1 are satisfied, into another physical state ρ_t at time t. We can write this as a linear map $\rho_t = \mathscr{V}_t(\rho_0)$, where $\mathscr{V}_t$ is a super-operator[1] that must be completely positive and trace-preserving (to conserve probabilities), usually denoted by CPTP. Such maps can be expressed in terms of Kraus operators as $\rho_t = \sum_i M_i \rho_0 M_i^\dagger$. The last postulate tells us how to evolve a completely isolated quantum system:

Postulate 4 (about state evolution): Given that a system that is isolated, described by the Hamiltonian H and has a initial state ρ_0, its state evolution will be governed by the von Neumann equation, which is,

$$\partial_t \rho_t = -i[H, \rho_t] \tag{1.4}$$

[1] It has the some properties of a operator but it receives the *super* in front of it because it acts on operators.

One can readily show that Eqn.(1.4) conserves the purity of the state during the evolution, so that a pure state never becomes mixed and vice-versa.

1.2 Open quantum systems

Fortunately nature is not so simple. A quantum system is always embedded in an environment and the coupling between them, the smaller it may be, cannot be neglected in some circumstances. For instance, if a system is prepared with coherence and is weakly coupled with the electromagnetic vacuum, we can say that the environment continuously interact with it, so that coherence can vanish as time goes by, a phenomenon called decoherence. The theory that deals with quantum systems that are not isolated is called *open quantum systems* [13].

As we have seen in Postulate 4, a physical map must be CPTP, then a natural question one can make is: what is the most general dynamical CPTP map that encompasses the interaction of the system with its environment? This is a very hard question, and is still being the focus of research [33, 34]. A possible and useful answer is provided by the Lindblad theorem [35], which gives the form of the equation that describes the evolution of a markovian system, which means that the state in $t + \delta t$ depends only on the state at time t, interacting with its surroundings. The Lindblad master equation is,

$$\partial_t \rho = \mathscr{L}(\rho) = -i[H, \rho] + D(\rho) \tag{1.5}$$

where $\mathscr{L}$ is the Liouvillian superoperator and

$$D(\rho) = \sum_i 2\kappa_i \left(L_i \rho L_i^\dagger - \frac{1}{2}\{L_i^\dagger L_i, \rho\} \right) \tag{1.6}$$

is the Lindblad dissipator. Here H is the Hamiltonian operator, L_i are arbitrary operators and $\kappa_i \geq 0$ represent the coupling strength with the environment. It is not the purpose of this dissertation to prove that this is the structure. For that we refer to Refs. [13, 14, 35]. We mention that the main hypotheses for this to work is that initially system and environment are uncorrelated, $\rho_o^{\text{Total}} = \rho_0 \otimes \rho^{\text{env}}$ and the environment is markovian. We mention that eqn. (1.6) can also describe a non-markovian system, if the dissipation rates are

negative [13].

Eqn.(1.5) describes a non-equilibrium dynamics and we can view it as a competition between different terms. Each term pushes the system to a different state, and eventually it reaches a (generally) non-equilibrium steady state (NESS), which will be a compromise between the strength of each term. This kind of competition will give rise to the *driven-dissipative phase transitions* that are the main topic of this dissertation. We note that if $\kappa_i = 0$ for all i we recover the von Neumann Eqn.(1.4).

Next, we apply this formalism to two simple and illuminating examples, one with finite dimension and the other with infinite dimension.

1.2.1 Exemple 1: Dynamics of a single qubit

A qubit is a two level system, and the simplest Hamiltonian to describe it is,

$$H = \frac{\Omega}{2}\sigma_z, \tag{1.7}$$

where Ω is the energy gap between the two possible states and σ_z is a Pauli matrix. We can introduce an environment where the Lindblad operator is $L = \sigma_z$, then

$$D(\rho) = 2\kappa(\sigma_z\rho\sigma_z - \rho) \tag{1.8}$$

This is a dephasing noise, and is responsible for washing out coherences of the system. Since it is a simple two dimensional system we can parametrize its density matrix as

$$\rho = \begin{bmatrix} p & q \\ \bar{q} & 1-p \end{bmatrix} \tag{1.9}$$

where p stands for the population on the ground state and q is the coherence term. Writting the Lindblad equation $\partial_t\rho = -i[H,\rho] + D(\rho)$ and solving for initial conditions $p(0) = p_0$ and $q(0) = q_0$, one finds,

$$p(t) = p_0 \tag{1.10}$$

$$q(t) = q_0 e^{-(i\Omega+4\kappa)t} \tag{1.11}$$

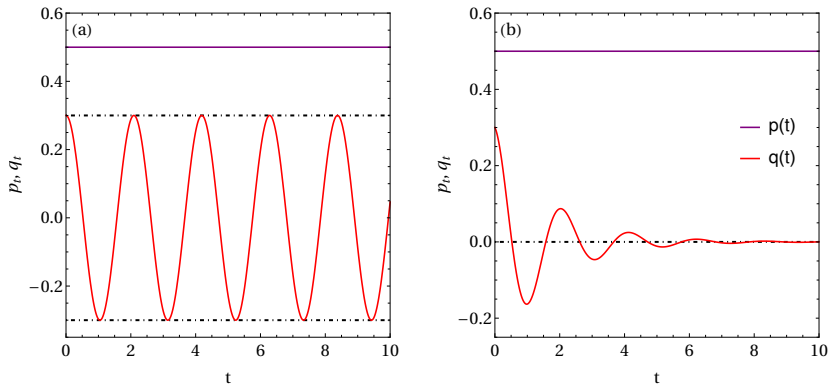

Figure 1.1: **Population and coherence dynamics for the Dephasing noise:** The initial population and coherence were set $p_0 = 0.5$, $q_0 = 0.3$ and the energy gap is $\Omega = 3$. In panel (a) $\kappa = 0$, i.e. there is no dissipation, while in panel (b) $\kappa = 0.15$.

In Fig.1.1(a) we can see the dynamics given by Eqn.(1.10) in absence of dissipation $\kappa = 0$, i.e. the system is isolated. The population is always constant while the coherences oscillates between $\pm q_0$. In Fig.1.1(b) we have turned on the interaction with the environment by setting $\kappa = 0.15$. In this case, again the population remains constant but as time goes by the coherences are washed away from the system. This simple example sheds light on the role of the environment for quantum system, it is responsible for decoherence that happens exponentially in time $e^{-4\kappa t}$, for this example.

1.2.2 Exemple 2: Driven-dissipative quantum harmonic oscillator at finite temperature

As a second example we take a driven-dissipative quantum harmonic oscillator described by a single mode a. The annihilation operator a and its conjugate, the creation operator $a^\dagger$, are related to the quadrature operators by $q = (a^\dagger + a)/\sqrt{2}$ and $p = i(a^\dagger - a)/\sqrt{2}$. The Hamiltonian of the system, in the interaction picture (see App. B), is

$$H = \Delta a^\dagger a + i\mathscr{E}(a^\dagger - a) \tag{1.12}$$

where Δ is the detuning and $\mathscr{E}$ is the driving amplitude. The finite temperature dissipator is,

$$D(\rho) = 2\kappa(N+1)\left(a\rho a^\dagger - \frac{1}{2}\{a^\dagger a, \rho\}\right) + 2\kappa N\left(a^\dagger \rho a - \frac{1}{2}\{aa^\dagger, \rho\}\right) \tag{1.13}$$

where $N = (e^{\omega/T} - 1)^{-1}$ is the Bose-Einstein occupation with ω being the free oscillator frequency. We note that when $T = 0$ the occupation vanishes $N = 0$, hence the only term that survive in the dissipator is the first one. We say in advance that this is the kind of dissipators we will be concerned with in this dissertation, since driven-dissipative phase transitions occur at zero temperature. One can write the Lindblad equation as,

$$\partial_t \rho = -i[H, \rho] + D(\rho), \tag{1.14}$$

which is possible to solve numerically truncating the dimension of the Hilbert space, since it is infinite. In this case, it is more informative and feasible to study the evolution of some observable rather than the dynamics of the state itself. Henceforth, when dealing with infinite dimensional systems we will study quantities such as the number of quanta $\langle a^\dagger a \rangle_t$. The dynamics of the the first and second moments is given by (see App.A),

$$\partial_t \langle a \rangle_t = -(i\Delta + \kappa)\langle a \rangle + \mathscr{E} \tag{1.15}$$

$$\partial_t \langle a^\dagger a \rangle_t = \mathscr{E}(\langle a \rangle + \langle a^\dagger \rangle) + 2\kappa(N - \langle a^\dagger a \rangle) \tag{1.16}$$

It is important to note that the second moment $\langle a^\dagger a \rangle$ only depends on the first moment, which in turn depends only on itself. Then, it is possible to obtain an analytical expression for both $\langle a \rangle_t$ and $\langle a^\dagger a \rangle_t$. The steady state value can be readily found by equating both to zero. The result is,

$$\langle a \rangle_{\text{SS}} = \frac{\mathscr{E}(\kappa - i\Delta)}{\Delta^2 + \kappa^2} \tag{1.17}$$

$$\langle a^\dagger a \rangle_{\text{SS}} = N + \frac{\mathscr{E}^2}{\kappa^2 + \Delta^2} \tag{1.18}$$

The result for the second moment, which is related to the number of quanta of the system, shows that in the absence of a pump $\mathscr{E} = 0$, temperature will push the number of excitations towards the Bose-Einstein occupation number N. Otherwise, we have a positive contribution to the N proportional to $\mathscr{E}^2$, the greater the pump, the more excitations we have on the system. This contribution is also inversely proportional to the dissipation κ^2. The competition between driving and dissipation will ultimately define how far from N

the NESS will be. The following plots can clarify this discussion:

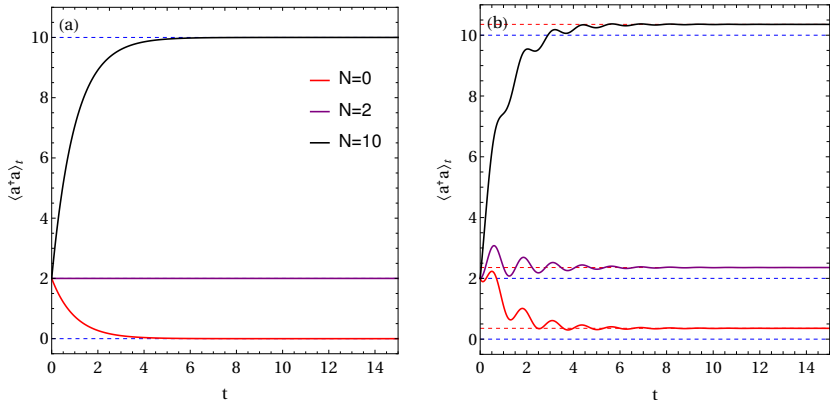

Figure 1.2: **Number of quanta dynamics for a driven-dissipative quantum harmonic oscillator at finite temperature:** (a) $\mathscr{E} = 0$ (b) $\mathscr{E} = 3$. The plots are for three different Bose-Einstein occupation number, as shown in panel (a). The initial condition was set with $\langle a^\dagger a\rangle_0 = 2$ and $\langle a\rangle_0 = 0$. The blue ($\mathscr{E} = 0$) and orange ($\mathscr{E} \neq 0$) dashed lines correspond to the NESS as given by Eqn.(1.18). Other parameters were set: $\Delta = 5$, $\kappa = 0.5$.

In Fig.1.2(a) we see the dynamics of the number of quanta $\langle a^\dagger a\rangle$ of a quantum harmonic oscillator, $\mathscr{E} = 0$ subjected to dissipation κ. The role of temperature is to take the system to the occupation Bose-Einstein occupation number N. In Fig.1.2(b) we plot the same for a forced quantum harmonic oscillator, $\mathscr{E} \neq 0$. Again, temperature pushes the system into N but the pump is responsible to take the system to a state with more excitations as can be seen in Eqn.(1.18).

1.3 Coherent states

In the last section we studied the dynamics of a forced quantum harmonic oscillator. This system has an infinite number of discrete levels and is usually referred to as a *continuous variable*. The study of continuous variables is important because it is useful to describe many experimental platforms, the most prominent in quantum optics where one uses harmonic oscillators to represent the electromagnetic field [36, 37]. Other platforms one can cite are trapped ions, optomechanical oscillators and Bose-Einstein condensates.

A suitable set of states to form the basis of continuous variables systems is that of coherent states $|\mu\rangle$, which are the states defined as the eigenvector of the annihilation

operator,

$$a\left|\mu\right\rangle = \mu\left|\mu\right\rangle . \tag{1.19}$$

Coherent states minimize the uncertainty relation $[q,p]=i$ where q,p are the quadrature operators. We will list below some important properties for the development of this dissertation. For a more detailed explanation on these states, we recommend Refs. [1, 38].

I) A coherent state can be expressed in terms of number states $|n\rangle$, which are the eigenstates of the number operator $a^{\dagger}a\left|n\right\rangle = n\left|n\right\rangle$, as,

$$\left|\mu\right\rangle = e^{-\frac{1}{2}|\mu|^2}\sum_{n=0}^{\infty}\frac{\mu^n}{\sqrt{n!}}\left|n\right\rangle \tag{1.20}$$

II) The scalar product between two coherent states $\left|\mu\right\rangle, \left|\nu\right\rangle$ is

$$\left\langle\nu|\mu\right\rangle = e^{\bar{\nu}\mu-\frac{1}{2}|\nu|^2-\frac{1}{2}|\mu|^2} \qquad \rightarrow \qquad |\left\langle\nu|\mu\right\rangle|^2 = e^{-|\nu-\mu|^2}, \tag{1.21}$$

we can see that different coherent states $\left|\nu\right\rangle, \left|\mu\right\rangle$ are not orthogonal to each other. However, their overlap decays exponentially with the difference $|\mu-\nu|$.

III) The completeness relation for coherent states is,

$$\frac{1}{\pi}\int d^2\mu \ \left|\mu\right\rangle\left\langle\mu\right| = 1, \tag{1.22}$$

where the integral is taken over the entire complex plane. The $1/\pi$ reflects the fact that the coherent state basis is overcomplete.

IV) The expectation value of any operator $\mathscr{O}$ in a coherent state can be written as

$$\left\langle\mu\right|\mathscr{O}\left|\mu\right\rangle = \sum_{n,m}\frac{\left\langle n\right|\mathscr{O}\left|m\right\rangle}{\sqrt{n!\,m!}}e^{-|\mu|^2}\bar{\mu}^n\mu^m. \tag{1.23}$$

This result shows that the diagonal elements in the coherent state basis fully determine all matrix elements of $\mathscr{O}$, since:

$$\left\langle n\right|\mathscr{O}\left|m\right\rangle = \frac{1}{\sqrt{n!\,m!}}\partial_{\bar{\mu}}^n\partial_{\mu}^m(e^{|\mu|^2}\left\langle\mu\right|\mathscr{O}\left|\mu\right\rangle)|_{\mu=0}, \tag{1.24}$$

where the derivatives are formal derivatives.

V) The probability of observing a coherent state μ with n quanta is given by,

$$P_\mu(n) = |\langle n|\mu\rangle|^2 = \frac{|\mu|^{2n} e^{-|\mu|^2}}{n!}, \tag{1.25}$$

which is the Poisson distribution with mean $|\mu|^2$.

One can also define Bargmann states,

$$||\mu\rangle = e^{\frac{1}{2}|\mu|^2} |\mu\rangle = \sum_{n=0}^{\infty} \frac{\mu^n}{\sqrt{n!}} |n\rangle , \tag{1.26}$$

They have the property that derivatives are translated into the action of an operator on it,

$$\partial_\mu ||\mu\rangle = a^\dagger ||\mu\rangle . \tag{1.27}$$

We say in advance that this identity together with the representation (I), will be used to numerically compute the entropy production in Chaps.5 and 6.

1.4 Quantum mechanics in phase space: The Husimi Q-function

In classical physics the dynamical state of a system can be fully characterized by its canonical coordinates in phase space. For continuous variable systems it is also possible to define a quantum phase space. There are many ways of describing it, the first one was introduced by Wigner [39], which is called the Wigner function. Here, we will introduce the Husimi Q-funtion proposed by Kôdi Husimi in Ref. [40] and discuss some of its main properties.

Let $|\mu\rangle$ be a coherent state, as defined by eqn. (1.19). We know, by property (IV), that any operator $\mathscr{O}$ can be determined by its diagonal coherent state matrix elements $\langle\mu|\,\mathscr{O}\,|\mu\rangle$ [1, 38]. This fact enables us to map the density matrix into a real function that will behave as a quasi-probability density for the system. We define the Husimi Q-function

corresponding to a density operator ρ as

$$Q(\mu,\bar{\mu}) = \frac{1}{\pi}\langle\mu|\,\rho\,|\mu\rangle\,, \tag{1.28}$$

where $\bar{\mu}$ denotes complex conjugation. In words , $Q(\mu,\bar{\mu})$ is the expectation value of the density matrix in a coherent state and it is interpreted as the probability distribution of the outcomes of a heterodyne experiment (see next section) [41, 42].

The Husimi Q-function is always positive, for instance take a density operator $\rho = \sum_i p_i\,|\psi_i\rangle\,\langle\psi_i|$, using the definition it is straightforward to see that

$$\begin{aligned} Q(\mu,\bar{\mu}) &= \frac{1}{\pi}\langle\mu|\,\rho\,|\mu\rangle \\ &= \frac{1}{\pi}\sum_i p_i|\langle\mu|\psi_i\rangle\,|^2 \geq 0. \end{aligned}$$

It is bounded as $0 \leq Q(\mu,\bar{\mu}) \leq 1/\pi$, because $\sum_i p_i|\langle\mu|\psi_i\rangle\,|^2 \leq 1$ and it is normalized due to the normalization of the density matrix ρ, indeed

$$1 = \mathrm{tr}\{\rho\} = \mathrm{tr}\left\{\frac{1}{\pi}\int d^2\mu\ |\mu\rangle\,\langle\mu|\,\rho\right\} = \int d^2\mu\ Q(\mu,\bar{\mu}) \tag{1.29}$$

where the integration extends over the entire complex plane.

Finally, the averages of the anti-normally ordered products of creation and annihilation operators are given by

$$\langle a^r(a^\dagger)^s\rangle = \int d^2\mu\ \mu^r(\bar{\mu})^s Q(\mu,\bar{\mu}). \tag{1.30}$$

The Q-function is a *quasi-probability*[2] distribution: it is normalized; always positive, which ensures that every physical state will be associated with a well defined Q-function and the antinormally ordered quantum moments can be determined in terms of simple moments of $Q(\mu,\bar{\mu})$.

To end this section we must know how the action of an operator in a state ρ is translated into a differential operator acting in $Q(\mu,\bar{\mu})$, the correspondence is given by the following

[2] $Q(\mu,\bar{\mu})$ does not represent the probability of mutually different states, because these are not orthogonal, this fact breaks down the third axiom of probability [43, 44].

table [1],

$$a_i\rho \to (\mu_i + \partial_{\bar{\mu}_i})Q(\mu_i, \bar{\mu}_i), \tag{1.31a}$$

$$a_i^\dagger\rho \to \bar{\mu}_i Q(\mu_i, \bar{\mu}_i), \tag{1.31b}$$

$$\rho a_i \to \mu_i Q(\mu_i, \bar{\mu}_i), \tag{1.31c}$$

$$\rho a_i^\dagger \to (\bar{\mu}_i + \partial_{\mu_i})Q(\mu_i, \bar{\mu}_i). \tag{1.31d}$$

The usefulness of this correspondence is that we can map a differential equation for an operator, such as the Lindblad equation into a partial differential equation, for Q. It is straightforward to generalize the above results for an arbitratry number of applications of the operators, for instance $a_i^r\rho \to (\mu_i + \partial_{\bar{\mu}_i})^r Q(\mu_i, \bar{\mu}_i)$.

1.5 Heterodyne measurements

In the last section it was claimed that the Husimi Q-function can be interpreted as the probability distribution of the outcomes of a *heterodyne measurement*. To see that, we will use Postulate 2, and consider the set of Kraus operators defined as

$$M_\mu = \frac{1}{\sqrt{\pi}} |\mu\rangle \langle\mu| \tag{1.32}$$

Due to the completeness relation Eqn.(1.22) of the coherent states basis, this set is properly normalized,

$$\int d^2\mu \; M_\mu^\dagger M_\mu = \int d^2\mu \; \frac{|\mu\rangle \langle\mu|}{\pi} = 1. \tag{1.33}$$

The probability of obtaining the outcome μ is given by,

$$p_\mu = \mathrm{tr}\{M_\mu \rho M_\mu^\dagger\} = \frac{1}{\pi} \langle\mu| \rho |\mu\rangle = Q(\mu, \bar{\mu}), \tag{1.34}$$

and that demonstrates our claim.

The idea of the heterodyne detection (see Fig. 1.3) is to mix the signal beam with a strong coherent signal, the local oscillator, before detecting it. It is called heterodyne because the local oscillator has a different frequency than the signal (if both have the

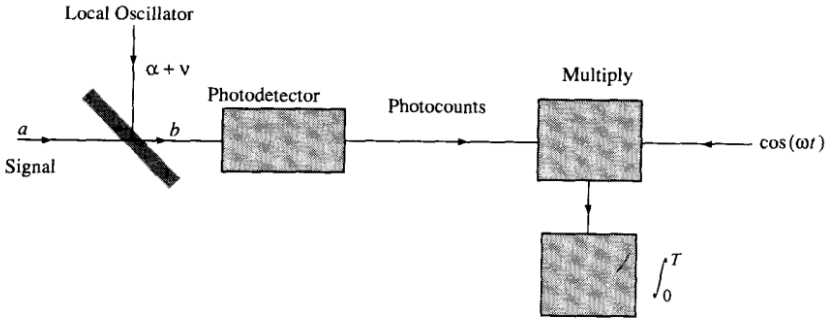

Figure 1.3: **Experimental arrangement:** for heterodyne detection. Taken from Ref. [1].

same frequency we have a homodyne detection) and it is done because this procedure has experimental advantages, such as gain in detection and reduction of noise to the shot noise limit [1]. The mixing is performed by the beam splitter. After that, the mixed signal goes to a photo-detector and some operations are performed to treat the signal, for further details on heterodyne measurements we refer to Ref. [1].

1.5.1 Examples of the Husimi Q-function

As a first example, we consider a number state $|n\rangle$, hence $\rho_n = |n\rangle\langle n|$. Its Husimi Q-function is,

$$Q_n(\mu,\bar{\mu}) = \frac{1}{\pi}|\langle n|\mu\rangle|^2 = \frac{1}{\pi}\frac{|\mu|^{2n}e^{-|\mu|^2}}{n!} \tag{1.35}$$

where we used Eqn. (1.25). So, up to a factor $1/\pi$ it is exactly the probability of observing n quanta in the coherent state $|\mu\rangle$.

Now, we consider the Husimi Q-function of a coherent state $|\alpha\rangle$, where $\rho = |\alpha\rangle\langle\alpha|$, in this case we obtain,

$$Q_\alpha(\mu,\bar{\mu}) = \frac{1}{\pi}|\langle\mu|\alpha\rangle|^2 = \frac{1}{\pi}\exp\{-|\mu-\alpha|^2\}, \tag{1.36}$$

where we used Eqn. (1.21). We observe that it is a gaussian distribution over the complex plane centered around α with unity variance. We note that in Eqn. (1.35) if we are at the ground state, i.e. $|0\rangle$ we obtain exactly Eqn. (1.36) centered around zero. This observation allows us to give another interesting interpretation for the coherent state as a displaced vacuum state, that is, it has the same distribution of the vacuum state but displaced by α

in the complex plane (see Fig. 1.4(f)). One can compute the mean value and variance of Eqn. (1.36) to find, $\langle|\mu|^2\rangle = \text{Var}(|\mu|^2) = n+1$. Hence, the larger the value of n is the distribution will be peaked around $|\mu|^2 = n+1$. Moreover, the exponential form of this function says that it will not be zero only when $\mu \approx \alpha$. In Fig. 1.4) we show some plots of representative Husimi Q-functions.

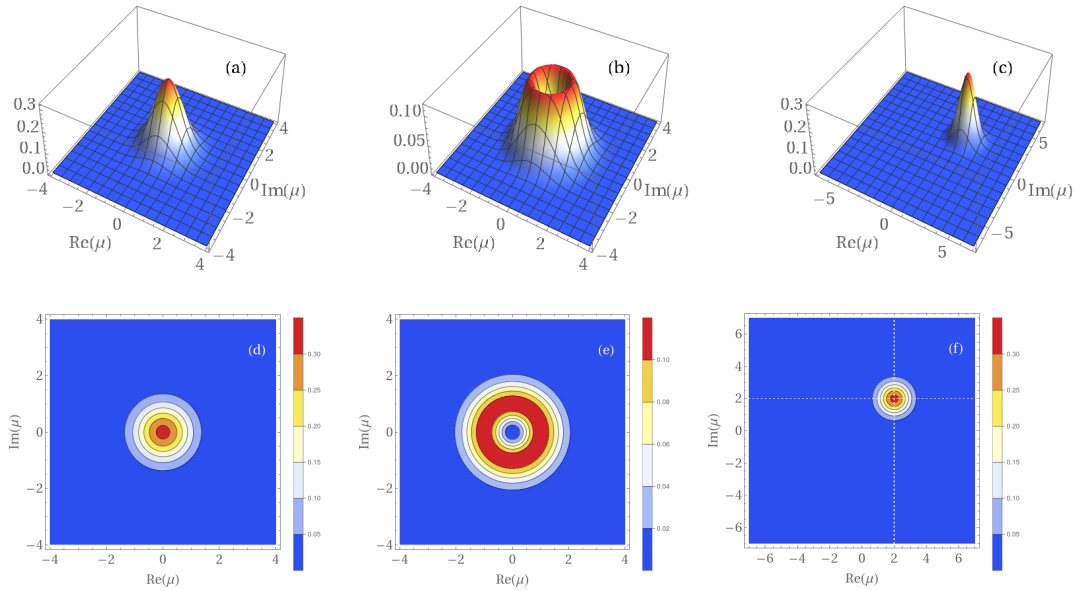

Figure 1.4: **Examples of Husimi Q-functions:** The Husimi Q-functions are $Q_{n=0}(\mu,\bar{\mu})$, $Q_{n=1}(\mu,\bar{\mu})$ and $Q_{\alpha=2+2i}(\mu,\bar{\mu})$, respectively. The upper line shows the $3D$ plots, while in the lower line we plot the contour of these functions.

Chapter 2

Entropy production: the second law of thermodynamics

Entropy is one of the most important concepts in physics. It was first introduced by Clausius as a function of a thermodynamic state useful to characterize the Carnot cycle. Later, within a microscopic description of thermodynamics, Boltzmann gave a physical meaning to it, in the context of micro-canonical ensemble. The entropy is a measure of how many micro-states are accessible to a macroscopic state. In information theory entropy is the function that provides the lack of information one have about a random variable [45]. It is ultimately the quantity that links physics with information theory [46].

For open systems, the entropy does not satisfy a conservation law. In addition to the entropy exchanged with the reservoir, entropy can also be spontaneously generated in the process. The latter is called *entropy production* and accounts for how irreversible a physical process is, or, equivalently, serve as a measure of how far from equilibrium a given process takes place [5,47]. The main contribution of this dissertation is the development of a theory of entropy production for non-equilibrium quantum systems tailored to a specific kind of open quantum system. Hence, in this chapter we review this concept. At the end of this chapter we aim to have answered the following questions:

- Why is entropy production important?
- What are the problems with the usual theory of entropy production (which we shall refer below as the "von Neumann formulation")?

Throughout this chapter we will refer to the equilibrium state of a system relative to its environment as defined by the *zeroth law of thermodynamics*: "If two systems are in thermal equilibrium with a third system, then they are in thermal equilibrium with each other". In Chap.3, the equilibrium state will be defined more formally in the context of statistical mechanics, which gives a microscopic interpretation for thermal phenomena.

The *first law of thermodynamics* states that energy is conserved. If we have a system, for instance a steam engine, we can change its internal energy by ΔU by providing some heat Q, and/or performing some work *on* it W,

$$\Delta U = Q + W. \tag{2.1}$$

Work can be interpreted as the controlled contribution to the change in internal energy, whereas heat is the amount of heat exchanged with a vast bath, which can not be controlled.

The *second law of thermodynamics* imposes restrictions on what type of transformations are allowed by nature. There are (at least) three equivalent statements of the 2nd law due to Carnot [48], Clausius [49] and Kelvin-Planck [5]. All of them are related to the aforementioned *entropy production*, which we will denote by Σ.

2.1 Entropy production in classical systems

In classical thermodynamics we learn the Clausius' inequality [4, 5], which states that the change in entropy from an initial state with S_i to a final one with S_f, defining $\Delta S = S_f - S_i$, is such that

$$\Delta S \geq \frac{Q}{T}, \tag{2.2}$$

where Q is the total heat delivered to the thermodynamic system and T is its absolute temperature. We mention that heat depends on the path taken, i.e. the steps of the thermodynamic process, so that it is usually written as $Q/T = \oint dQ/T$. The process is said to be *reversible* if $\Delta S = Q/T$, as occurs in idealized thermodynamic cycles, as will be exemplified by the Carnot cycle soon. A process is said to be *irreversible* if $\Delta S > Q/T$.

It is useful to rewrite the inequality (2.2) as the following equality,

$$\Delta S = \Sigma + \frac{Q}{T} \qquad \rightarrow \qquad \Sigma = \Delta S - \frac{Q}{T} \geq 0 \tag{2.3}$$

where $\Sigma \geq 0$ is the entropy production, that is, it is the entropy produced within the system during an irreversible process. The process is reversible if and only if $\Sigma = 0$, otherwise it is irreversible. Hence, the 2nd law can be stated in terms of entropy production as,

$$\boxed{\Sigma \geq 0} \tag{2.4}$$

We can differentiate Eqn.(2.3) with respect to time to obtain,

$$\frac{dS_t}{dt} = \Pi_t - \Phi_t, \tag{2.5}$$

where $\Pi_t = d\Sigma/dt \geq 0$ is the *entropy production rate* within the system and $\Phi = -(1/T)dQ/dt$ is the *entropy flux rate* from the system to the reservoir. The subscript t denotes the time dependence of these quantities.

Next, we will review three statements of the second law in classical thermodynamics and see how entropy production relates them.

Carnot statement

"If T_h and T_c, where $T_c < T_h$, are the absolute temperatures of a hot and cold bath, respectively, the maximum efficiency for a thermal machine operating between them is that of a Carnot machine, which is,"

$$\eta_C = 1 - \frac{T_c}{T_h} \tag{2.6}$$

The Carnot machine is an idealized machine in which every process is reversible. This means that by performing infinitesimal changes we can make the engine operate forward or backward. Physically, it means that there is no friction in the engine and that its heat reservoirs are *never* in contact with something colder or hotter than themselves. Suppose that we have a gas in a cylinder, initially occupying a volume V_1, with a frictionless piston

attached to it. It operates between two heat reservoirs, the hot at temperature T_h and the cold one at temperature T_c, where $T_h > T_c$. We consider the following four reversible steps (See Fig.2.1):

1. We put the cylinder in contact with the hot reservoir and then pull the piston slowly, to make sure that the temperature of the gas is never too different from the heat reservoir (which would not be possible if we pulled the piston fast) until the gas occupies a volume $V_2 > V_1$. This is an isothermal expansion of the gas, and a heat Q_h flows from the reservoir to the gas (heat absorption). In this case the internal energy is constant, so that $Q_h = W_{1,2}$;

2. The second step consists in taking the piston out of contact with any heat reservoir, so that no heat is exchanged. Again, one pulls the piston slowly until the gas temperature reaches T_c, in a volume $V_3 > V_2$. This is an adiabatic expansion and we have $\Delta U_{2,3} = W_{2,3}$;

3. In the third step, we put the system in contact with the heat reservoir at T_c and compress the piston slowly, so that the temperature of the gas does not change, until it reaches the volume $V_4 < V_3$. This is an isothermal compression, and an amount of heat Q_c will flow from the system to the reservoir. Here, we have $Q_c = -W_{3,4}$;

4. Finally, we take the cylinder out of contact with the cold reservoir and compress the piston slowly until the temperature reaches T_h, an adiabatic compression. This closes the cycle (see Fig.2.1). We can make all of these steps again or reverse the order, because it is composed of four reversible processes. Then, this cycle is reversible.

This is the Carnot cycle, by making the thermodynamic analysis of it [50] one obtains that its efficiency is precisely that given in Eqn. (2.6).

Now we consider, once again, a machine operating between a hot bath, with temperature T_h and a cold bath with temperature T_c, where $T_c < T_h$. To simplify the above analysis, we assume that each cycle operates very quickly (like the engine of a car) so that we can describe the thermodynamic quantities in a continuous fashion, instead of stroke-based. After the engine has reached a limit cycle, the rate of change of the internal energy and entropy will therefore no longer change, i.e. the limit cycle is the steady state cycle. The

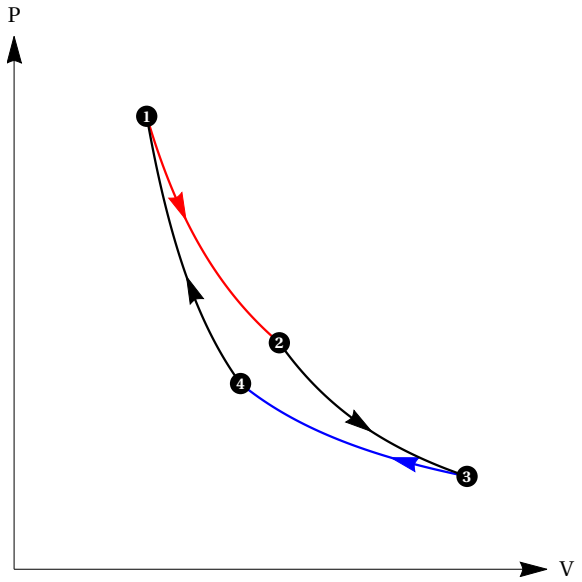

Figure 2.1: **Carnot cycle:** The red line corresponds to step (1), the isothermal expansion at T_h, while the blue line corresponds to step (3), the isothermal compression at T_c. The black lines correspond to the adiabatic process.

1st and 2nd laws therefore yield:

$$\frac{dU}{dt} = \dot{Q}_h + \dot{Q}_c + \dot{W} = 0 \tag{2.7}$$

$$\frac{dS}{dt} = \Pi + \frac{\dot{Q}_h}{T_h} + \frac{\dot{Q}_c}{T_c} = 0 \tag{2.8}$$

Using these relations, we can rewrite the efficiency as,

$$\eta = -\frac{\dot{W}}{\dot{Q}_h} = 1 + \frac{\dot{Q}_c}{\dot{Q}_h} = \left(1 - \frac{T_c}{T_h}\right) - \frac{T_c}{\dot{Q}_h}\Pi = \eta_C - \frac{T_c}{\dot{Q}_h}\Pi \tag{2.9}$$

from Eqn. (2.9) we see that the last term is always non-positive (because $\Pi \geq 0$). Whence, the efficiency of the machine will be smaller than Carnot's efficiency due to the entropy production. It will only be a Carnot machine if $\Pi = 0$.

Clausius' statement

"Heat can never pass from a colder to a warmer body without some other change, connected therewith, occurring at the same time."

Consider a process where we have two bodies, a hot one at T_h and a cold one at T_c,

where $T_c < T_h$. We *assume* there is no work involved, so the 1st law gives,

$$\dot{Q}_c = -\dot{Q}_h, \tag{2.10}$$

and the 2nd law, reads

$$\Pi = -\frac{\dot{Q}_h}{T_h} - \frac{\dot{Q}_c}{T_c} \geq 0. \tag{2.11}$$

Combining them,

$$\Pi = \left(\frac{1}{T_c} - \frac{1}{T_h}\right)\dot{Q}_h \geq 0. \tag{2.12}$$

Since $(1/T_c - 1/T_h) > 0$, Eqn.(2.12) yields $\dot{Q}_h \geq 0$. Physically, it means that heat flows from the hotter body to the cold one. This result is astonishing, the first law only says that energy must be conserved. So, in principle, as long as it is satisfied, we could have a heat flow from a colder body to a hot one. But the entropy production imposes a restriction on the flow of energy, this process is not allowed by nature unless we do something else.

Kelvin-Planck statement

"It is impossible to devise a cyclically operating device, whose the sole effect is to absorb energy in the form of heat from a single thermal reservoir and to deliver an equivalent amount of work."

Consider there is one heat bath at temperature T_h only, and there is no change in the internal energy ΔU. Then, the 1st and 2nd laws reads,

$$\dot{W} = -\dot{Q}_h, \tag{2.13}$$

$$\Pi = -\frac{\dot{Q}_h}{T_h} = \frac{\dot{W}}{T_h}. \tag{2.14}$$

Eqn.(2.14) says that positive work means there is an external agent performing work on the system.

The above analysis therefore shows quite clearly why entropy production is a central quantity in the characterization of thermodynamic processes out of equilibrium.

2.2 Entropy production and non-equilibrium steady states

We have seen that the entropy balance can be written as (see Eqn. (2.5)),

$$\frac{dS_t}{dt} = \Pi_t - \Phi_t,$$

where Π_t is the entropy production rate and Φ_t is the entropy flux rate. We say the system has reached a *steady state* when physical quantities do not change in time anymore. For an open system, there are two different kinds of steady states. We say the system is in an *equilibrium* steady state when it does not produce any entropy and there is no flux either, i.e. $\Pi = \Phi = 0$. Otherwise, if the system has a finite amount of entropy production rate $\Pi = \Phi > 0$ we say it has reached a *non-equilibrium steady state* (NESS). Hence, *NESSs are characterized by a finite entropy production rate*.

The theory of entropy production one has to use depends on the type of stochastic process under study. For classical systems, approaches based on classical master equations [51, 52] and Fokker-Planck equation [15, 53–56] have been extensively used.

In particular, in Ref. [56] the authors have developed a theory focused on systems described by linear Langevin equations. As an example, they studied the entropy production of a RL circuit in series. They showed that the NESS entropy production of such system is given by,

$$\Pi_{\text{RL}} = \frac{\mathscr{E}^2}{RT}, \tag{2.15}$$

where $\mathscr{E}$ is the electric potential of the battery, R is the resistance and T is the absolute temperature. This is the same result first obtained by Landauer in Ref. [57]. The system is completely classical as both the energy input, provided by the battery and the energy output due to dissipation thorough the system take place in a incoherent way. Remarkably, we will find a structurally similar result for a quantum system presenting criticality in Chap.5, that is why we mention Eqn. (2.15) at this point.

2.3 Entropy production for quantum systems

Regarding quantum systems, given a state ρ, von Neumann [14, 58] proposed the following definition of the entropy,

$$S_{\text{vN}} = -\operatorname{tr}\{\rho \ln \rho\} \tag{2.16}$$

where $\ln$ denotes the natural matrix logarithm. If the density matrix ρ is diagonalized as in Eqn.(1.2), we have

$$S_{\text{vN}} = -\sum_i p_i \ln p_i \tag{2.17}$$

where p_i is the population of the state $|\psi_i\rangle$. It measures the lack of information about the system. It is null in two cases only, if $p_i = 0$ or $p_i = 1$, which means there is no chance of finding the system in state $|\psi_i\rangle$ or it is certainly in state $|\psi_i\rangle$, respectively. Otherwise, $0 \leq S_{\text{vN}} \leq \ln d$, where d is the dimension of a finite dimensional Hilbert space.

The entropy flux for an open quantum system, described by a Lindblad master equation as Eqn.(1.5), is defined as,

$$\Phi = -\frac{1}{T}\operatorname{tr}\{HD(\rho)\} = \frac{\Phi_E}{T}. \tag{2.18}$$

where Φ_E is the energy flux *from* the system *to* the environment. Hence it relates entropy flux with heat, in accordance with classical thermodynamics. By Eqn.(2.5) we have that the von Neumann entropy production is

$$\Pi_{\text{vN}} = \frac{dS_{\text{vN}}}{dt} + \Phi. \tag{2.19}$$

The von Neumann formulation allows one to write Eqn.(2.19) in the following form,

$$\Pi_{\text{vN}} = -\partial_t K_{\text{vN}}(\rho||\rho^{\text{eq}}) \geq 0 \tag{2.20}$$

where $K_{\text{vN}}(\rho||\rho^{\text{eq}}) = \operatorname{tr}\{\rho(\ln\rho - \ln\rho^{\text{eq}})\}$ is the von Neumann relative entropy, which measures how distant the state ρ is from the equilibrium state $\rho^{\text{eq}} = \exp\{-\beta H\}/Z$, where β and Z are constants and H is the system Hamiltonian (it will be better understood in the

next chapter). This enables us to interpreted entropy production as a measure of how far from the equilibrium state ρ^{eq}, the state ρ is.

Despite the simple and familiar physical interpretations for the entropy production and flux, the von Neumann formulation combined with the way one defines the entropy flux rate in Eqn. (2.18), which is inspired by the classical structure and allows us to identify the entropy production as in Eqn. (2.19), leads to unphysical, divergent results when one takes the limit $T \to 0$. The zero temperature limit is commonly used in quantum optics, where the dynamics is well behaved and experimental results are theoretically reproduced in several situations. Even the entropy balance dS/dt is finite, despite the divergence of its individual contributions. This strange behavior was coined as *the zero temperature catastrophe* [59]. This is a clear inconsistency of the theory and it has led to approaches based on quantum Fokker-Planck equations using quantum phase space methods [27, 60, 61], inspired by the classical context [15, 52]. The same idea that will be used in Chap.4.

Chapter 3

Phase transitions

Last chapter was about thermodynamics, which allows one to determine relationships between various properties of materials with minimal information about its internal structure. For instance, to describe a glass of water one only needs to talk about its volume V, temperature T and pressure p, without ever thinking about all the complex interactions happening between the various molecules of water inside the glass.

However, due to the kinect interpretation, we know that thermal phenomena can be reduced to the study of the random motions of particles, so that the study of heat can be done in mechanical terms. Statistical mechanics is the bridge between the microscopic world, in which the system is composed of an enormous number of particles (an ensemble), and the macroscopic world, where we observe thermodynamic properties. Due to the randomness of the microscopic world, a detailed description of the state becomes unfeasible and one considers only the average properties of the ensemble. There are several ensembles, the most important being the Canonical (Gibbs) ensemble, which will be defined in the next section [6].

Among all phenomena statistical mechanics sheds light on, phase transitions are the most remarkable. They are abrupt changes in the characteristics of a physical system at certain specific points as a function of some parameter. They can happen for equilibrium or non-equilibrium states, in classical and quantum mechanical systems. The physical origin of phase transitions is due to interactions and a thermodynamic limit, which means that when we have a system that displays non-trivial interactions between a large number of particles one can expect a critical behavior to emerge. Basically, phase transitions are

all about some kind of *competition* between different terms of the operator that governs the dynamics (Hamiltonian or Liouvillian).

In this chapter, we will briefly review some concepts concerning classical and quantum phase transitions and study an example of a quantum phase transition in the Lipkin-Meshkov-Glick model. Then, we will discuss classical non-equilibrium phase transitions, where the entropy production rate has been shown to be able to characterize the critical behavior. Finally, we introduce and discuss driven-dissipative phase transitions, which are the critical systems of interest of the present work.

3.1 Equilibrium phase transitions: classical and quantum

In principle, any physical system can be described by a Hamiltonian operator that depends on some parameter $H(g)$, for which we can find the eigenvalues and eigenvectors,

$$H(g)\left|E_n\right\rangle = E_n(g)\left|E_n\right\rangle . \tag{3.1}$$

We can now define thermal equilibrium according to statistical mechanics: a physical system described by a Hamiltonian $H(g)$ is in *thermal equilibrium* at temperature T if the probability of finding the system in an eigenstate $|E_n\rangle$ is given by the *Gibbs distribution*

$$P_n = \frac{e^{-\beta E_n(g)}}{Z}, \tag{3.2}$$

where $\beta = 1/k_B T$, k_B is the Boltzmann's constant and Z is a normalization constant, called *partition function*

$$Z = \sum_n e^{-\beta E_n}. \tag{3.3}$$

The partition function is the central object of equilibrium statistical mechanics as it encodes all relevant equilibrium thermodynamic quantities. It is related to the free energy of the system via the identity (we set $k_B = 1$ from now on),

$$Z = e^{-\beta F} \qquad \rightarrow \qquad F = -T \ln Z \tag{3.4}$$

This equality is a bridge between the probabilities of the microscopic world that are encoded in the partition function and the macroscopic world, the thermodynamics of the system, through the free energy.

A classical phase transition occurs when thermodynamic potentials or some of its derivatives becomes non-analytic as a function of some parameter. For a temperature driven phase transition, the free energy F exhibits a non-analytic behavior at a critical temperature T_c. As an example of this type of transition we can imagine the liquid-vapor transition of water at a constant pressure p. In this scenario, there is a competition between the bounding energy of the molecules and the kinect energy they gain with temperature increase.

It is possible to observe phase transitions at zero temperature, these are the so called *quantum phase transitions* (QPT) [25]. In this case, some parameter g which measures the relative strength between competing terms in the Hamiltonian can change the ground state of the system, for a specific critical value g_c. This is the physical origin of the QPT. If $|\psi_0\rangle$ is the ground state with energy $E_0(g)$ and $|\psi_1\rangle$ is the first excited state with energy $E_1(g)$ of the Hamiltonian $H(g)$, then the energy gap is defined as the difference

$$\Delta(g) = E_1(g) - E_0(g), \tag{3.5}$$

and the QPT is associated with the closure of this gap, i.e. it takes place when $\Delta(g_c) = 0$.

To properly describe phase transitions it is useful to introduce a quantity denominated *order parameter*, which was first introduced by Lev Landau, in his theory of spontaneous symmetry breaking [9]. Its main property is to be null in one phase and non-zero in the other. The order parameter idea is extremely important and powerful because it works for both equilibrium or non-equilibrium phase transitions, in classical or quantum systems.

3.1.1 Example of a QPT: the Lipkin-Meshkov-Glick model

The Lipkin-Meshkov-Glick (LMG) [62] model describes the dynamics of a single macro-spin by the following Hamiltonian,

$$H = -hJ_z - \frac{\gamma_x}{2j}J_x^2, \tag{3.6}$$

where j is the total angular momentum, $h \geq 0$ is the transverse magnetic field and $\gamma_x \geq 0$ is the squeezing[1] strength along the x-direction (critical field $h_c = \gamma_x$). This Hamiltonian is symmetric under the transformation $J_x \to -J_x$ and $J_z \to J_z$, which is a discrete Z_2 symmetry. The thermodynamic limit corresponds in this case to $j \to \infty$. In such a limit the ground state (GS) of the system approaches a spin coherent state [63], defined by

$$|\theta, \phi\rangle = e^{-i\phi J_z} e^{-i\theta J_y} |j\rangle \,, \tag{3.7}$$

where $\theta \in [0, \pi]$, $\phi \in [0, 2\pi]$ and is $|j\rangle$ is the eigenstate of J_z with eigenvalue j. Bosonic coherent states are the quantum states that minimize the uncertainty relation, so they are the most "classical" states allowed by QM, as discussed in Sec.1.3. Spin coherent states share the same particularity: they make the averages of the spins to be equal to classical spins,

$$\mathbf{S} = (\langle J_x \rangle, \langle J_y \rangle, \langle J_z \rangle) = j(\sin\theta\cos\phi, \sin\theta\sin\phi, \cos\theta), \tag{3.8}$$

where $\langle J_i \rangle$, $i = x, y, z$ is the average of the macrospin J_i taken with respect with the state (3.7). Hence, the average energy in spin coherent states of Eqn.(3.6) is given by, in leading order [2],

$$\begin{aligned} E(\theta, \phi) &= \langle \theta, \phi | \, H \, | \theta, \phi \rangle \\ &= -hj\cos\theta - \frac{\gamma_x j}{2} \sin^2\theta \cos^2\phi. \end{aligned} \tag{3.9}$$

The GS is found by minimizing Eqn.(3.9) with respect to the angle variables, $\boldsymbol{\nabla} E(\theta, \phi) = \mathbf{0}$, which leads to the set of equations,

$$\begin{aligned} \sin\theta(h - \gamma_x \cos\theta \cos^2\phi) = 0 \\ \sin^2\theta(\gamma_x \cos\phi \sin\phi) = 0. \end{aligned} \tag{3.10}$$

There are two possible solutions for the set of Eqns.(3.10). The trivial one is $\theta = 0$, in this

[1] Squeezing acts by decreasing the variance, i.e. the quantum uncertainty of the angular momentum in a given direction.

[2] The term $\langle \theta, \phi | \, J_x^2 \, | \theta, \phi \rangle \approx j^2 \sin\theta\cos\phi + \mathscr{O}(j)$. In the thermodynamic limit we neglect the terms $\mathscr{O}(j)$ because, due to $1/(2j)$, their contribution is of order $\mathscr{O}(0)$.

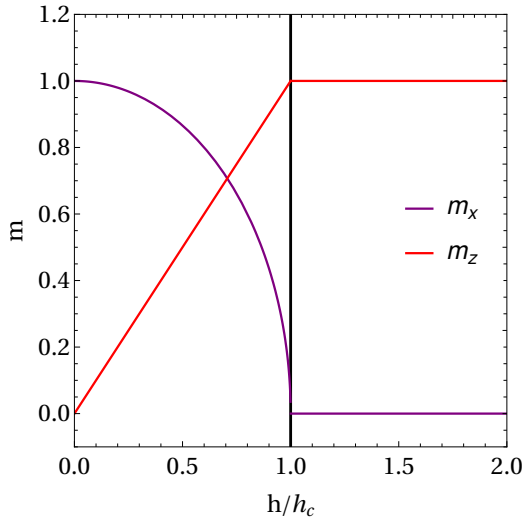

Figure 3.1: **Magnetization of the LMG model:** We plot the magnetization along the x and z direction as given by Eqns.(3.13) and (3.14). The black vertical line represents the critical point. The squeezing along the x direction was set $\gamma_x = 1$

case ϕ is arbitrary. But it is a minimum only when $h > h_c$. The other solution is given by,

$$\cos\theta = \frac{h}{\gamma_x} \leq 1 \tag{3.11}$$

with $\phi = 0$ or $\phi = \pi$ and is valid only if,

$$h \leq h_c = \gamma_x \tag{3.12}$$

It is insightful to look at the magnetization along the x and z directions. They are given by,

$$m_x = \frac{\langle J_x \rangle}{j} = \sin\theta\cos\phi = \begin{cases} \frac{1}{\gamma_x}\sqrt{h_c^2 - h^2}, & h \leq h_c \\ 0, & h \geq h_c \end{cases} \tag{3.13}$$

and,

$$m_z = \frac{\langle J_z \rangle}{j} = \cos\theta = \begin{cases} \frac{h}{\gamma_x}, & h \leq h_c \\ 1, & h \geq h_c. \end{cases} \tag{3.14}$$

In Fig.3.1 we can see the plot of both magnetizations. They have a kink at the critical point $h = \gamma_x$. The order parameter is m_x, since it is non-zero in the broken symmetry

phase and identically zero in the other phase (the symmetric one) where the magnetization in the z direction is maximal.

3.2 Classical non-equilibrium phase transitions and entropy production

Non-equilibrium phase transitions occur between two non-equilibrium steady states (NESSs). As discussed in the introduction and in Sec. 2.2, a NESS is a state where there is a constant flux of some physical quantity, such as charge and is characterized by a finite amount of entropy production rate $\Pi = \Phi > 0$. Moreover, what distinguishes NESSs from equilibrium steady states (ESS) is that the later satisfy the *detailed balance*. This concept is as follows, let $M_{i,j}$ be the transition probability from state j to state i, and let P_i^* denote the ESS distributions, detailed balance says that $M_{i,j}P_j^* = M_{j,i}P_i^*$, which means that going from state j to state i can occur with the same probability of the reversal process. It is related to the invariance under time reversal. However, the aforementioned fluxes lead to NESS distributions P_i^* that *break the detailed balance* condition and it creates *probability currents in phase space* that will be needed to characterize these states [47].

When a system is not in thermal equilibrium it becomes very hard to describe it because of the lack of a function such as the partition function Eqn. (3.3). Yet, one can use the idea of an order parameter to describe these type of phase transitions. However, this kind of description hides the non-equilibrium nature, and most importantly its behavior when the transition happen.

For that reason, it becomes interesting to study the behavior of entropy production, as it can give insights and even characterize them. Regarding this matter, there are several studies in the classical context [20–24] where the entropy production was calculated, indicating that it is always finite across a non-equilibrium transition and presents a kink or a discontinuity. Indeed, this behavior was shown to be universal for classical systems described by classical Pauli master equations and breaking a Z_2 symmetry in Ref. [2].

In Ref. [2], they consider the majority voter model [47], which presents both continuous and discontinuous phase transitions, depending on some parameters. This model is described by a classical master equation, for such systems one can use the Schnakenberg

expression for entropy production,

$$\Pi_t = \frac{k_B}{2}\sum_{i,j}(M_{j,i}P_i(t) - M_{i,j}P_j(t))\ln\frac{M_{j,i}P_i(t)}{M_{i,j}P_j(t)}. \tag{3.15}$$

This model is known to not satisfy the detailed balance, hence there is a finite entropy production rate. These facts characterize its non-equilibrium nature.

The model is defined as follows: consider an arbitrary lattice where each site i can assume integer values $\sigma_i = 0, 1, ..., q-1$. The dynamics depends on the fraction $w_{\sigma_i} = (1-\theta)\sum_{j=1}^{k}\delta(\sigma_i', \sigma_j) + \theta\delta(\sigma_i', \sigma_i)$, where σ_j denotes the spin of the k nearest neighbors of site i (k is the conectivity parameter). The term $\theta\delta(\sigma_i', \sigma_i)$ is the local spin dependence, proportional to the inertial term θ and σ_i' represents the spin of the majority neighborhood. We define a misalignment parameter f, so that with probability $1-f$ a local spin σ_i changes to σ_i' and with probability f it does not. We can think of the model as describing a community of individuals where each one has its own opinion about some subject and all of them are debating about it. As time goes by, they can change their opinion depending on their neighbors, we have individuals that change their minds according to the majority and others that do not. It was demonstrated that a discontinuous phase transition happens for large inertia term θ. Some plots for this model are shown in Fig. 3.2.

The authors consider a bidimensional lattice with conectivity $k = 20$ and inertial parameter $\theta = 0.375$. Panel (a) and (b) shows, respectively, the NESS entropy production and the order parameter $|m|$ at the vicinity of the critical parameter f_0, the inset shows the behavior of the NESS entropy production for a larger range of f, we observe that the entropy production is finite and has a discontinuity.

Panel (c) is the plot of the variance $\chi = N(\langle m^2\rangle - |m|^2)$ at the vicinity of the critical point, we note that as the volume N increases, the variance presents a finite peak approaching f_0. This is a *finite size* effect because the variance should diverge at the critical point. We must bear in mind that phase transitions occurs when one defines a thermodynamic limit, in this case that would be $N \to \infty$ (in the example of Sec. 3.1.1 it was the spin $j \to \infty$), but it is not possible to have something really infinite when performing computational simulations. It actually becomes harder to do when the system size increases. Although in this sense we cannot say we observe "real" phase transitions

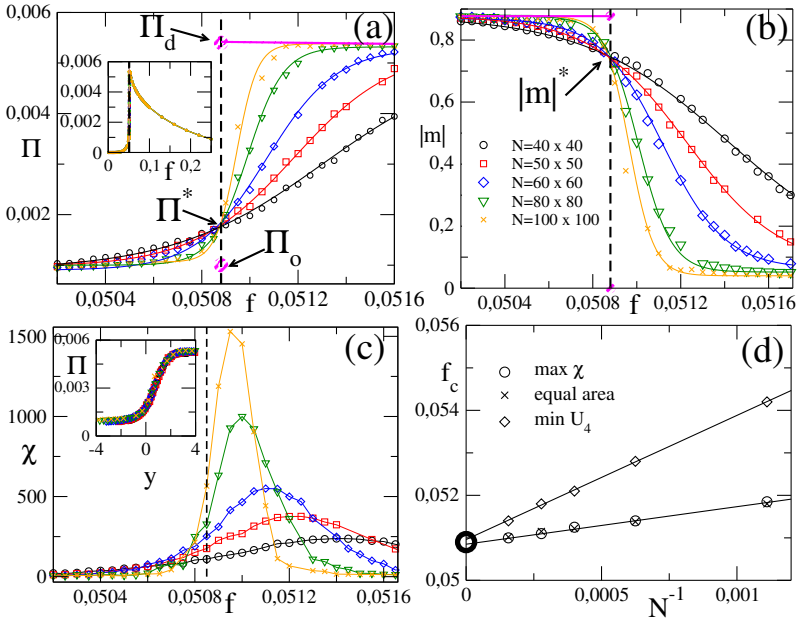

Figure 3.2: **Majority vote model presenting a discontinuous phase transition:** This panel was taken from Ref. [2]. The parameters were set $k = 20$ and $\theta = 0.375$. The plots are for different values of the system volume N as shown in panel (b). Panel (a) shows the steady entropy production rate Π,(b) shows the order parameter $|m|$ and (c) shows the variance χ versus f. All at the vicinity of phase coexistence. Dashed lines: Crossing point among entropy production curves. Continuous lines in (a) and (b) correspond to the theoretical description, Eqn.(28) of the paper. Top and bottom insets: Π for larger sets of f and collapse of data by taking the relation $y = (f - f_0)N$, respectively. In (d), the plot of the maximum of χ, minimum of U_4 and equal area order-parameter probability distribution versus N^{-1}.

in numerical simulations, it is true that a large enough finite system will have a phase-transition-like behavior, with its singularities and divergences smoothed. Hence, in order to use the finite size results for infinite system it is important to know how the finite variance change when one increases the system size. According to standard finite-size scaling, the variance behaves as $\chi = N^{\frac{\gamma}{\nu}} g(N^{\frac{1}{\nu}}|f - f_0|)$, where f is the control parameter, g being a scaling function and γ, ν the critical exponents. If one obtained the right critical point and critical exponents, then the data should collapse for every value of N, and we can extrapolate the results to the infinite system, where the phase transition takes place. This is shown in the inset of panel (c), where we observe data collapse for $y = (f - f_0)N$. It indicates the *universality* of the entropy production behavior.

In panel (d), we see the plot of the maximum of the variance χ, the minimum of the function $U_4 = 1 - \langle m^4 \rangle / (3\langle m^2 \rangle^2)$, which is the function used to find the critical value

f_0 as the point where, for diferent sizes, the curves intersect each other and equal area order-parameter probability.

Surprisingly, we will encounter a similar behavior, as shown in the insets of Fig.3.2 for one of the contributions to the entropy production in the quantum context at the end of Chap.5.

3.3 Driven-dissipative phase transitions

Driven-dissipative phase transitions (DDPTs) occur in systems whose state is governed by a Lindblad master equation of the form,

$$\partial_t\rho = -i[H_0 + i\sum_i \mathscr{E}_i(a_i^\dagger - a_i), \rho] + \sum_i 2\kappa_i \left(a_i\rho a_i^\dagger - \frac{1}{2}\{a_i^\dagger a_i, \rho\} \right),$$

where H_0 is the Hamiltonian of a particular model, $\mathscr{E}_i$ is the amplitude of the driving laser associated with the mode a_i in the interaction picture and we have a zero temperature dissipator (see Eqn.(1.13)). We note that the energy input is coherent while the dissipation occurs incoherently.

In fact, we can be more general and consider an evolution described by a Liouvillian that depends on a parameter g, which will be denoted by $\mathscr{L}(g)$,

$$\partial_t\rho_t = \mathscr{L}(g)\rho_t \tag{3.16}$$

We can apply the vectorization procedure (see App. D) and obtain the equation,

$$\partial_t \text{vec}(\rho_t) = \hat{\mathscr{L}}(g)\text{vec}(\rho_t) \tag{3.17}$$

where $\hat{\mathscr{L}}$ stands for the vectorized Liouvillian. From Eqn.(3.17) the solution is simply given by $\text{vec}(\rho_t) = \exp\Big\{\hat{\mathscr{L}}(g)t\Big\}\text{vec}(\rho_0)$. So that all information we need in order to know the state at time t is the spectrum of $\hat{\mathscr{L}}$. The Liouvillian spectrum is complex and has two important properties [13, 64],

1. It *always has a zero eigenvalue*, $\lambda_0 = 0$ and the steady-state is associated with it $\hat{\mathscr{L}}(g)\text{vec}(\rho_{\text{NESS}}) = 0$;

2. The eigenvalues are *always negative*, due to the stability of the state. If it were positive, then the exponential would diverge.

We may order the eigenvalues as $0 = |\Re[\lambda_0(g)]| < |\Re[\lambda_1(g)]| < ... < |\Re[\lambda_n(g)]|$. The eigenvalue $\lambda_1(g)$ is the one whose real part is the closest to zero. It plays a similar role as the first excited state in the energy gap $\Delta(g)$ in QPTs. Then, a dissipative phase transition is defined to happen when the real part of the first non-zero eigenvalue vanishes $\Re[\lambda_1(g_c)] = 0$ [65].

Physically, the interplay between the unitary dynamics and the dissipation is responsible for the emergence of the phase transition. Indeed, the system will eventually relax to a steady state as we have seen in Sec.1.2.2. The non-equilibrium nature can be physically visualized by the following reasoning: consider an optical cavity excited by a laser. The laser will continuously insert photons inside the cavity, this is the driving. But, photons can also leak out to the environment by a semitransparent mirror, this is the dissipation (see Fig.4.1). The competition between the driving and dissipation will lead the system to a NESS. In this sense, DDPTs are the non-equilibrium analogue of quantum phase transitions.

The main advantage of exploring DDPTs is due to the possibility of realizing phases that have *no* equilibrium counterpart. It provides a richer physics playground and this is due to the several terms of the model H_0 that will compete not only between them as in the QPT, but also with the dissipation channel to determine the NESS.

DDPTs have been extensively studied theoretically in recent years for various platforms, to mention some we can talk about nonlinear photonic resonators [65–74] , spin lattices [75–82] and exciton-polariton condesates [83–85].

The main concepts of this chapter can be summarized into the following table [77]:

	TPT	**QPT**	**DPT**
Operator	Hamiltonian $H = H^\dagger$	Hamiltonian $H(g) = H^\dagger(g)$	Liouvillian $\mathscr{L}(g)$
Relevant quantity	Free energy $F = -T \ln Z$	Energy eigenvalues $H(g)\left\|\psi_i\right\rangle = E_i(g)\left\|\psi_i\right\rangle$	Eigenvalues $\mathscr{L}(g)\rho = \lambda_i(g)\rho$
State	Gibbs $\rho \propto \exp\{-\beta H\}$	Ground state $(H(g) - E_0(g))\left\|\psi_0\right\rangle = 0$	Non-equilibrium steady state $\mathscr{L}(g)\rho = 0$
Phase transition	Non-analiticity in F	Energy gap $\Delta(g) = E_1(g) - E_0(g)$	Vanishing real part of eigenvalue closest to zero $\Re[\lambda_1(g_c)] = 0$

Table 3.1: **Table of phase transitions:** The first colunm stands for thermal phase transitions (TPT), the sencond for quantum phase transition (QPT) and the last for Dissipative phase transitions (DPT). Based on the table of Ref. [77]

Next chapter, we will put forward our theory of entropy production suited for driven-dissipative phase transitions, the key result of this dissertation.

Chapter 4

Wehrl entropy production rate

In this chapter we develop and present the main result of this work, the theoretical framework coined as *Wehrl entropy production rate*. A phase transition can always be characterized by an order parameter, but such quantities do not hold neither the irreversible nature of the system nor the role of quantum fluctuations. We recall that entropy production serves to characterize NESSs [47], as it measures how far from equilibrium a quantum state is. Since driven-dissipative phase transitions are the quantum analogue of non-equilibrium phase transitions, some natural questions one can come up with are:

1. How does Π behaves as one crosses the transition?

2. What is the role of quantum fluctuations?

Driven-dissipative phase transitions occur at zero temperature and the states are not gaussian, in general. These are the technical problems that arises when trying to define entropy production for critical quantum systems. The usual theory of entropy production breaks down for zero temperature, leading to the *zero temperature catastrophe* [59], and the non-gaussianity of the state prevents us from using the Wigner entropy production rate proposed in Ref. [27], once the Wigner function can be negative and bad behaved near the criticality.

Our proposal is to use the Husimi Q-function to define entropy production for systems that undergo driven-dissipative phase transitions. The chapter is organized as follows: first, we use the Wehrl entropy [86] to obtain closed expressions for the entropy production and entropy flux rate for general driven-dissipative systems described by a Lindblad master

equation, that can be mapped into a Fokker-Planck like equation [15, 53], it is applied to example 2 of Chap.1 for the driven-dissipative harmonic oscillator at zero temperature where one can easily obtain an analytical expression for the NESS entropy production. Finally, the results are specialized for critical driven-dissipative systems and the role of quantum fluctuations becomes clear. This chapter is based on Ref. [28]

4.1 Wehrl entropy production rate for driven-dissipative systems

We consider a bosonic system described by a set of modes a_i subjected to external coherent drives with amplitude $\mathscr{E}_i$ and incoherent photon losses at rate κ_i (see fig. 4.1) evolving according to the Lindblad master equation

$$\partial_t \rho = -i[H_0 + i\sum_i \mathscr{E}_i(a_i^\dagger - a_i), \rho] + \sum_i 2\kappa_i \left(a_i \rho a_i^\dagger - \frac{1}{2}\{a_i^\dagger a_i, \rho\} \right), \tag{4.1}$$

where the first term is the coherent evolution of the dynamics, H_0 is the Hamiltonian of the model and the sum runs over all modes. The second term is the usual Lindblad dissipator describing the incoherent one-photon losses for the enviroment at zero temperature (see Eqn. (1.13)).

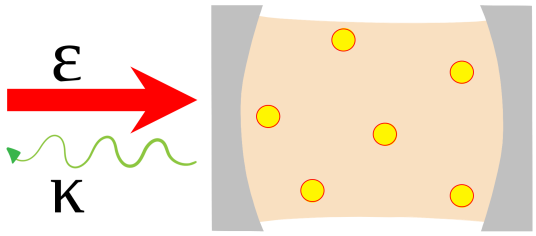

Figure 4.1: **Standard driven-dissipative scenario:** an optical cavity filled with a non-linear medium subjected to an external pump $\mathscr{E}$ and a photon loss at rate κ.

We move to phase space by defining the Husimi Q-function $Q(\mu, \bar{\mu}) = \langle \mu | \rho | \mu \rangle / \pi$ where $|\mu\rangle = \bigotimes_i |\mu_i\rangle$, with $a_i |\mu_i\rangle = \mu_i |\mu_i\rangle$ being coherent states. Using Eqns. (1.31) the

master equation (4.1) is converted into a Quantum Fokker-Planck equation

$$\partial_t \rho \to \partial_t Q(\mu, \bar{\mu}) = \mathscr{U}(Q) + \mathscr{D}(Q), \tag{4.2}$$

where $\mathscr{U}(Q)$ stands for the unitary differential operator operator (which will depend on the specific form of the Hamiltonian H_0) and $\mathscr{D}(Q)$ is the differential operator related to the dissipator. For the sake of generality, we consider the finite temperature dissipator as in Eqn. (1.13),

$$D(\rho) = \sum_i 2\kappa_i(N_i+1)\left(a\rho a^\dagger - \frac{1}{2}\{a^\dagger a, \rho\}\right) + 2\kappa_i N_i\left(a^\dagger \rho a - \frac{1}{2}\{aa^\dagger, \rho\}\right) \tag{4.3}$$

where $N_i = (e^{\omega_i/T} - 1)^{-1}$ is the Bose-Einstein occupation with ω_i being the free oscillator frequency of each mode a_i. It leads to,

$$\mathscr{D}(Q) = \sum_i \kappa_i(2Q + \mu_i \partial_{\mu_i} Q + \bar{\mu}_i \partial_{\bar{\mu}_i} Q + 2(N_i+1)\partial_{\bar{\mu}_i}\partial_{\mu_i} Q). \tag{4.4}$$

At this point it turns out to be convenient to define the quantity,

$$J_i(Q) \doteq -\kappa_i[\mu Q + (N_i+1)\partial_{\bar{\mu}} Q], \tag{4.5}$$

which becomes for $N_i = 0$ (zero temperature limit),

$$J_i(Q) = -\kappa_i(\mu_i Q + \partial_{\bar{\mu}_i} Q). \tag{4.6}$$

It allows one to write Eqn. (4.4) more neatly as,

$$\mathscr{D}(Q) = -\sum_i (\partial_{\mu_i} J_i(Q) + \partial_{\bar{\mu}_i} \bar{J}_i(Q)), \tag{4.7}$$

so that the dissipative operator can be viewed as a divergence in the complex plane.[1] The quantities $J_i(Q)$ have a rich physical meaning. First, we highlight that by introducing $J_i(Q)$ one can interpret Quantum Fokker-Planck equation (4.2) as a continuity equation for the quasiprobability distribution $Q(\mu, \bar{\mu})$. Secondly, we note that when the system

[1] Explicitly, one can see that $\mathscr{D}(Q) = -\boldsymbol{\nabla} \cdot \mathbf{J}$, where $\boldsymbol{\nabla} = (\partial_{\mu_i}, \partial_{\bar{\mu}_i})$, $\mathbf{J} = (J_i, \bar{J}_i)$

reaches the vacuum state, defined as $|\mathbf{0}\rangle = |00.....0\rangle$, which is the fixed point (equilibrium state) of the dissipator, i.e. $D(\rho_{vac}) = 0$ where $\rho_{vac} = |\mathbf{0}\rangle\langle\mathbf{0}|$, the Q-function will be $Q_{vac}(\mu,\bar{\mu}) = \frac{1}{\pi}|\langle\mu|\mathbf{0}\rangle|^2 = \frac{1}{\pi}\exp\Big\{-\sum_j|\mu_j|^2\Big\}$ and then it is trivial to verify that $J_i(Q_{vac}) = 0$. Thus, the quantities $J_i(Q)$ vanish in the equilibrium state of the dissipator (which will, in general, not be the steady-state of the full master equation due to the Hamiltonian contributions). All these observations induces us to interpret $J_i(Q)$ as *irreversible quasiprobability currents* in the quantum phase space associated with the mechanism of photon losses (dissipation). We can say in advance that these quantities will have a substantial role in entropy production [15, 47, 53].

To proceed we choose as our entropic quantifier the *Wehrl entropy* defined as [86],

$$S(Q) = -\int d^2\mu\; Q\ln Q, \tag{4.8}$$

since $Q(\mu,\bar{\mu})$ is the probability distribution of a heterodyne measurement, we have that $S(Q)$ can be interpreted as the entropy of the system convoluted with additional noise due to the heterodyning measurement. Indeed, one can show that it is an upper bound for the von Neummann entropy $S(\rho) \leq S(Q)$ [86].

We differentiate (4.8) in time to obtain,

$$\begin{aligned}\frac{dS(Q)}{dt} &= -\int d^2\mu\;\frac{d}{dt}[Q\ln Q]\\ &= -\int d^2\mu\;\partial_t Q\ln Q.\end{aligned}$$

Our goal now is to separate this as in Eqn. (2.5) ,

$$\frac{dS(Q)}{dt} = \Pi_t - \Phi_t, \tag{4.9}$$

where Π_t is the rate of entropy production within the system and Φ_t is the entropy flux rate from the system to the reservoir. Inserting Eqn.(4.2) into (4.9), inspired by a standard procedure developed for classical systems in Ref. [15] we identify the entropy production

rate and the entropy flux rate as,

$$\Pi_t \doteq \Pi_{\mathscr{U}} + \Pi_J, \tag{4.10}$$

$$\Pi_{\mathscr{U}} = -\int d^2\mu\ \mathscr{U}(Q)\ln Q, \tag{4.11}$$

$$\Pi_J - \Phi_t \doteq -\int d^2\mu\ \mathscr{D}(Q)\ln Q. \tag{4.12}$$

Physically Eqn. (4.12) essentially amounts to the fact that dissipation is an irreversible process, so that it must be related to the flux of entropy and must produce some entropy. The unitary dynamics is identified as a contribution to the entropy production because it is related to something that happens within the system, the act of heterodyning may produce entropy for certain systems, it depends on H_0 (it is trivial to demonstrate that the pumping contribution vanishes). We proceed by identifying the entropy production rate and entropy flux rate associated with dissipation. The only assumption we make is that the Q-function and its derivatives vanish at the infinity, applying integration by parts,

$$\begin{aligned}
\Pi_J - \Phi_t &= -\int d^2\mu\ \mathscr{D}(Q)\ln Q \\
&= \int d^2\mu\ \sum_i (\partial_{\mu_i} J_i(Q) + \partial_{\bar{\mu}_i}\bar{J}_i(Q))\ln Q \\
&= -\sum_i \left(\int d^2\mu\ \frac{\partial_{\mu_i} Q}{Q} J_i(Q) + \frac{\partial_{\bar{\mu}_i} Q}{Q}\bar{J}_i(Q)\right) \\
&= \sum_i \frac{2}{\kappa_i(N_i+1)}\int d^2\mu\ \frac{|J_i(Q)|^2}{Q} + \sum_i \int d^2\mu\ (\mu_i\bar{J}_i + \bar{\mu}_i J_i) \\
&= \sum_i \frac{2}{\kappa_i(N_i+1)}\int d^2\mu\ \frac{|J_i(Q)|^2}{Q} - \sum_i \frac{2\kappa_i}{N_i+1}(\langle a_i^\dagger a\rangle - N_i),
\end{aligned}$$

where in the third line we used Eqn. (4.5) to write $\frac{\partial_{\bar{\mu}_i} Q}{Q} = -\frac{1}{(N_i+1)}\left[\frac{1}{\kappa_i}\frac{J_i(Q)}{Q} + \mu_i\right]$. Whence, we find for the entropy flux rate,

$$\Phi_t = \sum_i \frac{2\kappa_i}{N_i+1}(\langle a_i^\dagger a\rangle - N_i), \tag{4.13}$$

which, for $N_i = 0$ (zero temperature limit) simplifies to,

$$\Phi_t = \sum_i 2\kappa_i \langle a_i^\dagger a \rangle, \tag{4.14}$$

which is a simple and beautiful formula. The flux of entropy to the reservoir is directly proportional to the number of photons inside the cavity: the more photons you have, the more the dissipator will act throwing them away, then the greater the flux will be. For the dissipative contribution to the entropy production we find,

$$\Pi_J = \sum_i \frac{2}{\kappa_i(N_i+1)} \int d^2\mu \, \frac{|J_i(Q)|^2}{Q} \geq 0, \tag{4.15}$$

it is directly related to the irreversible quasi-probability currents, for each mode, in quantum phase space. Indeed, it can be seen as the average of $|J_i(Q)/Q|^2$, where $J_i(Q)/Q$ may be interpreted as the velocity of the currents according to Ref. [15], then Π_J is a sum over the average of the squared velocities. Thus, the emergence of irreversibility at the quantum level is associated with the probability current of the dissipative process.

The unitary contribution to the entropy production (4.11) is a model dependent term, it may vanish or not. We will soon specialize it for critical systems where it is possible to provide a formula for this contribution.

4.1.1 Application: driven-dissipative quantum harmonic oscillator

As a simple, yet illuminating, application of our results, we revisit example 2 of Chap.1. Consider a single bosonic mode with Hamiltonian $H_0 = \Delta a^\dagger a$, driven with an amplitude $\mathscr{E}$ and subjected to dissipation at zero temperature with rate κ. Explicitly, Eqn.(4.1) becomes

$$\partial_t \rho = -i[\Delta a^\dagger a + i\mathscr{E}(a^\dagger - a), \rho] + 2\kappa \left(a\rho a^\dagger - \frac{1}{2}\{a^\dagger a, \rho\} \right), \tag{4.16}$$

The unitary differential operator is $\mathscr{U}(Q) = \mathscr{U}_\Delta + \mathscr{U}_\mathscr{E}$, where

$$\mathscr{U}_\Delta = i\Delta(\mu\partial_\mu Q - \bar{\mu}\partial_{\bar{\mu}} Q), \tag{4.17}$$

$$\mathscr{U}_\mathscr{E} = -\mathscr{E}(\partial_\mu Q + \partial_{\bar{\mu}} Q) \tag{4.18}$$

To compute the $\Pi_{\mathscr{U}}$ explicitly, we make use of integration by parts repeatedly and assume that $Q(\mu,\bar{\mu})$ and its derivatives vanishes as μ goes to infinity. Then,

$$\begin{aligned}
\Pi_{\Delta} &= -\int d^2\mu \mathscr{U}_{\Delta}\ln(Q) \\
&= -i\Delta\int d^2\mu\ln(Q)\mu\partial_{\mu}Q - \ln(Q)\bar{\mu}\partial_{\bar{\mu}}Q \\
&= -i\Delta\left(-\int d^2\mu(Q\ln Q+\mu\partial_{\mu}Q)+\int d^2\mu(Q\ln Q+\bar{\mu}\partial_{\bar{\mu}}Q)\right) \\
&= -i\Delta\left(-\int d^2\mu\mu\partial_{\mu}Q+\int d^2\mu\bar{\mu}\partial_{\bar{\mu}}Q\right) \\
&= -i\Delta\left(-\int d^2\mu Q+\int d^2\mu Q\right)=0
\end{aligned}$$

and,

$$\begin{aligned}
\Pi_{\mathscr{E}} &= -\int d^2\mu \mathscr{U}_{\mathscr{E}}\ln(Q) \\
&= \mathscr{E}\int d^2\mu\ln(Q)\partial_{\bar{\mu}}Q+\ln(Q)\partial_{\mu}Q \\
&= -\mathscr{E}\int d^2\mu\partial_{\bar{\mu}}Q+\partial_{\mu}Q=0
\end{aligned}$$

Hence $\Pi_{\mathscr{U}}=0$, which yields $\Pi_t=\Pi_J$ and $\Phi_t=2\kappa\langle a^{\dagger}a\rangle_t$. The NESS entropy production rate is such that $dS/dt=0$, which implies

$$\Pi_{\mathrm{SS}}=\Phi_{\mathrm{SS}}=2\kappa\langle a^{\dagger}a\rangle_{\mathrm{SS}}. \tag{4.19}$$

The value of $\langle a^{\dagger}a\rangle_{\mathrm{SS}}$ can be easily found by writing the temporal evolution for the moments (we repeat these equations for the sake of clarity),

$$\partial_t\langle a\rangle = -(i\Delta+\kappa)\langle a\rangle+\mathscr{E} \tag{4.20}$$

$$\partial_t\langle a^{\dagger}a\rangle = -2\kappa\langle a^{\dagger}a\rangle+\mathscr{E}(\langle a^{\dagger}\rangle+\langle a\rangle) \tag{4.21}$$

and setting them to zero. The results are,

$$\langle a\rangle_{\rm SS} = \frac{\mathscr{E}(\kappa - i\Delta)}{\kappa^2+\Delta^2}, \tag{4.22}$$

$$\langle a^\dagger a\rangle_{\rm SS} = \frac{\mathscr{E}^2}{\kappa^2+\Delta^2}. \tag{4.23}$$

Finally, the NESS entropy production rate will be

$$\Pi_{\rm SS} = \frac{2\kappa\mathscr{E}^2}{\kappa^2+\Delta^2}. \tag{4.24}$$

In case we have a driven-dissipative cavity $\Delta = 0$ we find that $\Pi_{\rm SS} = 2\mathscr{E}^2/\kappa$, which is similar to the entropy production of the RL circuit discussed in 2.2, $\Pi_{RL} = \mathscr{E}^2/RT$. It is important to notice that, although the results have the same structure, the physical processes behind them are quite different, in the RL circuit both energy and dissipation occur in an incoherent way, while in the driven cavity the energy input is coherent.

Our formalism also enables us to obtain the dynamics of the entropy production rate. To illustrate this, we consider a quench scenario for its simplicity: we choose an initial $\mathscr{E}_0$ and let the system relax to the corresponding NESS, then at time $t = 0$ the amplitude is abruptly changed to $\mathscr{E}_f$, the temporal evolution of the system is given by solving the Lindblad equation with this new parameter. After some transient dynamics it settles down into the NESS of the final amplitude. In fig. 4.2 we show the entropy production as a function of time in this scenario.

In panels (a) and (c) we simply have a driven-dissipative cavity, as $\Delta = 0$, in this case the entropy production monotonically increases (decreases) as $\mathscr{E}_f > (<)\mathscr{E}_i$ until it reaches the value for the NESS entropy production of the final pump and it never becomes greater (lower) than this value. In panels (a) and (c) we simply have a driven-dissipative cavity, as $\Delta = 0$, in this case the entropy production monotonically increases (decreases) as $\mathscr{E}_f > (<)\mathscr{E}_i$ until it reaches the value for the NESS entropy production of the final pump and it never becomes greater (lower) than this value.

In panels (b) and (d) we have the harmonic oscillator term $\Delta = -2$, for quenchs such that $\mathscr{E}_f > (<)\mathscr{E}_i$. During the transient dynamics the entropy production becomes greater (lower) than the entropy production of the NESS for which the system will relax. Hence

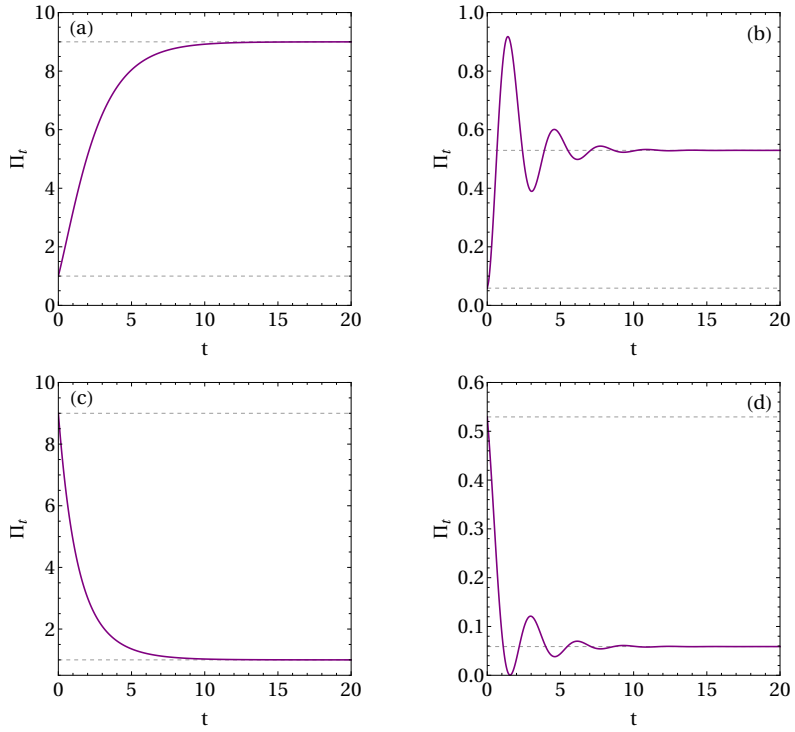

Figure 4.2: **Entropy production rate for a driven-dissipative cavity**: Entropy production computed numerically in a quench dynamics scenario. In the first column $\Delta = 0$ while in the second $\Delta = -2$. Panels (a) and (b) show the quench from $\mathscr{E}_i = 0.5$ to $\mathscr{E}_f = 1.5$. Panels (c) and (d) show the quench from $\mathscr{E}_i = 1.5$ to $\mathscr{E}_f = 0.5$. The dashed horizontal lines represent the NESS entropy production as given by Eqn. (4.24). The dissipation rate is $\kappa = 1/2$.

the Δ contribution acts by taking the system farther from equilibrium when $\mathscr{E}_f > \mathscr{E}_i$. In the case $\mathscr{E}_f < \mathscr{E}_i$ there is a certain time where the entropy production tends asymptotically to zero, i.e. at this time the dissipator is almost leaving no photons inside, and the system gets close to the equilibrium, but the continuous pump prevents it from happening.

4.2 Thermodynamic limit in critical systems

Now we reach the core result of this dissertation, where we define the thermodynamic limit for driven-dissipative systems at zero temperature, i.e. along this section we consider $N_i = 0$, and specialize the results of the last section to critical systems. To do so we need to define the notion of a *thermodynamic limit*. For the class of driven-dissipative systems described by Eqn.(4.1) criticality emerges when the pump intensity becomes very large, $\mathscr{E}_i \to \infty$, which physically translates to injecting a lot of photons into the

cavity. To represent the thermodynamic limit we define an adimensional parameter N and parametrize

$$\mathscr{E}_i = \epsilon_i \sqrt{N}, \tag{4.25}$$

with ϵ_i finite and $N \to \infty$. In a driven system, $\langle a_i \rangle$ scales proportionally to the amplitude $\mathscr{E}_i$, so that we also define

$$\langle a_i \rangle = \mu_i = \alpha_i \sqrt{N}, \tag{4.26}$$

where α_i are finite and represent the *order parameters* of the system. The scaling (4.26) is such that $\langle a^\dagger a \rangle \propto N$, so the parameter N is directly related to the number of photons inside the cavity. In our case, however, the parameter N is only introduced as a bookkeeping device, so we can tune the model towards a critical behaviour in a controlled way. The combination of scalings in Eqns.(4.25) and (4.26) makes $\mathscr{E}_i(\langle a_i^\dagger \rangle - \langle a_i \rangle) \propto O(N)$ in the mean field level, where a_i are replaced by $\langle a_i \rangle$, this means that the pumping term is *extensive* in N. We shall henceforth assume that this holds for the model hamiltonian H_0.

Next we introduce the displacement operators,

$$a_i = \langle a_i \rangle + \delta a_i = \alpha_i \sqrt{N} + \delta a_i, \tag{4.27}$$

where $\langle \delta a_i \rangle = 0$. Inserting this into Eqn.(4.14) the entropy flux naturally splits as

$$\Phi_t = \sum_i 2\kappa_i N |\alpha_i|^2 + \sum_i 2\kappa_i \langle \delta a_i^\dagger \delta a_i \rangle \doteq \Phi_{\text{ext}} + \Phi_q, \tag{4.28}$$

so that we have an extensive contribution, that depends only on the mean field values $|\alpha_i|^2$ and an intensive term proportional to the variance of the order parameter, thus related to quantum fluctuations.

A similar splitting is found for the dissipative contribution of the entropy production rate (4.15) by introducing *displaced phase space variables* $\mu_i = \langle a_i \rangle + \nu_i = \alpha_i \sqrt{N} + \nu_i$, where $\langle \nu_i \rangle = 0$. We note that the displacement does not affect the derivative $\partial_{\mu_i} = \partial_{\nu_i}$ so that, placing this into (4.6) we find the displaced currents to be

$$J_i(Q) = \kappa_i [(\alpha_i \sqrt{N} + \nu_i) Q + \partial_{\bar{\nu}_i} Q] = \sqrt{N} \kappa_i \alpha_i Q + J_i^\nu(Q), \tag{4.29}$$

where $J_i^\nu(Q) = \kappa_i(\nu_i Q + \partial_{\bar{\nu}_i} Q)$. Placing (4.29) into (4.15), with $N_i = 0$, it is straightforward to show that the entropy production rate associated with the dissipative contribution splits as

$$\Pi_J = \sum_i 2N\kappa_i|\alpha_i|^2 + \sum_i \frac{2}{\kappa_i}\int d^2\nu \, \frac{|J_i^\nu(Q)|^2}{Q} \doteq \Pi_{\text{ext}} + \Pi_d, \tag{4.30}$$

which is the main result of this chapter: the entropy production rate for *critical* driven-dissipative systems splits into three contributions

$$\Pi_t = \Pi_{\mathscr{U}} + \Pi_{\text{ext}} + \Pi_d. \tag{4.31}$$

The first one related to the unitary part and the coarse-graining of the Wehrl entropy, the second is extensive in N, so that it is completely independent of fluctuations, indeed

$$\Pi_{\text{ext}} = \Phi_{\text{ext}} = \sum_i 2N\kappa_i|\alpha_i|^2, \tag{4.32}$$

while the last term is related with the probability currents J_i^ν of the fluctuation operators. The entropy balance (4.9) becomes,

$$\frac{dS(Q)}{dt} = \Pi_{\mathscr{U}} + \Pi_d - \Phi_q. \tag{4.33}$$

One can see clearly that $\Pi_{\mathscr{U}}$ and Π_d are associated with quantum fluctuations when the system reaches the NESS, i.e. when $dS/dt = 0$, thus $\Pi_{\mathscr{U}} + \Pi_d = \Phi_q$. They may be interpreted as two sources for the quantum entropy flux rate Φ_q. We also note that $\Pi_d \geq 0$ but we can *not* say that, in general, the same will be true for $\Pi_{\mathscr{U}}$. We shall come back to this issue below.

4.2.1 Properties of the unitary contribution to entropy production

In order to understand the physics of the unitary contribution to the entropy production rate given by Eqn.(4.12) we will consider the case of a system described by a single mode normal ordered Hamiltonian,

$$H = \sum_{r,s} H_{rs}(a^\dagger)^r a^s, \tag{4.34}$$

where H_{rs} are some coefficients. As discussed above, an important assumption about the total Hamiltonian H is that at the mean field level ($a \to \langle a \rangle$) it is at most extensive in N, i.e. it must be of order $O(N)$. To ensure this condition is satisfied we parametrize the coefficients as $H_{rs} = h_{rs} N^{1-\frac{r+s}{2}}$ with h_{rs} finite and independent of N. As an example we can think about a term proportional to $a^\dagger a^\dagger a^\dagger a a$, here $r = 3$ and $s = 2$, thus the coefficient must be proportional to $N^{-3/2}$. Eqn.(4.34) acquires the form

$$H = N \sum_{r,s} h_{rs} \left(\frac{a^\dagger}{\sqrt{N}} \right)^r \left(\frac{a}{\sqrt{N}} \right)^s . \tag{4.35}$$

The unitary differential operator $\mathscr{U}(Q)$ is found straightforwardly using the correspondence table in Eqns.(1.31) repeatedly in $-i[H, \rho]$. The normal ordering becomes useful at this step, once it pulls all the derivatives to the right. The result is,

$$-i[H, \rho] \to \mathscr{U}(Q) = -i \sum_{r,s} h_{r,s} N^{1-\frac{(r+s)}{2}} [\bar{\mu}^r (\mu + \partial_{\bar{\mu}})^s - \mu^s (\bar{\mu} + \partial_\mu)^r] Q, \tag{4.36}$$

next we insert the displaced phase space variables $\nu = \sqrt{N}\alpha + \mu$ and expand the result in a power series of N. The result, to leading order in N is

$$\begin{aligned} \mathscr{U}(Q) = \; & - \; i\sqrt{N} \sum_{r,s} h_{r,s} \alpha^{s-1} \bar{\alpha}^{r-1} (s\bar{\alpha}\partial_{\bar{\nu}} - r\alpha\partial_\nu) Q \\ & - \; i \sum_{r,s} h_{r,s} \frac{\alpha^{s-2} \bar{\alpha}^{r-2}}{2} \left(s(s-1)\bar{\alpha}^2 (2\nu\partial_{\bar{\nu}} + \partial_{\bar{\nu}}^2) - r(r-1)\alpha^2 (2\bar{\nu}\partial_\nu + \partial_\nu^2) \right) Q \\ & - \; i \sum_{r,s} h_{r,s} 2rs|\alpha|^2 (\bar{\nu}\partial_{\bar{\nu}} - \nu\partial_\nu) Q \\ & + \; O(N^{-\frac{1}{2}}), \end{aligned} \tag{4.37}$$

where terms of $O(N^{-\frac{1}{2}})$ are suppressed in the limit $N \to \infty$. To simplify the cumbersome expression (4.37) we introduce the constants,

$$\Lambda_1 = -i \sum_{r,s} h_{rs}\, \alpha^{s-1} \bar{\alpha}^r s, \tag{4.38}$$

$$\Lambda_2 = -i \sum_{r,s} h_{rs}\, \alpha^{s-2} \bar{\alpha}^r s(s-1), \tag{4.39}$$

$$\Lambda_{11} = -i \sum_{r,s} h_{rs}\, \alpha^{s-1} \bar{\alpha}^{r-1} rs. \tag{4.40}$$

Using these constants and the Hermiticity of the Hamiltonian, i.e. $h_{rs} = \bar{h}_{rs}$, Eqn.(4.37) becomes,

$$\begin{aligned} \mathscr{U}(Q) &= \sqrt{N}\left(\Lambda_1 \partial_{\bar{\nu}} + \bar{\Lambda_1} \partial_{\nu}\right) Q \\ &+ \frac{1}{2}[\Lambda_2(2\nu\partial_{\bar{\nu}} + \partial_{\bar{\nu}}^2) + \bar{\Lambda}_2(2\bar{\nu}\partial_{\nu} + \partial_{\nu}^2) + 2\Lambda_{11}(\bar{\nu}\partial_{\bar{\nu}} - \nu\partial_{\nu})]Q \\ &+ O(N^{-\frac{1}{2}}). \end{aligned} \tag{4.41}$$

These are the leading terms of the unitary dynamics in the thermodynamic limit to the quantum Fokker-Planck equation. A characteristic feature of the Husimi Q-function becomes apparent here, which is the second derivatives terms, interpreted as diffusive terms. These diffusive terms, however, appear here in the unitary contribution. This is a unique feature of quantum dynamics and is ultimately a consequence of the coarse-graining nature of the Wehrl entropy.

Next, we plug Eqn.(4.41) into Eqn.(4.11) and perform multiple integration by parts, always assuming that the Q function, as well as its derivatives vanish at the infinity. This yields

$$\Pi_{\mathscr{U}} = \frac{1}{2} \int \frac{d^2\nu}{Q} \left[\Lambda_2(\partial_{\bar{\nu}} Q)^2 + \bar{\Lambda}_2(\partial_{\nu} Q)^2\right], \tag{4.42}$$

which is the analytical expression of the entropy production rate due to the unitary dynamics in the thermodynamic limit.

Finally, the summary of the main analytical results for critical driven-dissipative models

can be cast in the following table,

$$\boxed{\begin{aligned}&\frac{dS(Q)}{dt} = \Pi_{\mathscr{U}} + \Pi_d - \Phi_q,\\ &\Pi_{\mathscr{U}} = \frac{1}{2}\int \frac{d^2\nu}{Q}\left[\Lambda_2(\partial_{\bar{\nu}}Q)^2 + \bar{\Lambda}_2(\partial_\nu Q)^2\right],\\ &\Pi_d = \sum_i \frac{2}{\kappa_i}\int d^2\nu\ \frac{|J_i^\nu(Q)|^2}{Q},\\ &\Phi_q = 2\kappa\langle\delta a^\dagger \delta a\rangle.\end{aligned}} \tag{4.43}$$

where the expression for $\Pi_{\mathscr{U}}$ holds only in the thermodynamic limit.

Chapter 5

Kerr bistability model: non-equilibrium steady state

The term bistability refers to the existence of two stable states for a system to be and it is a known feature of classical non-linear systems [87, 88]. For instance, if one thinks about a conservative force field $U(x)$, it will be bistable if the potential energy has two local minima points, not necessarily symmetric, which are stable (see Fig.5.1). Between them there is always a local maximum, which is the unstable equilibrium point, in the sense that any perturbation makes the system go to one of the minima and it can be interpreted as a barrier between the minima. In classical systems, it is possible for the system to transition between the two minima as long as enough energy is given for it to overcome the barrier. This happens, for instance, when the system is in contact with a thermal bath which causes thermal fluctuations.

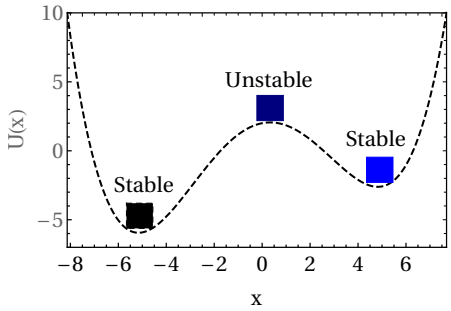

Figure 5.1: **Plot of a classical potential:** The plot stands for a potential of the type $U(x) = a_0 + a_1 x - a_2 x^2 + a_4 x^4$, with $a_i > 0$. The stable and unstable points of the potential are represented by the position of the bricks.

Optical bistability is the existence of two stable states with *different* photon numbers for the *same* driving conditions and it is a general feature of nonlinear systems described within a *mean field approximation*. It was first observed in Ref. [89] and formalized theoretically in the seminal paper by Drummond and Walls [3] where they developed a fully quantum mechanical model for the dispersive optical bistability, here referred to as the *Kerr bistability model* (KBM). This model describes a cavity filled with a nonlinear medium. The system is also assumed to lie within the driven-dissipative scenario described in the previous chapter: the cavity is pumped by an external laser source, injected through one of its mirrors. This mirror has to be semi-transparent, so photons also leak out. Since its introduction, it has been a topic of various studies and recently the physics emerging from fluctuations of nonlinear models that appears in various KBM-like plataforms [90–95] has received a lot of interest mainly due to the possibility of studying quantum many body phases [96–98] and critical phenomena [99–102]. In particular, the KBM is a paradigmatic model when one talks about driven-dissipative phase transitions (DDPT), both in theoretical [71, 103, 104] and experimental [96, 105] realms, as it presents a discontinuous DDPT.

This chapter is devoted to explaining the KBM in detail and applying the formalism developed in the previous chapter to its non-equilibrium steady state (NESS). In the next chapter we will present the time evolution of entropic quantities in a quench dynamics scenario for this same model.

5.1 The model

We consider the Kerr bistability model (KBM) that describes an optical cavity filled with a medium whose polarization vector is non-linear, going up to third order, i.e. $\mathbf{P} = \chi\mathbf{E} + \chi^{(2)}\mathbf{E}^2 + \chi^{(3)}\mathbf{E}^3$ with χs denoting the polarizability tensor and $\mathbf{E}$ the electric field, which will be described by a single mode a. The effect of the non-linear medium is to promote an effective interaction between the photons, with strength U. The cavity is coherently driven by a laser with an amplitude $\mathscr{E}$, which will behave as a classical field. And finally, there is a dissipation channel at rate κ that describes single photon losses due to the contact with the electromagnetic field, an environment at zero temperature.

This setup fits precisely into the formulation developed in the last chapter and presents a *discontinuous* driven-dissipative phase transition. Before studying the Wehrl entropy production rate, we will give further details of the model.

The KBM Hamiltonian was derived from the Maxwell-Bloch equations in Ref. [3] and reads,

$$\tilde{H} = \omega_c a^\dagger a + i(\mathscr{E} e^{-i\omega_p t} a^\dagger - \bar{\mathscr{E}} e^{i\omega_p t} a) + \frac{U}{2} a^\dagger a^\dagger a a. \tag{5.1}$$

The first term describes the cavity mode oscillating with the cavity frequency ω_c which is related with its geometry; the second describes the pump of the laser with a frequency ω_p and amplitude $\mathscr{E}$, that from now on, without loss of generality, will be assumed to be real. The last term is due to the nonlinearity of the medium and describes the effective interaction between the photons inside the cavity. The hamiltonian is time dependent, to simplify we can go to a frame rotating at a frequency ω_p (see App. B) and obtain a time independent Hamiltonian,

$$H = \Delta a^\dagger a + i\mathscr{E}(a^\dagger - a) + \frac{U}{2} a^\dagger a^\dagger a a, \tag{5.2}$$

where we basically took away the time dependency of the pump at the cost of replacing $\omega_c \to \Delta = \omega_c - \omega_p$ where Δ is the detuning between the cavity and the pump frequency. The bistable behaviour is directly linked to this quantity. We can say in advance that bistable behaviour only occurs when $\Delta < 0$, i.e. the frequency of the intracavity mode ω_c is lower than the frequency of the laser ω_p. This is the condition to observe the phase transition.

The one photon losses are described by the usual Lindblad dissipator,

$$D(\rho) = 2\kappa \left(a^\dagger \rho a - \frac{1}{2}\{a^\dagger a, \rho\} \right), \tag{5.3}$$

so that the dynamics of the system state ρ is described by the Lindblad master equation,

$$\partial_t \rho = -i[H_0 + i\mathscr{E}(a^\dagger - a), \rho] + D(\rho). \tag{5.4}$$

which is precisely Eqn.(4.1) with $H_0 = \Delta a^\dagger a + (U/2) a^\dagger a^\dagger a a$.

5.2 Dynamical equations for the moments

Once the dynamics of the state of the system is given by Eqn.(5.4), it is possible to write equations for the time evolution of the quantities of interest such as the moments $\langle a\rangle$, $\langle a^\dagger a\rangle$, an so on. The equation for the mean value of the amplitude $\langle a\rangle = \mu$ is (see App.A),

$$\partial_t \mu = -(\kappa + i\Delta)\mu + \mathscr{E} - iU\langle a^\dagger aa\rangle. \tag{5.5}$$

This formula is exact but we end up with a *hierarchy* problem. Due to the interaction term the equation for $\langle a\rangle$ depends on a higher order moment, $\langle a^\dagger aa\rangle$ and this will go on for every moment equation we write. Hence, the set of differential equations is not closed and it is impossible to obtain analytical formulas for μ following this approach.

In order to obtain μ, $\langle a^\dagger a\rangle$ and $\langle aa\rangle$ at the non-equilibrium steady state (NESS), i.e. when the mean values do not change in time, we will use two different approaches: the first one will be the *mean field approximation*, where we replace the operator by its mean values plus some fluctuation (which is described by an operator) around it. The second is a *numerically exact* approach based on a vectorization procedure (see App.D) where we find the NESS ρ_{SS} and compute the moments numerically. It is worthy saying that there is an exact solution for the NESS moments $\langle (a^\dagger)^r (a)^s\rangle$ [3, 106–109].

5.2.1 Mean Field approximation

The simplest way to solve the Eqn. (5.5) at the NESS is to perform a mean field approximation (MFA) [6], where the basic idea is to define a fluctuation operator δa,

$$\delta a = a - \mu. \tag{5.6}$$

This way the triple product in Eqn.(5.5) of operators becomes,

$$a^\dagger aa = |\mu|^2\mu + O(\delta a) \tag{5.7}$$

the approximation takes place when we neglect terms of order δa and higher, which is justified when we consider a thermodynamic limit where these fluctuations are not expected

to play an important role. It is worth emphasizing that this approximation is quite rough. It is valid only when the number of photons $\langle a^\dagger a\rangle = |\mu|^2$ inside the cavity is "very high", in such a way that the interaction strength U becomes very weak. Whence, we loose any effects due to quantum fluctuations and that is the key point to understand why *bistability* appears. Eqn.(5.5) in the MFA then becomes,

$$\partial_t \mu = -(\kappa + i\Delta + iU|\mu|^2)\mu + \mathscr{E}. \tag{5.8}$$

We introduce the dimensionless parameter N as in Sec.4.2 to define a thermodynamic limit $N \to \infty$. Explicitly the scalings will be [65],

$$U = \frac{u}{N}, \tag{5.9}$$
$$\mathscr{E} = \sqrt{N}\epsilon, \tag{5.10}$$
$$\mu = \sqrt{N}\alpha, \tag{5.11}$$

such that the assumption of $H_0 \propto O(N)$ holds true. We also note that the product,

$$U\mathscr{E}^2 = u\epsilon^2 \sim O(0). \tag{5.12}$$

The equation of motion for the scaled amplitude α will be,

$$\partial_t \alpha = -(\kappa + i\Delta + iu|\alpha|^2)\alpha + \epsilon. \tag{5.13}$$

It is interesting to note that both (5.8) and (5.13) have the same structure and, from a mathematical point of view, have the same properties; in the next section we address the problem of the stability of this equation.

To know what are the conditions to have stable solutions for the Eqn. (5.8) in the long-time limit $t \to \infty$ where the system reaches the NESS we will perform a linearization procedure (see App. C) closely following Ref. [3].

We begin by writing the system of differential equations,

$$\begin{cases} \partial_t \alpha = -[\kappa + i(\Delta + u|\alpha|^2)]\alpha + \mathscr{E} = G(\alpha, \bar{\alpha}), \\ \partial_t \bar{\alpha} = -[\kappa - i(\Delta + u|\alpha|^2)]\bar{\alpha} + \mathscr{E} = \bar{G}(\alpha, \bar{\alpha}). \end{cases} \tag{5.14}$$

The NESS is,

$$\begin{cases} \partial_t \alpha_0 = 0 \rightarrow \mathscr{E} = [\kappa + i(\Delta + u|\alpha|^2)]\alpha = f(|\alpha|^2)\alpha, \\ \partial_t \bar{\alpha}_0 = 0 \rightarrow \mathscr{E} = [\kappa - i(\Delta + u|\alpha|^2)]\bar{\alpha} = \bar{f}(|\alpha|^2)\bar{\alpha}. \end{cases} \tag{5.15}$$

where we defined the function $f(|\alpha|^2) = [\kappa + i(\Delta + u|\alpha|^2)]$. To simplify the notation along this section, we set $|\alpha|^2 = n$ so that the NESS can be summarized by the equation,

$$\mathscr{E}^2 = |f(n)|^2 n \tag{5.16}$$

5.2.2 Stability analysis of the steady state

To begin the stability analysis we consider small fluctuations $\alpha_1(t)$ around the NESS, $\alpha_1(t) = \alpha - \alpha_0$, we obtain the following equation,

$$\partial_t \alpha_1(t) = \partial_\alpha G(\alpha_0, \bar{\alpha_0})\alpha_1 + \partial_{\bar{\alpha}} G(\alpha_0, \bar{\alpha_0})\bar{\alpha}_1, \tag{5.17}$$

where

$$\partial_\alpha G(\alpha, \bar{\alpha}) \;\; = -\left[\partial_n f(n) n + f(n)\right] \partial_{\bar{\alpha}} G(\alpha, \bar{\alpha}) \;\; = -\partial_n f(n)\alpha^2. \tag{5.18}$$

The linearized system therefore is,

$$\partial_t \begin{bmatrix} \alpha_1(t) \\ \bar{\alpha}_1(t) \end{bmatrix} = \begin{bmatrix} -[\partial_n f(n) n + f(n)] & -\partial_n f(n)\alpha_0^2 \\ -\partial_n \bar{f}(n)(\bar{\alpha_0})^2 & -[\partial_n \bar{f}(n) n + \bar{f}(n)] \end{bmatrix} \begin{bmatrix} \alpha_1(t) \\ \bar{\alpha}_1(t) \end{bmatrix}, \tag{5.19}$$

which can be put into the neat matrix form,

$$\partial_t \vec{\alpha_1} = -J\vec{\alpha_1}. \tag{5.20}$$

We want the *stable* solutions of Eqn.(5.20). In this case, due to the minus sign of J, a stable solution requires both eigenvalues to be positive. This will be true if both the trace and the determinant of J are positive,

$$\begin{aligned} \mathrm{Tr}\{J\} &= 2\Re f(n) + n\partial_n f(n) > 0, & (5.21)\\ \det\{J\} &= |f(n)|^2 + n\left(\bar{f}(n)\partial_n f(n) + f(n)\partial_n \bar{f}(n)\right) > 0. & (5.22) \end{aligned}$$

If the $\mathrm{Tr}\{J\}$ or the $\det\{J\}$ changes sign then we have a change in the stability properties. The first condition gives us that $\mathrm{Tr}\{J\} = 2\kappa > 0$, so the dissipation rate must be positive, which is in agreement with the Lindblad formalism. Now, note that using (5.16) we can write,

$$\begin{aligned} \det\{J\} = \partial_n \mathscr{E}^2 &> 0, & (5.23)\\ 3u^2n^2 + 4\Delta u n + (\kappa^2 + \Delta^2) &> 0. & (5.24) \end{aligned}$$

Hence, the quadratic equation (5.24) on n gives us that the solution is stable if $n < n_-$ or $n > n_+$ where,

$$n_\pm = \frac{-2\Delta \pm \sqrt{\Delta^2 - 3\kappa^2}}{3u}. \quad (5.25)$$

This equation sheds light into the conditions for the existence of bistability (see Fig.5.2): $n_\pm$ is related to the number of photons inside the cavity, so it must be real, which is ensured by imposing $\Delta^2 \geq 3\kappa^2$. Also, it must be always positve, otherwise we would have unphysical results. From the first term we see that $\Delta/u < 0$, but u is assumed to be positive due to its physical interpretation of an interaction strength between the photons, hence $\Delta < 0$. This condition tells us that to have a bistable behavior we must have that the cavity frequency is smaller than the pump frequency $\omega_c < \omega_p$. Finally, combining $\Delta < 0$ with $\Delta^2 \geq 3\kappa^2$ yields $\Delta \leq -\sqrt{3}\kappa$.

5.3 Exact solution for the moments

In the last two sections, we have performed a MFA and a linearized analysis for the NESS in a well defined thermodynamic limit, this constitutes a semiclassical approach

to the problem which is given by Eqn. (5.7). The price we pay is to neglect quantum fluctuations.

It turns out, however, that it is possible to find the NESS analytically for this model. This was first done in Ref. [3] using the complex P-representation to map Eqn.(5.4) into a Fokker-Planck equation. Later, [106] revisited the problem and used different quasiprobabilities distributions, such as the Wigner and the Husimi Q-function.

Recently, in Ref. [107] the authors used again the complex P-function and generalized it for the case with two photon losses. The NESS moments obtained by these methods is always unique, therefore pointing to no bistable behavior. To reconcile this with the bistability predicted by the MFA one has to take into account quantum fluctuations. They are responsible for triggering a switching between the states and the unique solution is a weighted average over the two states given by MFA. Indeed, experiments with two-mode laser evidenced that the switching times were extremely long [110], and were predicted to diverge when the fluctuations are weak and (or) if the number of photons were large [111]. There is yet another approach introduced in Ref. [108], called *coherent quantum absorber*, where the authors applied it to a cascaded spin network and for the KBM as we have been considering here. It was generalized in Ref. [109] for Kerr resonators pumped up to three photons and with a two photon loss mechanism.

The expression found in [3] for the moments is:

$$\langle (a^\dagger)^n a^m \rangle = \sqrt{2}\frac{\bar{\xi}^n \xi^m \Gamma(\bar{x})\Gamma(x)}{\Gamma(\bar{x}+n)\Gamma(x+m)} \frac{{}_0F_2(\bar{x}+n, x+m; |\xi|^2)}{{}_0F_2(\bar{x}, x; |\xi|^2)}, \tag{5.26}$$

where $\xi = 2\mathscr{E}/iU$, $x = 2(i\Delta + \kappa)/iU$, ${}_0F_2(a, b; c)$ denotes the hyper-geometric function and Γ is the gamma function. Eqn.(5.26) is of paramount importance: first it solves the problem of bistable states introduced by the MFA, secondly it gives us the exact form of the entropy production at the NESS, $\Pi_{\text{SS}} = \Phi_{\text{SS}} = 2\kappa\langle a^\dagger a \rangle$; and finally it serves as a solid ground where we can check our results and test the accuracy of our numerical simulations.

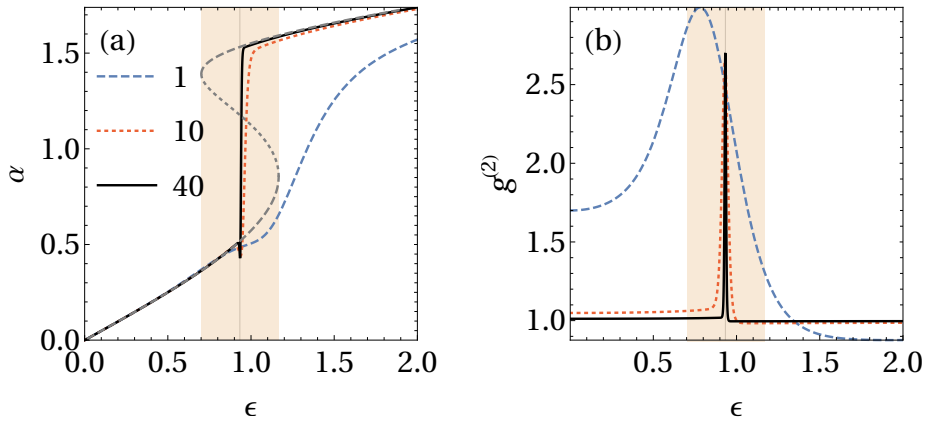

Figure 5.2: **First moment $|\alpha|$ and $g^{(2)}$ correlation function NESS:** of the Kerr bistability model as a function of ϵ, computed from the exact solution Eqn.(5.26). The curves are for three different values of N, as shown in image (a). In image (a) the dashed gray curve corresponds to the mean-field prediction for this moment. The vertical line represents the critical value ϵ_c computed from the numerically exact solution. The orange patch marks the bistable region, as predicted from mean-field theory Eqn.5.25. Other parameters were fixed at $\kappa = 1/2$, $\Delta = -2$ and $u = 1$.

In Fig.5.2(a) we show the first moment α of the model comparing the exact solution Eqn.(5.26) with three different values of N with the mean-field prediction Eqn. (5.25), denoted by the gray dashed line. Indeed, we see that as N increases the exact solution matches the MFA prediction, but instead of having a bistable behaviour, we observe an abrupt jump from the lower to the upper branch, i.e. a phase transition.

In Fig.5.2(b) we show the second order correlation function, defined as

$$g^{(2)}(0) = \frac{\langle a^\dagger a^\dagger a a \rangle}{|\langle a^\dagger a \rangle|^2}, \tag{5.27}$$

this is an important function from the experimental point of view because it is related to the *variance of the intensity* of the light beam, which in turn is associated with the number of photons counted in a detector. Thus, it tells us how often we detect two photons at times very close to each other. Measuring this function allows an experimentalist to classify the type of light being measured i.e. if it is coherent, bunched or antibunched. It is not the purpose of this dissertation to get into the details of this function, for that we recommend Refs. [36, 37]. The important thing to know is that it has a peak at the criticality ϵ_c, which allows us to obtain the value of this parameter. Moreover it is worth mentioning the light is classified as coherent, as that emitted by a laser, if $g^{(2)}(0) = 1$, in which case two detection

events are uncorrelated. It is bunched if $g^{(2)}(0) > 1$ where there is a tendency for detection events to be closer to each other. So at criticality the coherent light presents itself as bunched light. Finally, it is called anti-bunched when $g^{(2)}(0) < 1$.

5.3.1 On the coherent quantum absorber method

In this section we present the coherent absorber method closely following Ref. [108], where it was introduced. The method relies on considering a cascaded quantum network as show in Fig.5.3. The physical set up can be composed of $N \geq 2$ subsystems fixed at some positions x_i. These subsystems are coupled to a 1D continuum of right propagating bosonic modes, that may represent for instance photons traveling inside a wave-guide. The interaction is such that time-reversal symmetry is broken. It means that photons can be emitted from the left to the right, drive other subsystems and eventually leave the network. It is assumed that the Born-Markov approximation is valid for this system coupled to the wave-guide such that the cascaded master equation for the reduced system density matrix ρ is,

$$\partial_t \rho = \sum_i -i[H_i, \rho] + 2\kappa \left(c_i \rho c_i^\dagger - \frac{1}{2}\{c_i^\dagger c_i, \rho\} \right) + 2\kappa \sum_{j>i} ([c_i \rho, c_j^\dagger] + [c_j, \rho c_i^\dagger]), \quad (5.28)$$

where the first sum describes the Lindblad evolution of each subsystem and the second sum accounts for the unidirectionality of the bath and describes the possibility of a photon emitted by subsystem in x_i be reabsorbed in a subsystem $x_j > x_i$. Manipulating the terms of (5.28) and defining $c = \sum_i c_i$, Eqn. (5.28) becomes,

$$\partial_t \rho = -i[H_{\text{casc}}, \rho] + 2\kappa \left(c \rho c^\dagger - \frac{1}{2}\{c^\dagger c, \rho\} \right) \quad (5.29)$$

where,

$$H_{\text{casc}} = \sum_i H_i - i\kappa \sum_{j>i} (c_j^\dagger c_i - c_i^\dagger c_j) \quad (5.30)$$

is the cascaded Hamiltonian featuring non-local coherent dynamics of the coupling mediated by the environment.

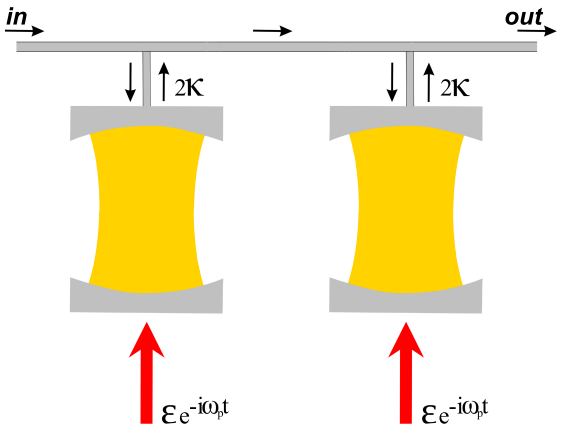

Figure 5.3: **Sketch of the coherent absorber method for the KBM:** Two non-linear optical cavities coupled to a waveguide at rate κ. Both are driven by a laser with amplitude $\mathscr{E}$ with frequency ω_p.

To apply the method for the KBM model, we consider a network composed of two subsystems A and B. The *Coherent quantum absorber* (CQA) is the B subsystem, which is constructed artificially, so to act by perfectly reabsorbing the photons emitted by subsystem A. It ensures that there are no photons leaking out of the wave-guide and will make the system relax to a pure state $\rho_0 = |\psi_0\rangle \langle\psi_0|$ [112]. Another requirement is that the steady-state has non-trivial correlations between subsystems A and B, so that they cannot be partioned into smaller subsystems. So let a and b, be the annihilation bosonic operators associated with each subsystem, respectively. The following properties must hold,

1. $(a + b)\,|\psi_0\rangle = 0$, which ensures no photons will escape from the wave-guide;
2. $[H_{\text{casc}}, \rho] = 0$, which ensures the system is in the stationary state;
3. $\mathscr{C} = -2(\langle c_A^\dagger c_A\rangle - |\langle c_A\rangle|^2) \neq 0$, which ensures there are non-trivial correlations between the subsystems.

The idea builds on choosing the Hamiltonian H_B, for system B such that it creates a *dark entangled state*, i.e. a state $|\psi_0\rangle$ with the aforementioned properties.

For the KBM we have,

$$H_A = \Delta a^\dagger a + i\mathscr{E}(a^\dagger - a) + \frac{U}{2} a^\dagger a^\dagger a a, \tag{5.31}$$

to make up the system H_B we make use of the *educated guess* introduced in Ref. [108]. Hence, we define the system B with bosonic modes b with the exact same parameters of A, but with a minus sign in the first and last terms,

$$H_B = -\Delta b^\dagger b + i\mathscr{E}(b^\dagger - b) - \frac{U}{2} b^\dagger b^\dagger b b. \tag{5.32}$$

Thus the cascaded Hamiltonian Eqn. (5.30) becomes,

$$H_{\text{casc}} = H_A + H_B - i\kappa(b^\dagger a - a^\dagger b). \tag{5.33}$$

We define the composite symmetric c_+ and anti-symmetric c_- bosonic operators as,

$$c_\pm = \frac{a \pm b}{\sqrt{2}} \tag{5.34}$$

now using Eqn.(5.34) we can rewrite the Hamiltonian Eqn. (5.33) as,

$$\begin{aligned} H_{\text{casc}} &= i\sqrt{2}\mathscr{E}c_+ + (\Delta - i\kappa)c_+^\dagger c_- + \left[\frac{U}{2}(c_+^\dagger c_+ + c_-^\dagger c_- - 1)\right] c_+^\dagger c_- + \text{h.c.} \\ &= H_1 + H_2 + H_3 + \text{h.c.} \end{aligned} \tag{5.35}$$

Condition (1) imposes $c_+ |\psi_0\rangle \propto (a+b)|\psi_0\rangle = 0$, so that the steady state symmetric mode *must be* in the vacuum state $|0\rangle_+$. Then, we write the dark state *ansatz*,

$$|\Psi_0\rangle = |0\rangle_+ \otimes |\xi_0\rangle_- \tag{5.36}$$

and using the occupation number basis $\{|n\rangle\}$, we have

$$|\xi_0\rangle_- = \sum_n \alpha_n |n\rangle, \tag{5.37}$$

for some coefficients α_n. The next step is to use condition (2), which is equivalent to $H_{\text{casc}}|\psi_0\rangle = \lambda|\psi_0\rangle$, where λ is some complex number. Moreover, using the fact that $c_+|0\rangle_+ = 0$ and performing the projection $\langle\psi_0| H_{\text{casc}}|\psi_0\rangle = 0$, we obtain that $\lambda = 0$.

Computing $H_{\text{casc}} |\psi_0\rangle$ we find,

$$H_1 |\psi_0\rangle = i\sqrt{2}\mathscr{E} |1\rangle_+ \otimes |\xi_0\rangle \tag{5.38}$$

$$H_2 |\psi_0\rangle = \sum_n \alpha_n \sqrt{n}(\Delta - i\kappa) |1\rangle_+ \otimes |n-1\rangle_- \tag{5.39}$$

$$H_3 |\psi_0\rangle = \sum_n \alpha_n \frac{U}{2}(n-1) |1\rangle_+ \otimes |n-1\rangle_- \tag{5.40}$$

and the hermitian conjugate term is identically zero. Hence,

$$|1\rangle_+ \otimes \sum_n i\sqrt{2}\mathscr{E}\alpha_n |n\rangle + \left[(\Delta - i\kappa) + \frac{U}{2}(n-1)\right] \sqrt{n}\alpha_n |n-1\rangle = 0 \tag{5.41}$$

which yields,

$$\sum_n i\sqrt{2}\mathscr{E}\alpha_n |n\rangle + \left[(\Delta - i\kappa) + \frac{U}{2}(n-1)\right] \sqrt{n}\alpha_n |n-1\rangle = 0 \tag{5.42}$$

Projecting Eqn. (5.42) into $\langle n-1|$ we find,

$$i\sqrt{2}\mathscr{E}\alpha_{n-1} + \left[(\Delta - i\kappa) + \frac{U}{2}(n-1)\right] \sqrt{n}\alpha_n = 0 \tag{5.43}$$

Finally, after some algebraic manipulation, Eqn. (5.43) becomes the following recursion relation for the coefficients,

$$\alpha_n = \sqrt{\frac{2}{n}} \frac{\xi}{n+x-1} \alpha_{n-1}, \tag{5.44}$$

where $\xi = 2\mathscr{E}/iU$ and $x = 2(\kappa + i\Delta)/iU$. This recursion is readily solved [113], such that the solution that fulfills conditions (1)-(3) is,

$$|\xi_0\rangle_- = \frac{1}{N} \sum_{n=0}^{\infty} \frac{(\sqrt{2}\xi)^n}{\sqrt{n!}} \frac{\Gamma(x)}{\Gamma(x+n)} |n\rangle \tag{5.45}$$

with $N = \sqrt{{}_0F_2(x, \bar{x}; 2|\xi|^2)}$ being the generalized hyper-geometric function. Since $|\psi_0\rangle$ is a tensor product and the symmetric mode is in the vacuum state, the non-zero normally

ordered operator are those of the anti-symmetric mode. Hence,

$$\langle (c_-^\dagger)^n (c_-)^m \rangle = 2^{\frac{n+m}{2}} \frac{\bar{\xi}^n \xi^m \Gamma(\bar{x})\Gamma(x)}{\Gamma(\bar{x}+n)\Gamma(x+m)} \frac{{}_0F_2(\bar{x}+n, x+m; 2|\xi|^2)}{{}_0F_2(\bar{x}, x; 2|\xi|^2)} \tag{5.46}$$

and going back to the original modes we find,

$$\langle (a^\dagger)^n (b^\dagger)^k b^l a^m \rangle = \frac{(-1)^{k+l}}{2^{(n+k+l+m)/2}} \langle (c_-^\dagger)^{n+k} (c_-)^{m+l} \rangle, \tag{5.47}$$

setting $k = l = 0$, we obtain Eqn.(5.26). The main advantage of the CQA method is that the problem is reduced to a simple recursion formula Eqn. (5.44), instead of solving a Fokker-Planck equation for the P-representation, which is much more complicated from a mathematical point of view.

5.4 The Wehrl entropy production rate for the Kerr bistability model

We apply the formalism developed in the last chapter to the KBM. We may repeat some of the equations here for completeness. The first step is to transform the Lindblad master equation (5.4) into a Fokker-Planck equation [106, 114] of the form,

$$\partial_t Q(\mu, \bar{\mu}) = \mathscr{U}(Q) + \mathscr{D}(Q), \tag{5.48}$$

where the one mode dissipative contribution is $\mathscr{D}(Q) = -(\partial_\mu J(Q) + \partial_{\bar{\mu}} \bar{J}(Q))$ according to (4.7) with $J(Q)$ being the one mode irreversible quasi-probability current as in Eqn.(4.6). The unitary differential operator $\mathscr{U}(Q)$ can be split into three terms,

$$\mathscr{U}(Q) = \mathscr{U}_\Delta + \mathscr{U}_\mathscr{E} + \mathscr{U}_U, \tag{5.49}$$

where,

$$\mathscr{U}_{\Delta} = i\Delta(\mu\partial_{\mu}Q - \bar{\mu}\partial_{\bar{\mu}}Q), \tag{5.50}$$

$$\mathscr{U}_{\mathscr{E}} = -\mathscr{E}(\partial_{\mu}Q + \partial_{\bar{\mu}}Q), \tag{5.51}$$

$$\mathscr{U}_{U} = \frac{iU}{2}[2|\mu|^2(\mu\partial_{\mu}Q - \bar{\mu}\partial_{\bar{\mu}}Q) + \mu^2\partial_{\mu}^2Q - \bar{\mu}^2\partial_{\bar{\mu}}^2Q]. \tag{5.52}$$

We note that Eqns. (5.50) and (5.51) are precisely the same of Sec.4.1.1, so we know they do not contribute to the entropy production rate, i.e. $\Pi_{\Delta} = \Pi_{\mathscr{E}} = 0$. The interaction term Eqn.(5.52) has diffusion contributions (second derivatives), so we may expect it will not vanish, as discussed in Sec.4.2.1. We compute explicitly the unitary contribution for the entropy production rate Eqn. (4.11) $\Pi_{\mathscr{U}} = \Pi_U$,

$$\begin{aligned}\Pi_U &= -\int d^2\mu \mathscr{U}_U \ln(Q) = -N\int d^2\alpha \mathscr{U}_u \ln(Q),\\ &= N\Pi_u^{(1)} + \Pi_u^{(0)}.\end{aligned}$$

In the first line we used the scalings (5.10) and (5.11), which allowed us to split Π into an extensive and an intensive term. The first one is,

$$\Pi_u^{(1)} = -iu\int d^2\alpha \ln(Q)|\alpha|^2(\alpha\partial_{\alpha}Q - \bar{\alpha}\partial_{\bar{\alpha}}Q) = 0,$$

and vanishes, as it should according to the discussion presented in Sec.4.2.1. Now the intensive term reads,

$$\begin{aligned}\Pi_u^{(0)} &= -\frac{iu}{2}\int d^2\alpha \ln(Q)(\alpha^2\partial_{\alpha}^2Q - (\bar{\alpha})^2\partial_{\bar{\alpha}}^2(Q))\\ &= \frac{iu}{2}\int d^2\alpha \frac{(\alpha^2(\partial_{\alpha}Q)^2 - \bar{\alpha}^2(\partial_{\bar{\alpha}}(Q))^2)}{Q} \neq 0.\end{aligned}$$

Which is the same expression we would have found if, instead we have used Eqn.(4.42) directly.

For the entropy production and entropy flux we can readly use Eqns.(4.28) and (4.30) specialized for a single mode. The results are presented in Fig. 5.4.

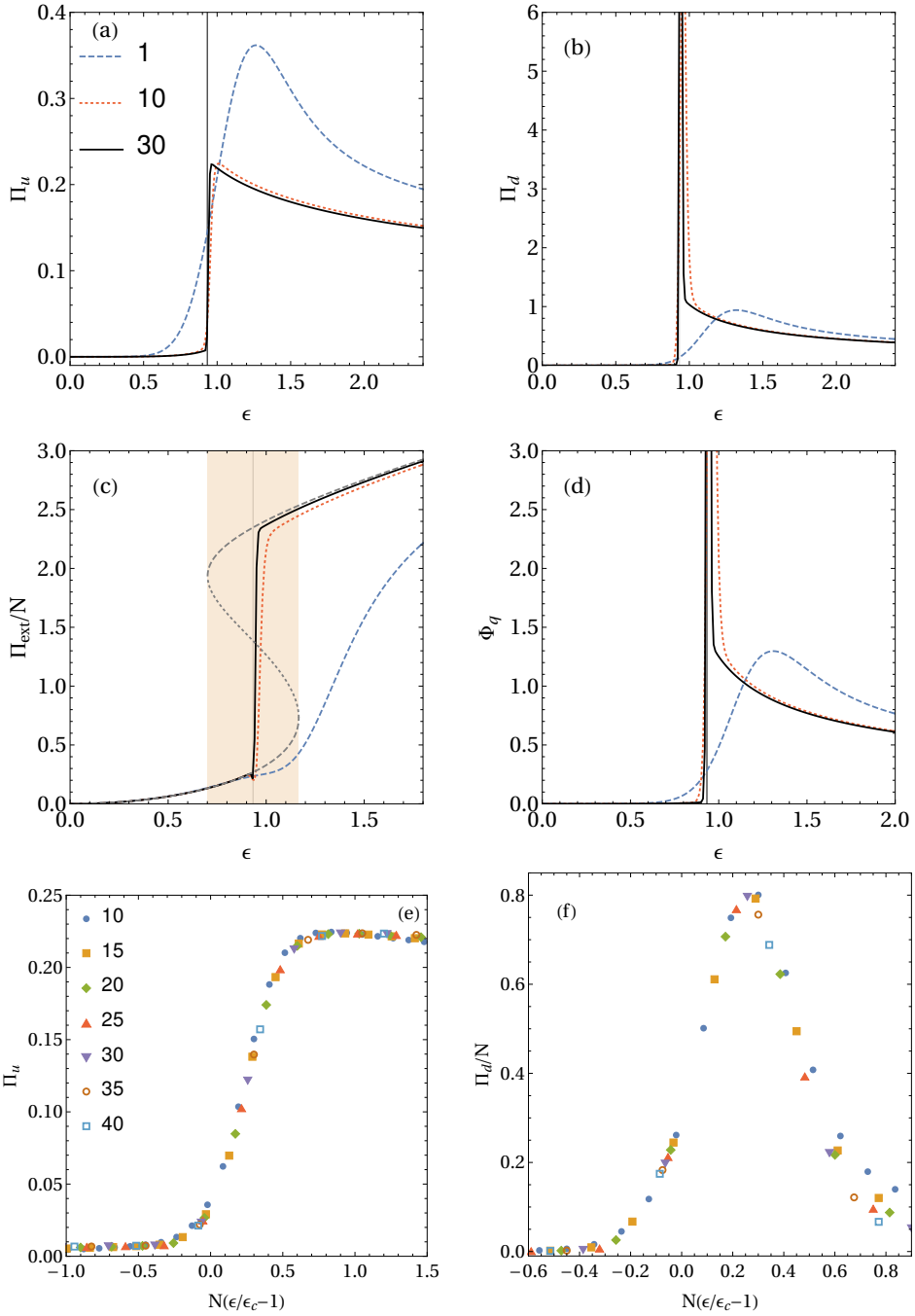

Figure 5.4: **Intensive contributions to entropy production, extensive contribution, quantum entropy flux at the NESS and finite size analysis:** of the Kerr bistability model as a function of ϵ. (a) and (b) were computed numerically while (c) and (d) were computed from the exact solution Eqn.(5.26). The curves (a-d) are for three different values of N, as shown in image (a), meanwhile Figs.(e-f) are for N varying from 10 to 40 in steps of five, as shown in panel (e). In Fig.(c) the dashed gray line represents the mean field prediction $\Pi_J = 2\kappa|\alpha|^2$, with the orange patch highlighting the bistable region. In images (a-d) the solid black curve corresponds to the critical point. Other parameters were fixed at $\kappa = 1/2$, $\Delta = -2$ and $u = 1$.

In Fig. 5.4(a) we plot Π_u, we note it is finite and present a discontinuity at the critical point. In panel (e) we observe the data collapse by plotting Π_u against $N(\epsilon/\epsilon_c - 1)$ for various values of N, showing the universality. Hence, this contribution mimics the behavior of entropy production in classical non-equilibrium phase transitions, discussed in Sec. 3.2.

In Fig. 5.4(b) and (d) we plot the dissipative quantum contribution Π_d to the entropy production and the quantum entropy flux Φ_q, respectively. In view of Eqn. (4.33) the dissipative contribution Π_d will behave like the variance of the order parameter $\langle \delta a^\dagger \delta a \rangle$ (the entropy flux rate), which diverges at the critical point. Such a behavior matches experimental observation of the irreversible entropy production in mesoscopic systems, reported in Ref. [26]. Moreover, in panel (f) we observe the data collapse of Π_d/N against $N(\epsilon/\epsilon_c - 1)$ for various values of N, demonstrating the universality of this behavior.

In panel (c) we show the rescaled extensive contribution to entropy production (and flux) rate Π_{ext}/N with the mean field prediction, the orange patch highlights the bistable region.

In conclusion, we applied the formalism developed in chap. 4 to the paradigmatic Kerr bistability model, which undergoes a discontinuous driven-dissipative phase transition. To that end, we studied the model in detail deducing the conditions to observe the phase transition by means of MFA and using the exact solution. We found that the contribution to the entropy production due to unitary dynamics Π_u is finite and presents a discontinuity at the critical point, thus behaving similarly to the entropy production across a classical non-equilibrium phase transition, as discussed in sec. 3.2. The contribution due to the dissipative contribution Π_d presents a divergence at the critical point, as the quantum entropy flux Φ_q, in accordance with recent experimental investigations. Moreover, a finite size scaling analysis of Π_u and Π_d ensures the universality of the results for the thermodynamic limit.

Chapter 6

Kerr bistability model: quench dynamics scenario

The formalism developed in Chap. 4 was able to capture some interesting features of entropy production at the NESS of the KBM model, as reported in Ref. [28]. It is also able to shed light on the entropic dynamics. So, in this chapter we address the following question:

- How does the entropy rate components behave when one abruptly changes the driving amplitude?

A sudden change in the driving amplitude (called a *quantum quench*) will cause the system to evolve from one non-equilibrium state to another. On top of the entropy that is already being constantly produced in these systems, there will therefore be an additional entropy production associated with this dynamics. The goal of this chapter is to probe this entropy production and understand how they are influenced by different quench protocols.

There are the so called gaussian states for which we are able to obtain the entropic quantities easily since the Husimi Q-function is known. Some features of the KBM lead to Gaussian states in the thermodynamic limit. If the dynamics were Gaussian, this would therefore be an enormous simplification, since it would allow for very efficient means to study the entropy production.

With that in mind, first we study the gaussianity of the state during the dynamics, and we show that unfortunately it is not the case for our system. A study of quench dynamics

in the KBM model therefore requires a full numerical approach, based on the vectorization method discussed in App. D. Later, we present the results of our numerical simulations to the entropic quantities, which demonstrates the usefulness of the formalism out of the static scenario.

6.1 State gaussianity test during the dynamics

A quantum state is gaussian, which will be denoted by ρ_g, if its Husimi Q-function is a Gaussian function of the coherent state variable μ [42, 115].

An example of a gaussian state is the thermal state $\rho_T = \exp\{-\beta\omega a^\dagger a\}/Z$, where $Z = (1 - e^{-\beta\omega})^{-1}$. The Q-function $Q_T(\mu, \bar{\mu}) = \langle\mu| \rho_T |\mu\rangle / \pi$ is,

$$Q_T(\mu, \bar{\mu}) = \frac{1}{\pi(\bar{n}+1)} \exp\left\{-\frac{|\mu|^2}{\bar{n}+1}\right\}, \tag{6.1}$$

where $\bar{n} = (e^{\beta\omega} - 1)^{-1}$ is the Bose-Einstein occupation number. And as an example of a non-gaussian state we take the superposition of coherent states, known as Schrödinger cat state. These states are defined as $|\psi\rangle = (|\alpha\rangle + |-\alpha\rangle)/\sqrt{2}$, then $\rho_{SC} = |\psi\rangle\langle\psi|$ and its Husimi-Q function is,

$$Q_{SC}(\mu, \bar{\mu}) = \frac{e^{-|\mu|^2-|\alpha|^2}}{2\pi}(e^{\bar{\mu}\alpha+\bar{\alpha}\mu} + e^{-(\bar{\mu}\alpha+\bar{\alpha}\mu)} + e^{\bar{\mu}\alpha-\bar{\alpha}\mu} + e^{-(\bar{\mu}\alpha-\bar{\alpha}\mu)}), \tag{6.2}$$

which is clearly *not* a gaussian function. There is also the concept of gaussian preserving maps, which takes gaussian states into gaussian states. If we have a system described by an arbitrary number of bosonic modes a_i, the most general map with this property is a gaussian Hamiltonian. This means the Hamiltonian is *at most quadratic* in a_i and $a_i^\dagger$ which is not the case of the KBM model Eqn.(5.2), since it has an interaction term $a^\dagger a^\dagger aa$.

Gaussian states are nice because they can be *fully* characterized by the moments [42]:

$\langle a\rangle, \langle a^\dagger a\rangle$ and $\langle aa\rangle$ and their conjugates. We define,

$$\mu = \langle a\rangle \tag{6.3}$$

$$\langle \delta a^\dagger \delta a\rangle = \langle a^\dagger a\rangle - \langle a^\dagger\rangle\langle a\rangle \tag{6.4}$$

$$\langle \delta a \delta a\rangle = \langle aa\rangle - \langle a\rangle^2. \tag{6.5}$$

Moreover, the Husimi Q-function of a gaussian state $Q(\lambda,\bar{\lambda}) = \langle\lambda|\,\rho_g\,|\lambda\rangle/\pi$ has a neat analytical form [42], which is

$$Q(\lambda,\bar{\lambda}) = \frac{1}{\pi\sqrt{|\Theta_Q|}}\exp\left(-\frac{1}{2}\vec{v}^\dagger\Theta_Q^{-1}\vec{v}\right) \tag{6.6}$$

where

$$\Theta_Q = \begin{bmatrix} \langle \delta a^\dagger \delta a\rangle + 1 & \langle \delta a \delta a\rangle \\ \langle \delta \bar{a} \delta a\rangle & \langle \delta a^\dagger \delta a\rangle + 1 \end{bmatrix} \tag{6.7}$$

is the covariance matrix, $\vec{v} = (\lambda-\mu, \bar{\lambda}-\bar{\mu})^T$.

If the state of the KBM model were gaussian during the dynamics we could easily obtain all entropic quantities by making use of Eqn.(6.6) in Eqns. (4.43).

However, as we now show, the state is unfortunately not Gaussian. To prove this, we shall carry out a test based on the fourth moment. As is well known, for Gaussian states, all higher order moments can be expressed solely in terms of the mean and the covariance matrix. We shall therefore compare this prediction with that obtained from the full numerics using vectorization. From Eqn.(6.6), we can obtain $\langle a^r(a^\dagger)^s\rangle$ by performing an integral over the λ space variables,

$$\langle a^r(a^\dagger)^s\rangle = \int d^2\lambda\ \lambda^r\bar{\lambda}^s Q(\lambda,\bar{\lambda},\mu,\bar{\mu}), \tag{6.8}$$

we obtain the moments symbolically using the software Mathematica®. Parametrizing $\lambda = x+iy$, we can make the the integration over λ becomes a double integral over x, y.

Using the commutation relation $[a, a^\dagger] = 1$ it is straightforward to show that the normal ordered fourth moment is

$$\langle a^\dagger a^\dagger aa\rangle = \langle aaa^\dagger a^\dagger\rangle - 4\langle aa^\dagger\rangle + 2, \tag{6.9}$$

the two terms of this expression can be computed symbolically using Eqns.(6.6) and (6.8), which yields,

$$\langle aa^\dagger \rangle = 1 + \langle \delta a^\dagger \delta a \rangle + |\mu|^2 \tag{6.10}$$

and

$$\begin{aligned}\langle aaa^\dagger a^\dagger \rangle = |\langle \delta a \delta a \rangle|^2 + 4\langle \delta a^\dagger \delta a \rangle (1 + |\mu|^2) \\ + 2(1 + \langle \delta a^\dagger \delta a \rangle^2) + |\mu|^2(4 + |\mu|^2) + (\langle \delta a^\dagger \delta a^\dagger \rangle \mu^2 + \langle \delta a \delta a \rangle \bar{\mu}^2),\end{aligned} \tag{6.11}$$

Thus, Eqn.(6.9) becomes,

$$\langle a^\dagger a^\dagger a a \rangle_g = 2\langle \delta a^\dagger \delta a \rangle + |\mu|^2(4\langle \delta a^\dagger \delta a \rangle + |\mu|^2) + |\langle \delta a \delta a \rangle|^2 + \mu^2 \langle \delta a^\dagger \delta a^\dagger \rangle + \bar{\mu}\langle \delta a \delta a \rangle. \tag{6.12}$$

where we introduced the notation $\langle ... \rangle_g$ to emphasize that Eqn.(6.12) is valid *only* for gaussian states. We note that Eqn.(6.12) depends only on second order moments, a result known as Isserlis' theorem [116](also called Wick's theorem in the context of quantum field theory [117]).

We choose nine representative quenches to study the dynamics of this moment, as will be explained below. To test the gaussianity we computed $\langle a^\dagger a^\dagger a a \rangle$ exactly using vectorization to obtain the state ρ_t for each time t and compared it with the value of Eqn.(6.12) by means of the following quotient,

$$\mathscr{G} = \frac{\langle a^\dagger a^\dagger a a \rangle}{\langle a^\dagger a^\dagger a a \rangle_g} \tag{6.13}$$

where $\langle a^\dagger a^\dagger a a \rangle_g$ is computed from Eqn.(6.12), with the elements on the RHS computed from the exact numerics. This way, the state is gaussian if $\mathscr{G} = 1$ and non-gaussian otherwise. The results are summarized in Fig. 6.1.

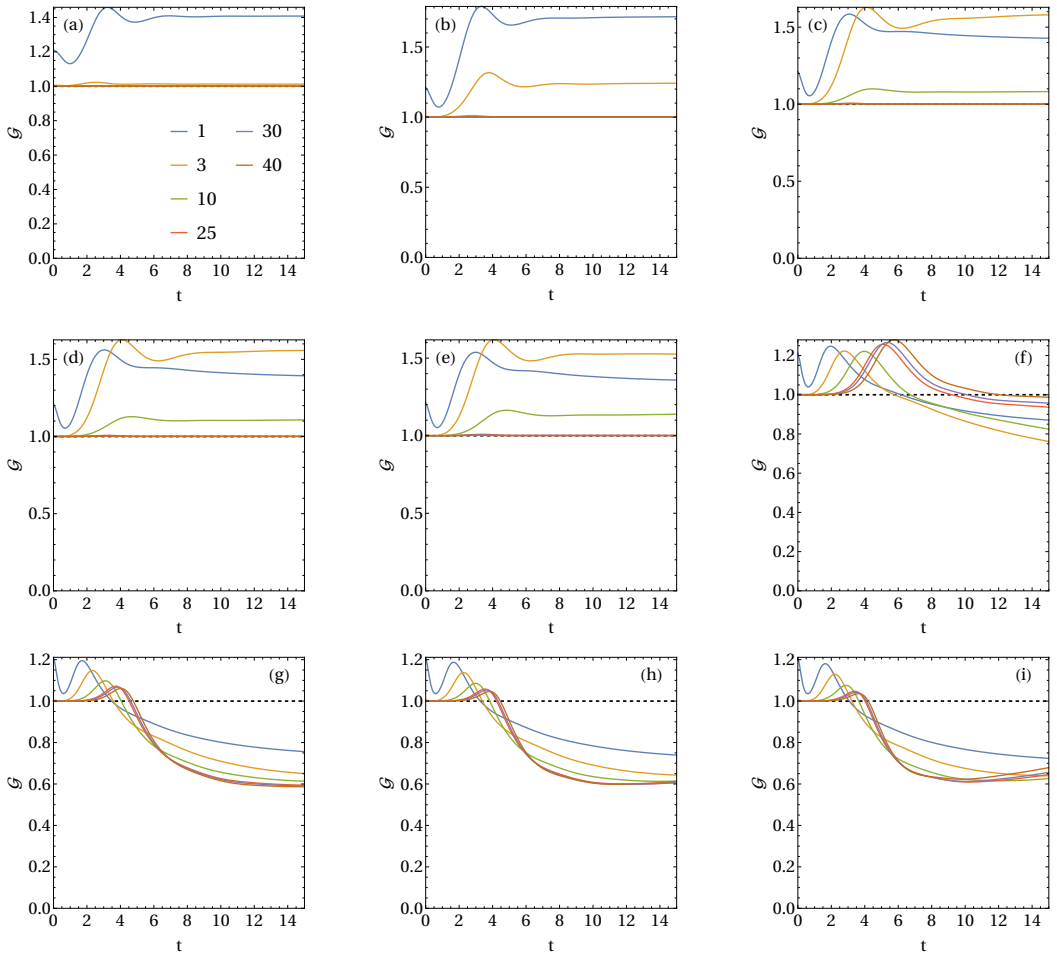

Figure 6.1: **Testing the gaussianity of the state during the dynamics:** $\mathscr{G}$, with $\langle a^\dagger a^\dagger a a\rangle_g$ given by Eqn.(6.12) for quenches from $\epsilon_i = 0.5$ to (a) $\epsilon_f = 0.6$ (b) $\epsilon_f = 0.8$ (c) $\epsilon_f = \epsilon_c - 0.01$ (d) $\epsilon_f = \epsilon_c$ (e) $\epsilon_f = \epsilon_c + 0.01$ (f) $\epsilon_f = 1.1$ (g) $\epsilon_f = \epsilon_+ - 0.01$ (h) $\epsilon_f = \epsilon_+$ (i) $\epsilon_f = \epsilon_+ + 0.01$. Where ϵ_c stands for the critical pump amplitude and ϵ_+ is the upper limit of the bistable region as found by MFA in Eqn.(5.13). The simulations are for six different values of N as shown in panel (a). Other parameters were fixed at $\kappa = 1/2$, $\Delta = -2$ and $u = 1$.

Throughout this chapter, we will make frequent reference to Fig. 6.2(a), which shows the different bistability regions in ϵ for the choice of parameters we are using. In this case, recall, the mean-field bistability region occurs between $\epsilon_- = 0.701373$ and $\epsilon_+ = 1.16616$, where $\epsilon_\pm$ is given by Eqn.(5.25). Moreover, the exact critical point is at $\epsilon_c = 0.933$. The initial $\epsilon_i = 0.5 < \epsilon_-$ was chosen to be in the lower branch. This is the case for all quenches presented in this chapter.

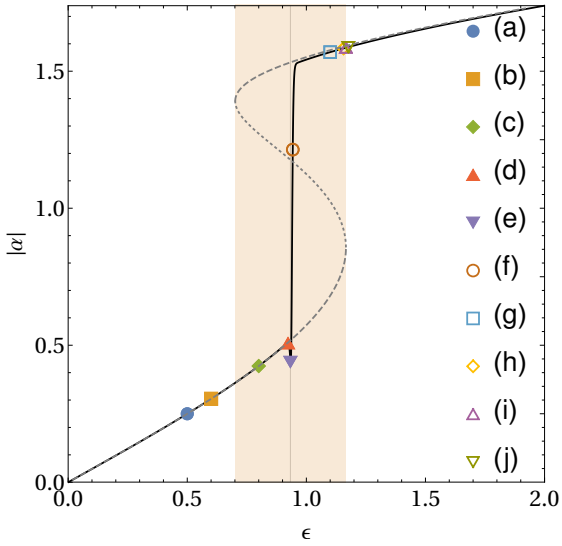

Figure 6.2: **Plot of the first moment:** where the chosen values of ϵ to study the quench dynamics are marked. (a) $\epsilon = 0.5$, (b) $\epsilon = 0.6$, (c) $\epsilon = 0.8$, (d) $\epsilon = \epsilon_c - 0.01$, (e) $\epsilon = \epsilon_c$, (f) $\epsilon = \epsilon_c + 0.01$, (g) $\epsilon = 1.1$, (h) $\epsilon = \epsilon_p - 0.01$, (i) $\epsilon = \epsilon_p$, (j) $\epsilon = \epsilon_p + 0.01$

The quench in panel (a) goes to $\epsilon_f = 0.6$. It continues in the lower branch and out of the bistable region, i.e. $\epsilon_f < \epsilon_-$. We can see that the state is almost gaussian already for $N = 3$ and effectively gaussian from $N = 10$ onward.

In panel (b) the quench goes to $\epsilon_f = 0.8$. It is still in the lower branch, but now it is inside the bistable region and away from the critical point $\epsilon_- < \epsilon_f < \epsilon_c$. Now we observe that $N = 3$ is not even close to gaussian, but again from $N = 10$ onward it is.

Next, we have in panels (c) $\epsilon_f = \epsilon_c - 0.01$, (d) $\epsilon_f = \epsilon_c$ and (e) $\epsilon_f = \epsilon_c + 0.01$, i.e. the quenches going to pumps at the vicinity of and to the critical pump. We observe that for these three quenches the dynamics are not gaussian for $N = 10$ anymore, but it is still approximately gaussian from $N = 25$ onward.

In panel (f) $\epsilon_f = 1.1$, is such that it has crossed the critical point and lies inside the bistable region, away from the upper border $\epsilon_c < \epsilon_f < \epsilon_+$. This quench is the first one to present non-trivial behavior, being clearly not gaussian for any size of N.

Finally, the last three quenches are for the upper border and its vicinity, (g) $\epsilon_f = \epsilon_+ - 0.01$, (h) $\epsilon_f = \epsilon_+$ and (i) $\epsilon_f = \epsilon_+ + 0.01$. From these panels, we observe again that the states are non-gaussian during the dynamics for any size of N.

Hence, we have seen that the last four quenches present highly non-gaussian dynamics, we note that this is a specific feature of the dynamics. That is, the NESS may very well be

approximated by a Gaussian. But this does not mean that the state during the dynamics will.

6.2 Entropic dynamics in a quench scenario: results and discussion

Here we present the results of the simulations for the entropy dynamics focusing on the quantities defined in Chap. 4. Our results have four distinct behaviors, so that the quenches presenting the same behavior were grouped together in four panels. For each of the quenches, we plot: (1) the extensive entropy flux rate Φ/N Eqn. (4.14), (2) the extensive entropy production rate Π_J/N Eqn. (4.15), (3) quantum entropy flux rate Φ_q Eqn. (4.28), (4) dissipative contribution to the quantum entropy production rate Π_d Eqn. (4.30) and finally (5) the unitary contribution to the entropy production rate Π_u Eqn. (4.41).

As we have seen in the last section, the states are not gaussian during the dynamics. So the simulation of the quench protocol requires full numerics using the vectorization procedure of App. D. The quench protocol we used is as follows (it is the same used in Sec. 4.1.1):

1. The system is initialized in ϵ_i, which is associated with an initial Liovillian $\mathscr{L}_i$. The initial state is the NESS of this Liouvillian, i.e. $\mathscr{L}_i\rho_i = 0$;

2. At time $t = 0$ we abruptly change the pump to a certain ϵ_f, which defines a new Liouvillian $\mathscr{L}_f$;

3. The state evolution is governed by the final Liouvillian according to $\rho_t = \exp\{\mathscr{L}_f t\}\rho_i$. The evolution is computed discretizing time in small steps Δt;,

4. We compute the Husimi Q-function numerically for each instant of time t, by constructing approximate coherent states,

$$|\mu\rangle = e^{-|\mu|^2/2} \sum_{n=0}^{n_{\max}} \frac{\mu^n}{\sqrt{n!}} |n\rangle \,, \tag{6.14}$$

the convergence of the numerical evolution is ensured by choosing different truncation sizes $n_{\max}$;

5. To compute the entropic quantities we construct a grid of the Husimi function $Q(\mu, \bar{\mu})$, which will be integrated numerically using standard numerical integration algorithms;

6. The derivatives of Q are computed using Eqn.(1.27), which yields expressions like,

$$\partial_{\bar{\mu}} Q = -\mu Q + \frac{1}{\pi} \langle \mu | \, a\rho \, | \mu \rangle \,, \tag{6.15}$$

with such an expression, derivatives of the Husimi function can be computed directly from the obtained density matrix ρ_t.

All these steps are computationally costly. The main technical difficulties is that for each quench the dimension of the Fock space $n_{\max}$ is different, and depending on the quench it takes longer for the system to reach the new NESS. For more details on the parameters of the simulations see App.E.2. The results are presented in Figs. 6.3-6.6.

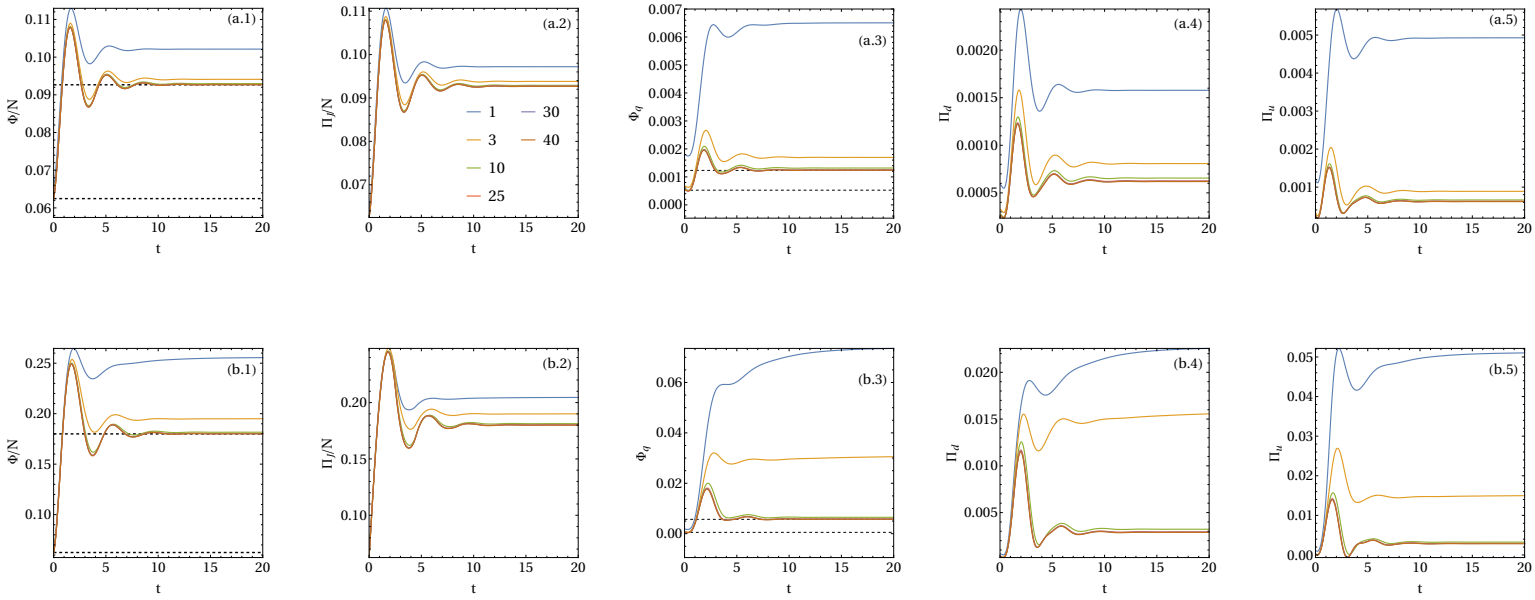

Figure 6.3: **Entropic dynamics for the quench dynamics (I):** The quenches are for (a) $\epsilon_f = 0.6$ in the upper row and (b) $\epsilon_f = 0.8$ in the lower row. Each column represent one entropic quantity: (1) Extensive entropy flux rate Φ/N, (2) Extensive entropy production rate Π_J/N, (3) Quantum entropy production rate Φ_q, (4) quantum entropy production rate due to dissipation Π_d and (5) quantum entropy production rate due to unitary dynamics Π_u. The plots are for different values of N as shown in panel (a.2). The dashed black lines represent the exact solutions for the entropy fluxes as given by Eqn.(5.26). Other parameters were fixed at $\kappa = 1/2$, $\Delta = -2$ and $u = 1$.

We observe that all entropic quantities are well behaved and they have a similar behavior for both quenches. In particular panels (a/b.1) Φ/N and (a/b.3) Φ_q shows that the system goes from the NESS of ϵ_i to the NESS of ϵ_f, which are denoted by the black dashed lines.

The extensive entropy production rate Π/N, shown in (a/b.2) has the same behavior as the flux, as expected by Eqn.(4.32)). This holds true for all the next quenches. Regarding the entropy production rate, we note that the order of magnitude of the quantum contribution due to dissipation Π_d (a/b.4) is the same as Φ_q (a/b.3) and also as the unitary contribution Π_u (a/b.5) for all N. The later observation does not hold for all quenches, as we will observe in the next quenches.

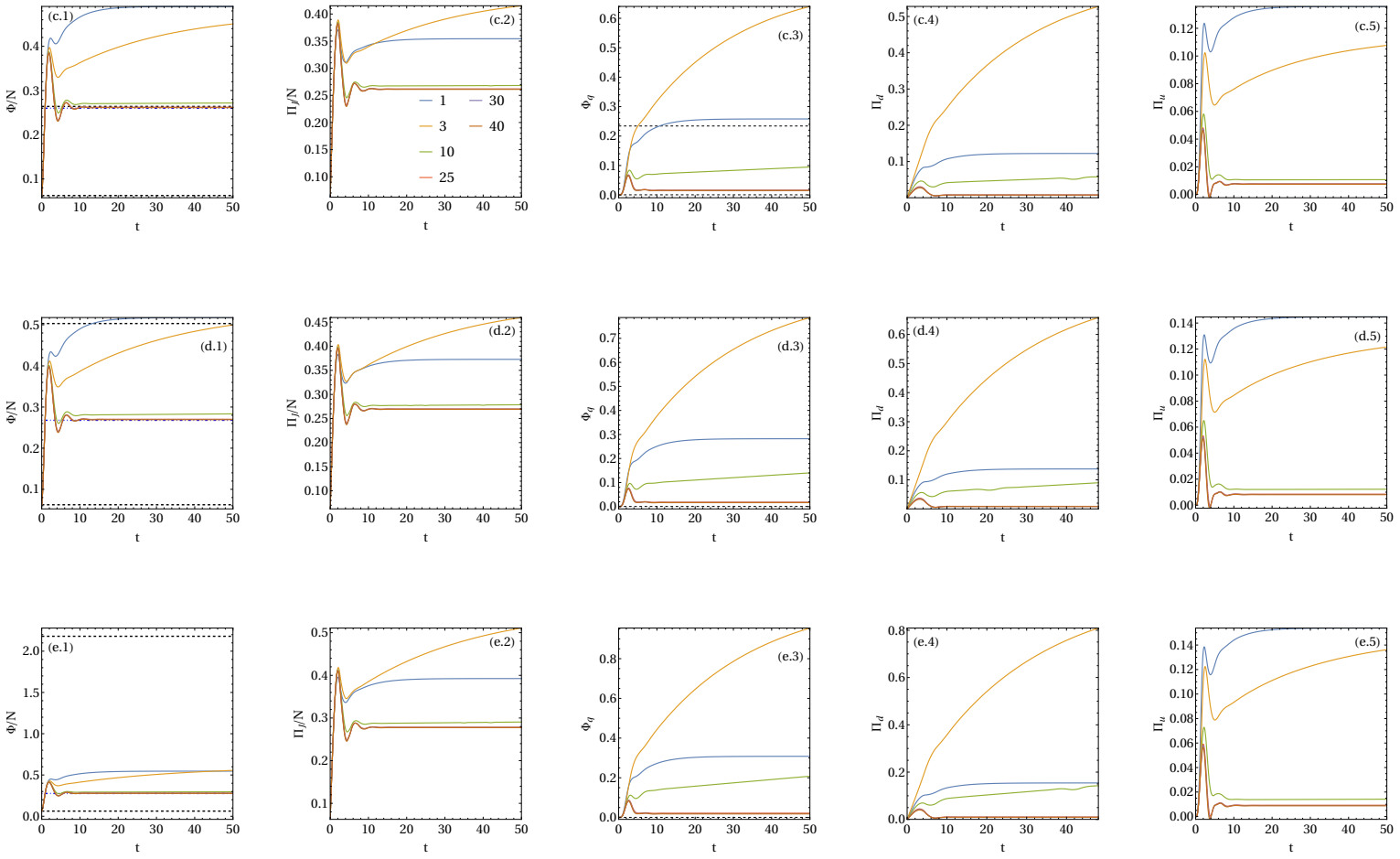

Figure 6.4: **Entropic dynamics for the quench dynamics (II):** The quenches are for (c) $\epsilon_f = \epsilon_c - 0.01$ in the first row, (d) $\epsilon_f = \epsilon_c$ in the second row and (e) $\epsilon_f = \epsilon_c + 0.01$ in the third row. The dashed black lines represent the exact solutions for the entropy fluxes as given by Eqn.(5.26) and the dot-dashed blue lines represent the MFA prediction for the NESS entropy flux Eqn.(5.16). The column ordering and other parameters were fixed as in Fig.6.3

In Fig.6.4 we show the entropic dynamics for the quenches to (c) $\epsilon_f = \epsilon_c - 0.01$ (d) $\epsilon_f = \epsilon_c$ and (e) $\epsilon_f = \epsilon_c + 0.01$. Interestingly, the extensive entropy flux rate Φ/N (c/d/e.1) does not relax to the exact final NESS value, denoted by the black dashed line in panels (c/d/e.1) in any case. Instead, it goes to the value predicted my MFA Eqn.(5.16), represented by the blue dot-dashed lines. Moreover, we note that it takes longer for the system to relax than it took in quenches presented before in Fig.6.3. Again, the extensive entropy production rate Π_J/N, shown in (c/d/e.2) has the same behavior as the extensive flux. Regarding the quantum entropy production rate, we note that, as in the first panel, the order of magnitude of the quantum contribution due to dissipation Π_d (c/d/e.4) is the

same as Φ_q (c/d/e.3) for all N. We also note that in this case Π_d is greater than the unitary contribution Π_u for $N = 3$ only but it is of the same order for other N.

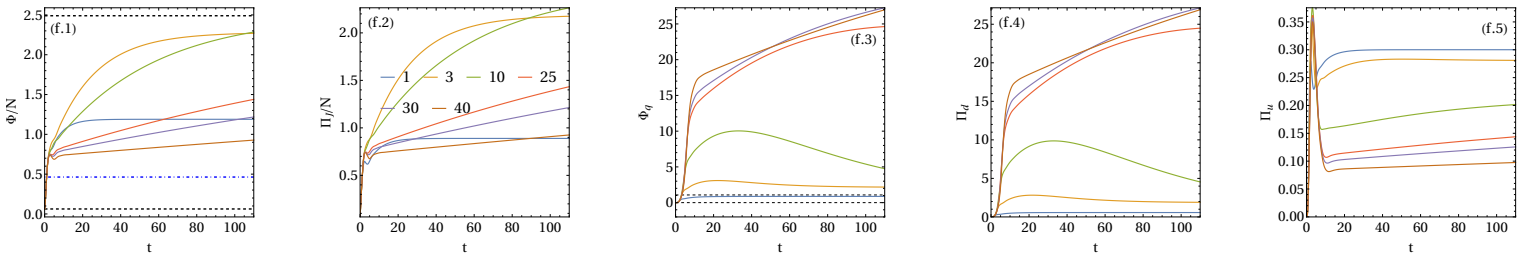

Figure 6.5: **Entropic dynamics for the quench dynamics (III):** The quench is for (f) $\epsilon_f = 1.1$. The column ordering and other parameters were fixed as in Fig.6.3.

Fig.6.5 shows the simulation for the quench to (f) $\epsilon_f = 1.1$. This pump frequency is such that we have crossed the critical point and is located inside the region of bistability. We emphasize that it was the first to display non-gaussian behavior (see Fig.6.1(f)). From panel (f.1) we see that the total entropy flux rate Φ/N does not relax nor to the exact solution neither to the MFA prediction, although it seems to be approaching the latter it as N increases. Again, the extensive entropy production rate Π/N, shown in (f.2) has the same behavior as the flux, as expected. The plot of the unitary contribution to the entropy production rate Π_u (f.5), suggests that its NESS depends on N, what is surprising, since this contribution is intensive, as Φ_q (f.3) and Π_d (f.4). We also note that the contribution Π_d is always greater than Π_u for all N, the same is observed in the next set of plots.

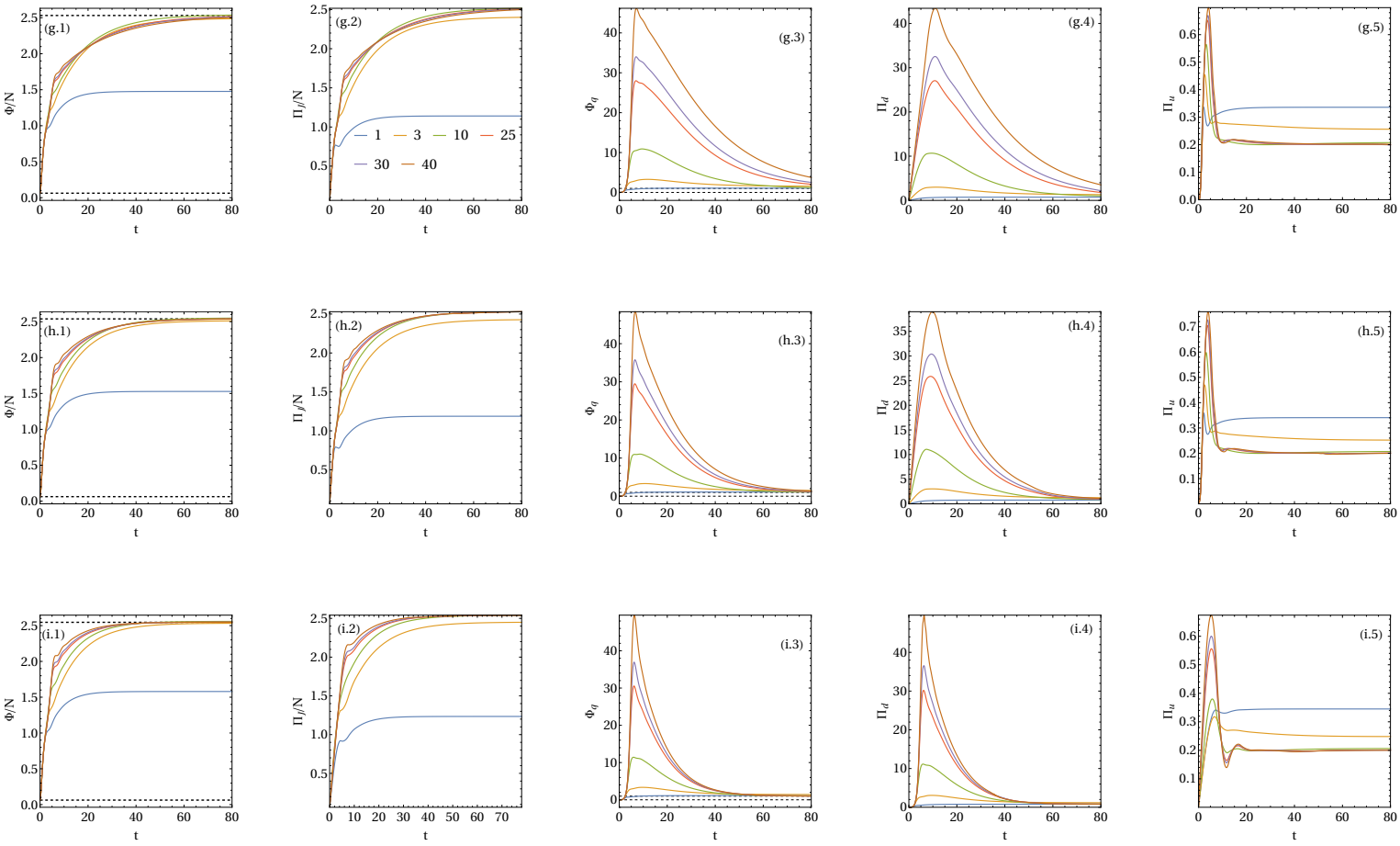

Figure 6.6: **Entropic dynamics for the quench dynamics (IV):** The quenches are for (g) $\epsilon_f = \epsilon_+ - 0.01$ (h) $\epsilon_f = \epsilon_+$ and (e) $\epsilon_f = \epsilon_+ + 0.01$. The column ordering and other parameters were fixed as in Fig.6.3.

From panels (g/h/i.1) where we plotted Φ/N and (g/h/i.3) where we plotted Φ_q we observe that the system asymptotically approaches the NESS predicted by the exact solution in a much longer time than the previous quenches. The most striking result for these quenches is that intensive quantities, such as Φ_q(g/h/i.3) and Π_d (g/h/i.4) presents a N-dependent very high peak during the transient dynamics, it is much greater than the NESS value. We also note that $\Pi_d \gg \Pi_u$. The N-dependency can also be noted in Π_u (g/h/i.5) during the transient dynamics.

As a conclusion of this section we can say that during the dynamics the extensive entropy production and flux are always the same, as predicted by Eqn.(4.32) and that the quantum entropy production Π_d has always the same behavior as the quantum entropy flux Φ_q. We have observed a dependency of the NESS according to where the final pump ϵ_f is located. And finally, we observed a dependency on the system size N of intensive

quantities such as Φ_q and Π_d for quenches crossing the critical pump, close to the upper border of the bistable region.

Chapter 7

Conclusions

In this dissertation we developed and presented a new theoretical framework of entropy production based on the Husimi Q-function. The main advantage of this theory is that it works well for zero temperature systems and does not impose any restriction on the type of Hamiltonian or state. The theory was specialized to driven-dissipative quantum systems displaying criticality, which has been the focus of intense research in recent years, both in theoretical and experimental branches. The main contribution of the formalism is to help to understand the behavior of entropy production across these quantum non-equilibrium transitions.

The entropy production rate was found to have two contributions, one of them due to the unitary dynamics of the system, hence a model dependent term. This contribution is related to the coarse-graining introduced by the Q-function, whose physical origin comes from the performance of a heterodyne measurement. The second contribution is related to the dissipation process, which is a usual source of irreversibility even in classical systems. Moreover, for critical systems we found a closed expression for the unitary contribution in Eqn. (4.42). We also found that the dissipative contribution splits into an extensive term and a second term solely due to quantum fluctuations in phase space in Eqn. (4.30). The entropy flux was found to be related to the number of photons inside the cavity, and for critical systems it also splits into a extensive term, which is equal to the extensive dissipative entropy production, and a quantum one related to the variance of the number of photons in Eqn. (4.28).

Afterwards, we applied out formalism to the paradigmatic model of Kerr bistability,

which was explained in detail in Sec. 5. We studied it in the NESS regime and in a quench dynamics scenario. We have found that the NESS quantum entropy production rate due to dissipation Π_d and flux Φ_q diverge at the critical point, thus behaving like a susceptibility. The unitary contribution Π_u behaved qualitatively similar to that of the entropy production in classical non-equilibrium transitions explained in Sec. 3.2. We emphasize that there is a fundamental difference between driven-dissipative and classical non-equilibrium phase transitions, in the former the energy input is coherent and the dissipation takes place incoherently; in the latter both energy input and output take place incoherently, through the transition rates in a classical master equation.

In the quench dynamics scenario we showed that the state is not gaussian during the dynamics, preventing a huge simplification in the study of the entropic quantities introduced by gaussian states. Then, by making use of vectorization we simulated the quench dynamics for nine representative quenches and found four distinct behaviors, which were discussed in detail. The most impressive result was that for some specific quenches, intensive quantities showed a N dependency during the transient dynamics, i.e. the greater the N, the further from equilibrium the state could get. A manuscript discussing these results for the quench scenario is currently in preparation.

As research perspectives of this work we can say that it would be valuable to explore models that presents DDPTs even in the presence of temperature ($T \neq 0$), in such a case we would have an interplay between thermal and quantum fluctuations. Another research line is to understand better the behavior of the unitary contribution to the entropy production rate. A first step towards this direction is currently being undertaken, where we are studying the Wehrl entropy production rate in the dynamical phase transition (DPT) of the LMG model. These are non-equilibrium phase transitions that appear as a non-analyticity in critical times in a quantity that has a formal similarity to the equilibrium partition function, called the Loschmidt echo. The results were reported in Ref. [118].

Appendix A

The time derivative of the mean of an operator

Given an operator $\mathscr{O}$, we may want to write the equation that governs the time evolution of its expectation value. Consider the dynamics is governed by a master equation,

$$\partial_t \rho = -i[H, \rho] + D(\rho), \tag{A.1}$$

where the dissipator due to some operator L is,

$$D(\rho) = 2\kappa \left(L\rho L^\dagger - \frac{1}{2}\{L^\dagger L, \rho\} \right). \tag{A.2}$$

The equation for the expectation value of the operator $\mathscr{O}$ will be,

$$\begin{aligned} \langle \mathscr{O} \rangle = \mathrm{tr}\{\mathscr{O}\rho\} \rightarrow \partial_t \langle \mathscr{O} \rangle &= \mathrm{tr}\{\mathscr{O}\partial_t \rho\} \\ &= -i\,\mathrm{tr}\{\mathscr{O}[H, \rho]\} + \mathrm{tr}\{\mathscr{O}D(\rho)\} \end{aligned} \tag{A.3}$$

Using the cyclic property of the trace,

$$\begin{aligned} \mathrm{tr}\{\mathscr{O}[H, \rho]\} &= \mathrm{tr}\left\{ \mathscr{O}H\rho - \underbrace{\mathscr{O}\rho H}_{H\mathscr{O}\rho} \right\} \\ &= \mathrm{tr}\{[\mathscr{O}, H]\rho\} = \langle [\mathscr{O}, H] \rangle \end{aligned} \tag{A.4}$$

$$\begin{aligned}
\mathrm{tr}\{\mathscr{O}D(\rho)\} &= \mathrm{tr}\left\{2\kappa\mathscr{O}\left[L\rho L^\dagger - \frac{1}{2}^\dagger L\rho - \frac{1}{2}\rho L^\dagger L\right]\right\} \\
&= \mathrm{tr}\left\{2\kappa\underbrace{\mathscr{O}L\rho L^\dagger}_{L^\dagger\mathscr{O}L\rho} - \frac{1}{2}\mathscr{O}L^\dagger L\rho - \frac{1}{2}\underbrace{\mathscr{O}\rho L^\dagger L}_{L^\dagger L\mathscr{O}\rho}\right\} \\
&= \mathrm{tr}\left\{2\kappa\left[L^\dagger\mathscr{O}L - \frac{1}{2}(\underbrace{\mathscr{O}L^\dagger L + L^\dagger L\mathscr{O}}_{\{L^\dagger L,\mathscr{O}\}})\right]\rho\right\} \\
&= 2\kappa\left\langle\left(L^\dagger\mathscr{O}L - \frac{1}{2}\{L^\dagger L,\mathscr{O}\}\right)\right\rangle
\end{aligned} \tag{A.5}$$

Finally, we can write:

$$\partial_t\langle\mathscr{O}\rangle = -i\langle[\mathscr{O},H]\rangle + 2\kappa\left\langle\left(L^\dagger\mathscr{O}L - \frac{1}{2}\{L^\dagger L,\mathscr{O}\}\right)\right\rangle \tag{A.6}$$

Appendix B

Rotating frame

The rotating frame is a generalization of the Heisenberg and interaction pictures [10] which is widely used in quantum optics in order to deal with time dependent Hamiltonians [36]. Consider a system described by a density matrix $\tilde{\rho}$ and let S_t be a time dependent unitary operator, $S_t^\dagger S_t = S_t S_t^\dagger = 1$, where 1 stands for the identity matrix. We assume that the system evolves according to the von Neumann equation under a time dependent Hamiltonian $\tilde{H}(t)$,

$$\partial_t \tilde{\rho} = -i[\tilde{H}(t), \tilde{\rho}]. \tag{B.1}$$

We move to the rotating frame by definig a new density matrix as,

$$\rho = S_t \tilde{\rho} S_t^\dagger, \tag{B.2}$$

taking the time derivative of Eqn.(B.2) and noting that $\partial_t(S_t S_t^\dagger) = \partial_t(S_t)S_t^\dagger + \partial_t(S_t^\dagger)S_t = 0$, which leads to $\partial_t(S_t)S_t^\dagger = -\partial_t(S_t^\dagger)S_t$, it is straightforward to show that the new density matrix also evolves according to a von Neumann equation

$$\partial_t \rho = -i[H(t), \rho] \tag{B.3}$$

where the the new Hamiltonian is,

$$H(t) = i\partial_t(S_t)S_t^\dagger + S_t H(t) S_t^\dagger \tag{B.4}$$

Eqn.(B.3) is general. By making a smart choice of S_t we may obtain a time independent $H(t)$. In the next section we show the details for the KBM of the main text.

B.1 Kerr bistability model in the rotating frame

The time dependent Hamiltonian of the KBM is,

$$\tilde{H} = \omega_c a^\dagger a + i\mathscr{E}(e^{-i\omega_p t}a^\dagger - e^{i\omega_p t}a) + \frac{U}{2}a^\dagger a^\dagger a a, \tag{B.5}$$

and the goal is to obtain a time independent hamiltonian. We define the unitary operator rotating with the pump frequency as,

$$S_t = e^{i\omega_p t a^\dagger a} \tag{B.6}$$

using Eqn.(B.6) with the Baker–Campbell–Hausdorff (BCH) formula,

$$e^{\lambda A}Be^{-\lambda A} = B + \lambda[A,B] + \frac{\lambda^2}{2!}[A,[A,B]] + \frac{\lambda^3}{3!}[A,[A,[A,B]]] + ... \tag{B.7}$$

one finds that,

$$\begin{aligned} S_t a S_t^\dagger &= e^{-i\omega_p t}a \\ S_t a^\dagger S_t^\dagger &= e^{i\omega_p t}a^\dagger \end{aligned} \tag{B.8}$$

Finally, using Eqns.(B.8), (B.4) and the fact that S_t is an unitary operator we obtain the time independent Hamiltonian Eqn.(5.2),

$$H = (\omega_c - \omega_p)a^\dagger a + i\mathscr{E}(a^\dagger - a) + \frac{U}{2}a^\dagger a^\dagger a a, \tag{B.9}$$

where in the main text we defined the detuning $\Delta = \omega_c - \omega_p$.

But the model obeys a Lindblad master equation, so we have to study the action of S_t in the dissipator $D(\tilde{\rho})$, again using Eqns.(B.8) and the unitarity of S_t it is straightforward to verify that,

$$S_t D(\tilde{\rho}) S_t^\dagger = D(S_t \tilde{\rho} S_t^\dagger) = D(\rho). \tag{B.10}$$

With this we have that the Lindblad master equation in the rotating frame is Eqn.(5.4) of the main text.

Appendix C

Linearization

Linearization is a procedure in which the basic idea is to approximate a nonlinear system by a linear one. We are interested in things that evolves with time. Our interest remain in two dimensional systems, but the results studied here are easy to generalize to n dimensions. For more details on this method we refer to Ref. [119].

Consider a system of two differential equations,

$$\begin{cases} d_t x(t) &= f(x,y), \\ d_t y(t) &= g(x,y). \end{cases} \tag{C.1}$$

The equilibrium, or fixed point of this system corresponds to the constant solution for $x(t)$ and $y(t)$. Let (x_0, y_0) be the equilibrium point, then $f(x_0, y_0) = g(x_0, y_0) = 0$.

Suppose $f(x,y)$ is a well behaved function. We want to know its behavior in the neighborhood of the equilibrum (x_0, y_0). From calculus the tangent plane approximation (linearization) of $f(x,y)$ at this point we have,

$$f(x,y) \approx f(x_0,y_0) + \partial_x f(x_0,y_0)(x-x_0) + \partial_y f(x_0,y_0)(y-y_0) + ... \tag{C.2}$$

Using Eqn.(C.2) it is possible to rewrite Eqn.(C.1) as

$$\begin{cases} d_t x &= f(x,y) = \underbrace{f(x_0,y_0)}_{=0} + \partial_x f(x_0,y_0)(x-x_0) + \partial_y f(x_0,y_0)(y-y_0) \\ d_t y &= g(x,y) = \underbrace{g(x_0,y_0)}_{=0} + \partial_x g(x_0,y_0)(x-x_0) + \partial_y g(x_0,y_0)(y-y_0) \end{cases} \tag{C.3}$$

Now, we define $u = x - x_0$ and $v = y - y_0$, this gives us, since x_0 and y_0 are just constants $d_t u = d_t x$ and $d_t v = d_t y$. With these new variables the system takes the form,

$$\begin{cases} d_t u &= \partial_x f(x_0,y_0)u + \partial_y f(x_0,y_0)v \\ d_t v &= \partial_x g(x_0,y_0)u + \partial_y g(x_0,y_0)v \end{cases} \tag{C.4}$$

which can be written in matricial notation as,

$$d_t \begin{bmatrix} u \\ v \end{bmatrix} = \begin{bmatrix} \partial_x f(x_0,y_0) & \partial_y f(x_0,y_0) \\ \partial_x g(x_0,y_0) & \partial_y g(x_0,y_0) \end{bmatrix} \begin{bmatrix} u \\ v \end{bmatrix} \rightarrow d_t \vec{\xi} = J\vec{\xi} \tag{C.5}$$

Where J is the Jacobian matrix and $\vec{\xi}$ is the column vector. Eqn.(C.5) is the linear approximation of the orignal problem and has the simple solution $\vec{\xi}(t) = e^{Jt}\vec{\xi}(0)$, where $\vec{\xi}(0)$ is the initial condition.

An important question to answer is: How well does this approximation work? If the real parts of both eigenvalues are nonzero, then the behavior of the system (C.1) near (x_0, y_0) is qualitatively **the same** as the behavior of the linear approximation (C.5).

Suppose we have $eigs(J) = \{\lambda_+, \lambda_-\}$ and the eigenvectors associated are $\vec{v_+}, \vec{v_-}$. Then, the solution can be written as

$$\vec{\xi}(t) = e^{\lambda_+ t}\vec{v_+} + e^{\lambda_- t}\vec{v_-} \tag{C.6}$$

Hence, there are three possible solutions, that depends on the eigenvalues. They are:

1. $\lambda_+ > 0$ and $\lambda_- > 0$, this solution is **unstable**, because $\vec{\xi}(t)$ explodes as $t \rightarrow \infty$;
2. $\lambda_{+(-)} > 0$ and $\lambda_{-(+)} < 0$, this is a **saddle point**;
3. $\lambda_+ < 0$ and $\lambda_- < 0$, this is a **stable** solution, because $\vec{\xi}(t) \rightarrow 0$as $t \rightarrow \infty$.

Appendix D

Vectorization

The vectorization is a linear transformation which converts a matrix into a column vector. Take three matrices A,B and C, the main property of the vectorization is the following [64],

$$\boxed{\text{Vec}(ABC) = (C^T \otimes A)\text{Vec}(B)}. \tag{D.1}$$

We will use this procedure to solve an "operator-eigenoperator" equation of the form,

$$\partial_t \rho = \mathscr{L}\rho \tag{D.2}$$

In Eqn.(D.2), ρ is the density matrix and $\mathscr{L}$ is the Louvillian superoperator. Using Eqn.(D.1) we can transform Eqn.(D.2) into an eigenvalue-eigenvector equation,

$$\partial_t \text{Vec}(\rho) = \text{Vec}(\mathscr{L}\rho) = \lambda \text{Vec}(\rho) \tag{D.3}$$

Applying it to a Lindblad equation,

$$\partial_t \rho = \mathscr{L}\rho = -i[H,\rho] + D(\rho) = -i(H\rho - \rho H) + 2\kappa \left[L\rho L^\dagger - \frac{1}{2}(\rho L^\dagger L + L^\dagger L \rho) \right] \tag{D.4}$$

yields,

$$\begin{cases} \text{Vec}(H\rho\mathbb{1}) = (\mathbb{1}^T \otimes H)\text{Vec}(\rho) \\ \text{Vec}(\mathbb{1}\rho H) = (H^T \otimes \mathbb{1})\text{Vec}(\rho) \\ \text{Vec}(L\rho L^\dagger) = [(L^\dagger)^T \otimes L]\text{Vec}(\rho) = [L^* \otimes L]\text{Vec}(\rho) \\ \text{Vec}(\mathbb{1}\rho(L^\dagger L)) = [(L^\dagger L)^T \otimes \mathbb{1}]\text{Vec}(\rho) \\ \text{Vec}((L^\dagger L)\rho\mathbb{1}) = [(\mathbb{1}^T \otimes (L^\dagger L)]\text{Vec}(\rho) \end{cases}$$

For instance, if we are dealing with a dephasing dissipator,

$$D(\rho) = \frac{\lambda}{2}(\sigma_z\rho\sigma_z - \rho)$$

the final equation will be

$$\begin{aligned} \text{Vec}(D'(\rho)) &= \frac{\lambda}{2}(\text{Vec}(\sigma_z\rho\sigma_z) - \text{Vec}(\rho)) \\ &= \frac{\lambda}{2}((\sigma_z^T \otimes \sigma_z) - 1)\text{Vec}(\rho) \\ &= \frac{\lambda}{2}((\sigma_z \otimes \sigma_z) - 1)\text{Vec}(\rho) \end{aligned}$$

Appendix E

Details of the numerical simulations

In this appendix we present some convergence/sanity checks of the numerical simulations that enabled us to obtain the entropy production and flux rate at the NESS and during the quench protocol.

We have the Liouvillian corresponding to the master equation (5.4) (with the scaling) as

$$\mathscr{L}(\rho) = -i\Big[H_0 + i\epsilon\sqrt{N}(a^\dagger - a), \rho\Big] + 2\kappa\bigg(a\rho a^\dagger - \frac{1}{2}\{a^\dagger a, \rho\}\bigg). \tag{E.1}$$

The steady-state equation,

$$\mathscr{L}(\rho) = 0, \tag{E.2}$$

is then transformed into a eigenvalue/eigenvector equation by making use of the vectorization procedure, explained in Sec.D. Then, ρ is the eigenvector of $\hat{\mathscr{L}}$ associated with the eigenvalue 0. To carry out the calculation, we decompose ρ in the Fock basis, using a sufficiently large dimension n_{max} for the Fock space to ensure convergence (see table E.1 and Fig.E.1).

N interval	$n_{\max}$
$N \leq 10$	60
$N \leq 35$	220
$N \leq 55$	300
$N \leq 80$	450
$N \leq 100$	520

Table E.1: **Truncated dimension of the Fock space given** N: For each interval of N on the left column, the truncated dimension of the Fock space was defined by the values on the right column. Convergence was ensured by comparing the numerical results of the NESS with the exact values as given in Ref. [3].

E.1 NESS convergence analysis

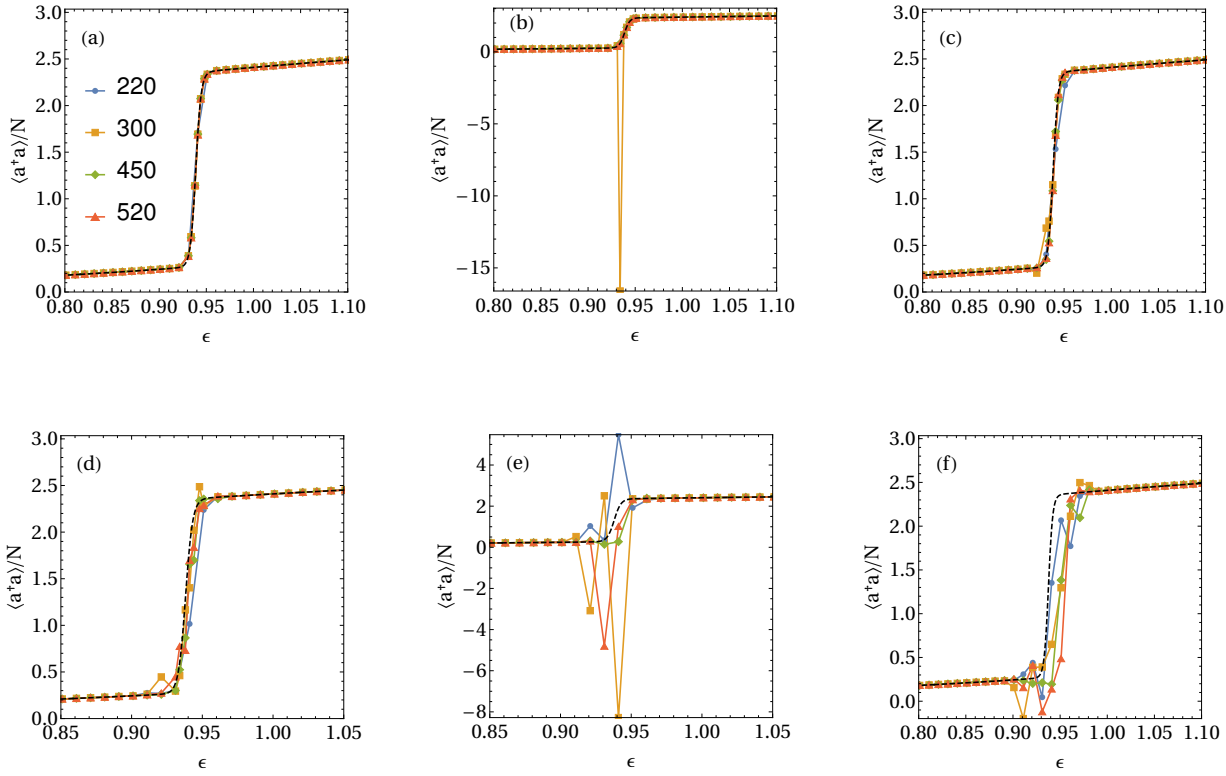

Figure E.1: **Convergence test for the truncated dimension given** N: Plot of the second moment $\langle a^\dagger a\rangle/N$ at the vicinity of criticallity for different values of truncated dimension $n_{\max}$ as shown in panel (a). The black dashed line stands for the exact solution of Ref. [3], while the dots are the numerical results obtained from vetorization for different dimensions. The plots are for: (a) $N = 40$ (b) $N = 41$ (c) $N = 43$ (d) $N = 45$ (e) $N = 47$ (f) $N = 50$

We found that for $N > 40$ our numerical procedure did not match the exact results in the critical region as can be seen in Fig.E.1, that is why all of our numerical results presented in the main text goes up to $N = 40$ only. The truncated dimension of the Fock space were chosen as showed in Tab.E.1 for all numerical computations.

E.2 Convergence analysis and sanity check: quench dynamics

To obtain the entropy flux $\Phi_t = 2\kappa\langle a^\dagger a\rangle_t$ we simply evolved the initial state in time, as described in the main text Sec. 6.2, and computed the trace with with the state ρ_t, for each step of time $\langle a^\dagger a\rangle_t = \mathrm{tr}\{a^\dagger a\rho_t\}$. In order to ensure the convergence of the simulations for the quench, we defined a control parameter δ and compared the results between N and $N + \delta$. The control parameter could take the values $\delta = 0$ and $\delta = 5$. This small contribution to N should not modify the results and that is precisely what is verified in Fig.E.2.

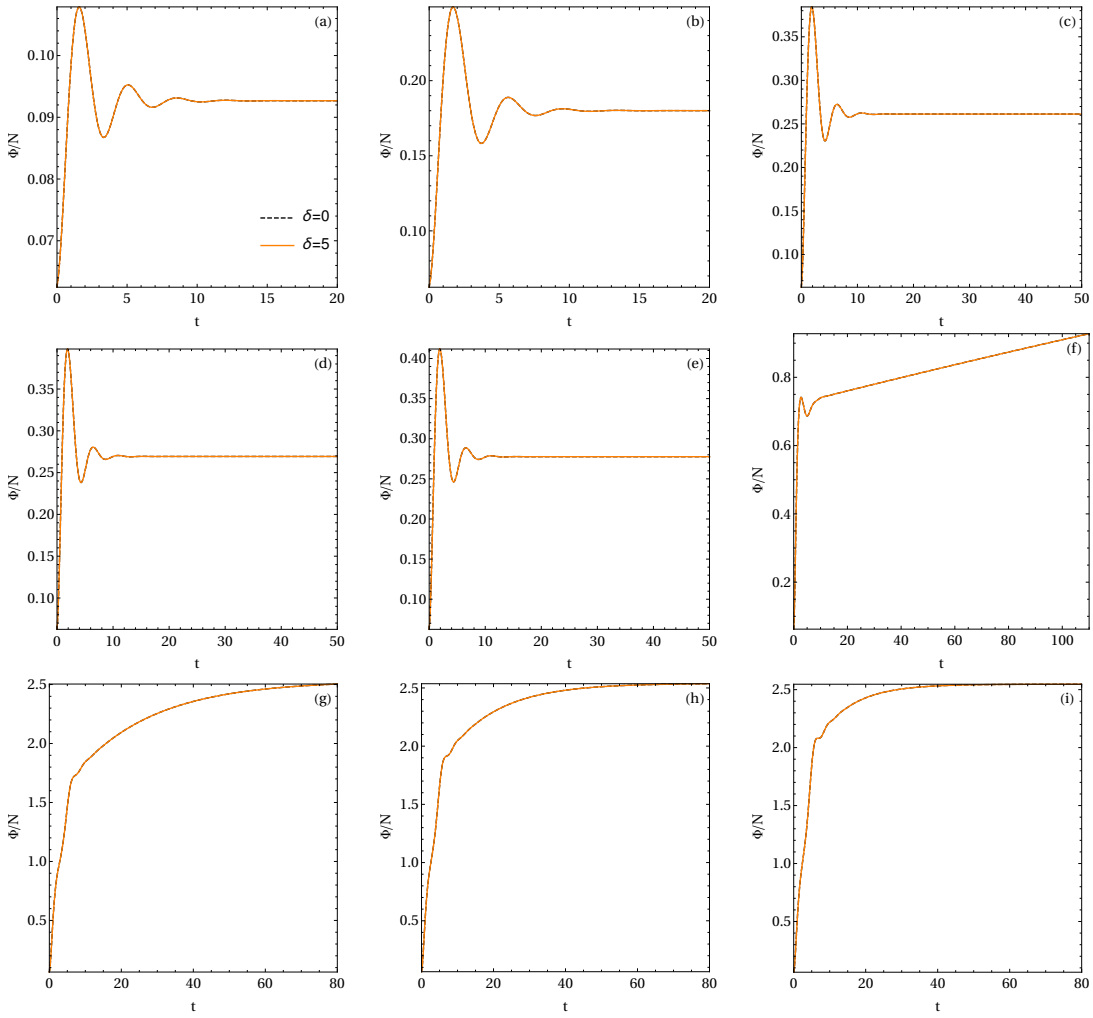

Figure E.2: **Convergence analysis of the total flux:** It was fixed $N = 40$. The plots are for two different values of the control parameter $\delta = 0$ and $\delta = 5$, as shown in panel (a). The quenches are from $\epsilon_i = 0.5$ to (a) $\epsilon_f = 0.6$ (b) $\epsilon_f = 0.8$ (c) $\epsilon_f = \epsilon_c - 0.01$ (d) $\epsilon_f = \epsilon_c$ (d) $\epsilon_f = \epsilon_c + 0.01$ (e) $\epsilon_f = 1.1$, (f) $\epsilon_f = \epsilon_p - 0.01$ (g) $\epsilon_f = \epsilon_p$ (h) $\epsilon_f = \epsilon_p + 0.01$. Other parameters were fixed as in Fig.6.3.

As a sanity check we test if after the quench dynamics the sum of the contributions of the entropy production rate matches the NESS entropy flux rate,

$$\frac{dS}{dt} = 0 \quad \rightarrow \quad \Pi_J + \Pi_u = \Phi_{\text{ext}}, \tag{E.3}$$

this behavior can be verified in Fig.E.5.

Given a matrix ρ we locate the Husimi Q-function and construct discretized surface grid as a xy-plane where $\mu = \langle a \rangle = x + iy$. This way $Q(\mu, \bar{\mu}) \rightarrow Q(x, y)$. The Q-function is approximately centralized around μ, we compute the standard deviation in x and y

direction, we choose the number of standard deviations "nstd" in both directions and the number of points of the grid "ngrid" so that the Q-function is null in the borders. To do so we use the following identities,

$$\langle aa^\dagger \rangle = \int d^2\mu \, |\mu|^2 Q(\mu, \bar{\mu}) \tag{E.4}$$

$$= \int dxdy \, (x^2 + y^2) Q(x, y) = \langle x^2 \rangle + \langle y^2 \rangle \tag{E.5}$$

and,

$$\langle aa \rangle = \int d^2\mu \, \mu^2 Q(\mu, \bar{\mu}) \tag{E.6}$$

$$= \int dxdy \, (x^2 + y^2 + 2ixy) Q(x, y) = \langle x^2 \rangle - \langle y^2 \rangle + 2i\langle xy \rangle \tag{E.7}$$

Hence, for instance $\langle x \rangle = \Re\mu$ and $\langle x^2 \rangle = (2\langle aa^\dagger \rangle + \langle aa \rangle - \langle \bar{aa} \rangle)/4$. This yields $\text{var}(x) = \sqrt{\langle x^2 \rangle - \langle x \rangle^2}$. This procedure gives the region of integration $\{x_i, x_f\} \times \{y_i, y_f\}$ and the spacing in each direction $\Delta x, \Delta y$. The code that locates the Husimi Q-function is shown in Fig. E.3.

```
LocateHusimi[ρ_, ngrid_:20, nstd_:6] := Module[{aveA, aveAAd, aveAA, aveX, aveY, aveX2, aveY2, stdX, stdY, xi, xf, yi, yf, Δx, Δy},

  aveA = Chop@Tr[a.ρ];
  aveAAd = Chop@Tr[a.a†.ρ];
  aveAA = Chop@Tr[a.a.ρ];

  aveX = Re[aveA];
  aveY = Im[aveA];
  aveX2 = (2 aveAAd + aveAA + aveAA*)/4 // Chop;
  aveY2 = (2 aveAAd - aveAA - aveAA*)/4 // Chop;

  stdX = √(aveX2 - aveX^2);
  stdY = √(aveY2 - aveY^2);

  xi = aveX - nstd stdX;
  xf = aveX + nstd stdX;
  yi = aveY - nstd stdY;
  yf = aveY + nstd stdY;
  Δx = First@Differences@linspace[xi, xf, ngrid];
  Δy = First@Differences@linspace[yi, yf, ngrid];
  {xi, xf, Δx, yi, yf, Δy}


];
```

Figure E.3: **Code 1:** Locate Husimi Q-function.

Once we localize the Q-function, we compute the components of Π_t for each step of time, where the state is ρ_t by the following steps:

1. We choose the number of points in the surface grid "ngrid" and a number of standard deviations "nstd" we use to center the Husimi Q-function. These numbers remain constant for a given quench. We locate the Husimi Q-function in order to have the region of integration aforementioned;

2. With the region of integration we compute the values of Π_J and Π_u, using the formulas of the main text. The code of the function *Q-Entropy Calculator* is shown in Fig. E.4;

```
QEntropyProdCalculator[{xi_, xf_, Δx}, {yi_, yf_, Δy}, ρ_] :=

 Module[{nmax = Length[ρ] - 1, α, inner1, inner2, aarho, arho, αvecmod, xrange, yrange, J2overQ, Q, ΠJandU, ΠJ, DαsQ, D2αsQ, ΠJtemp, Utemp, ΠU},

  xrange = range[xi , xf , Δx] + 10^-15;
  yrange = range[yi , yf , Δy] + 10^-15;

  arho = a.ρ;
  aarho = a.arho;

  ΠJandU = Table[
    α = x + I y;

    αvecmod =  Quiet@Chop@Table[Exp[-Abs[α]^2 / 2] α^n / Sqrt[n!], {n, 0, nmax}];

    Q = 1/π αvecmod*.ρ.αvecmod;

    inner1 = 1/π αvecmod*.arho.αvecmod;

    inner2 = 1/π αvecmod*.aarho.αvecmod;

    DαsQ = -α Q + inner1;

    D2αsQ = -α DαsQ - α (inner1) + (inner2);

    If[Abs[Q] < 10^-15, {0, 0}, {Abs[inner1]^2/Q, ((α*)^2 (Q D2αsQ - (DαsQ)^2)/Q) - ((α*)^2 (Q D2αsQ - (DαsQ)^2)/Q)*}]
    , {y, yrange}, {x, xrange}];

  ΠJ = Chop@Total@Flatten[Δx Δy ΠJandU[[All, All, 1]]];

  ΠU = Chop@Total@Flatten[Δx Δy ΠJandU[[All, All, 2]]];

  {ΠJ, ΠU}
 ]
```

Figure E.4: **Code 2:** Entropy calculator.

3. These steps are repeated for each step of time.

The parameters of the quench dynamics simulations were chosen as shown in Tab. E.2.

ϵ_f	Nstd	NGrid	t_f
0.6	6	35	20
0.8	6	35	20
$\epsilon_c - 0.01$	6	35	50
ϵ_c	6	35	50
$\epsilon_c + 0.01$	6	35	50
1.1	8	74	110
$\epsilon_p - 0.01$	7	65	80
ϵ_p	7	65	80
$\epsilon_p + 0.01$	7	65	80

Table E.2: **Parameters for the numerical entropy production computation:** "Nstd" stands for number of standard deviations chosen to locate the Husimi Q-function and "NGrid" is the number of points of the Husimi grid. Finally, t_f is the final time chosen for the final ϵ_f.

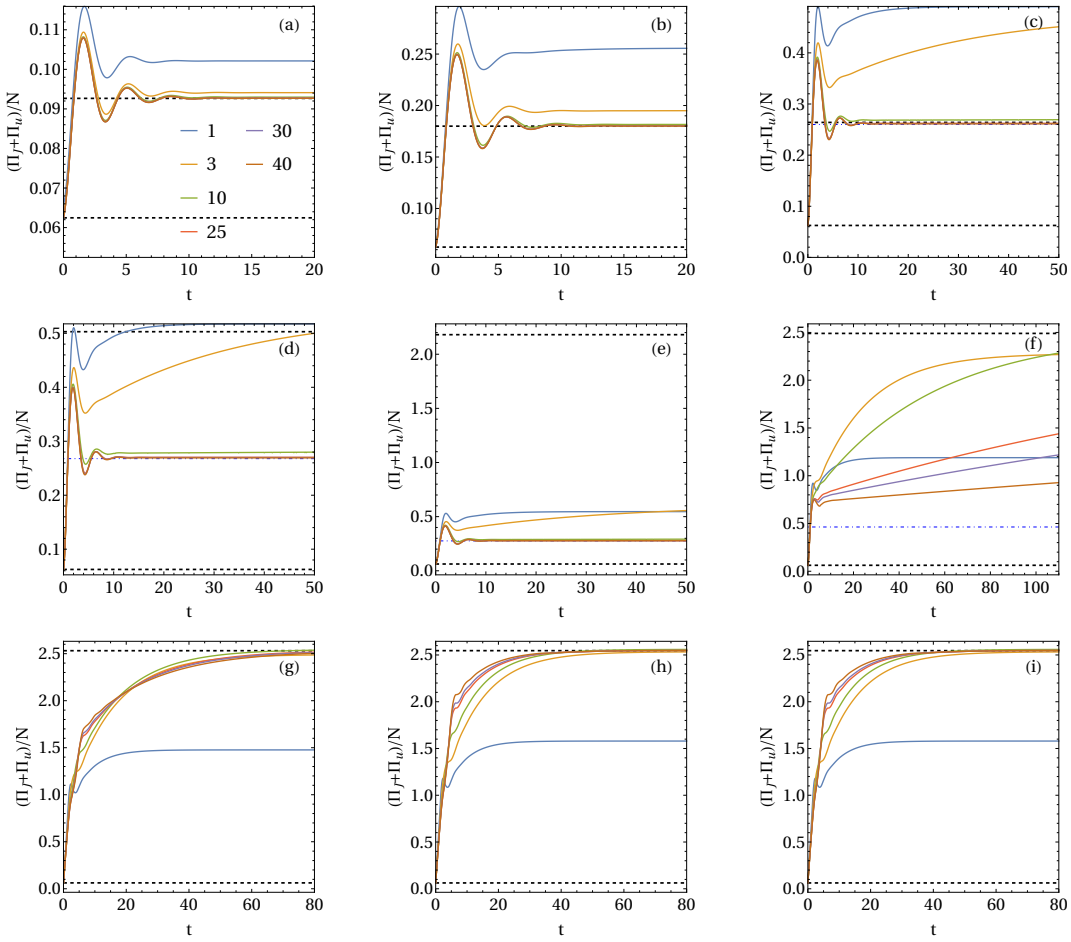

Figure E.5: **Sanity check :** The plot shows that $(\Pi_J + \Pi_u)/N \to \Phi_{\text{ext}}/N$ after the quench dynamics. The values of N are shown in panel (a). The order of the quenches and other parameters are as in Fig.E.2

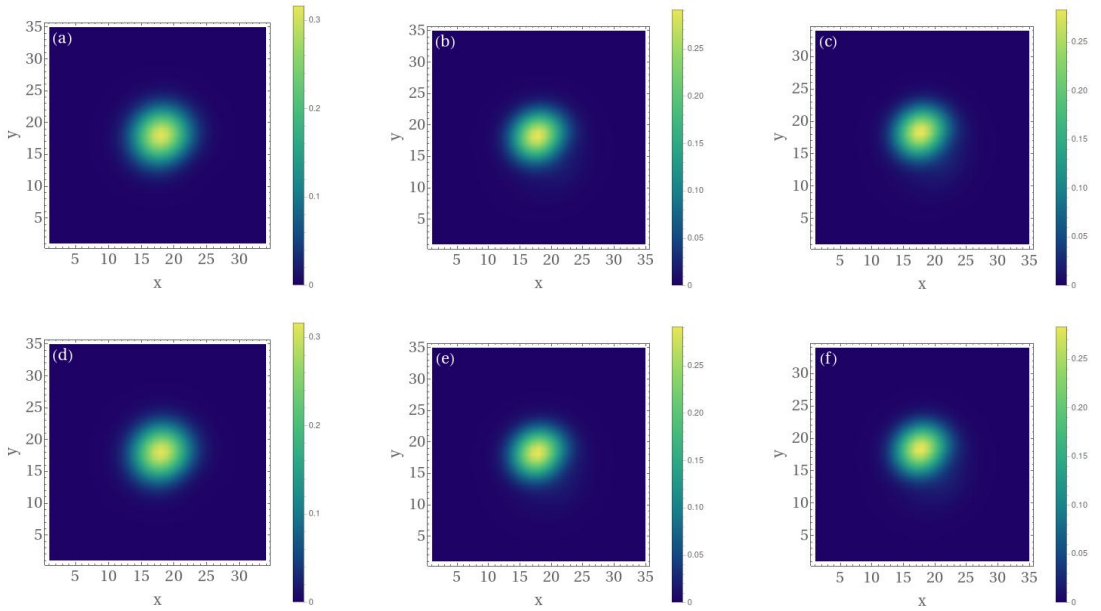

Figure E.6: **Husimi Q-function contour plot:** We plot the contour of the Husimi Q-function during the time evolution of the quench $(\epsilon_i, \epsilon_f) = (0.5, \epsilon_c)$. In the upper row we set $N = 1$ and time (a) $t = 1$, (b) $t = 6.5$, (c) $t = 15$, while in the lower row we set $N = 40$ and time (d) $t = 1$,(e) $t = 6.5$,(f) $t = 15$. The frames are $x = \Re\mu$ and $y = \Im\mu$. Other parameters are as in Fig.E.2

In Fig. E.6 we observe the evolution of the Husimi Q-function at certain times as given by the aforementioned algorithm, for $N = 1$ and $N = 40$. We note that it is always centralized and zero in the borders as required to computed the integrals of the entropy production rate numerically. It holds for all the quenches shown in Chap. 6.

Bibliography

[1] C. Gardiner and P. Zoller, *Quantum noise: a handbook of Markovian and non-Markovian quantum stochastic methods with applications to quantum optics*, vol. 56. Springer Science & Business Media, 2004.

[2] C. E. F. Noa, P. E. Harunari, M. J. de Oliveira, and C. E. Fiore, "Entropy production as a tool for characterizing nonequilibrium phase transitions," *Phys. Rev. E*, vol. 100, p. 012104, Jul 2019.

[3] P. Drummond and D. Walls, "Quantum theory of optical bistability. i. nonlinear polarisability model," *Journal of Physics A: Mathematical and General*, vol. 13, no. 2, p. 725, 1980.

[4] E. Fermi, *Thermodynamics*. Dover books in physics and mathematical physics, Dover Publications, 1956.

[5] H. Callen, H. Callen, N. F. R. C. of Australia. Research Division, and W. . Sons, *Thermodynamics and an Introduction to Thermostatistics*. Wiley, 1985.

[6] S. Salinas, *Introduction to statistical physics*. Springer Science & Business Media, 2001.

[7] R. Feynman, *Statistical Mechanics: A Set Of Lectures*. Advanced Books Classics, Avalon Publishing, 1998.

[8] D. C. Mattis, *The theory of magnetism I: Statics and Dynamics*, vol. 17. Springer Science & Business Media, 2012.

[9] L. Landau and E. Lifshitz, *Statistical Physics*. No. v. 5, Elsevier Science, 1980.

[10] J. J. Sakurai and J. Napolitano, *Modern Quantum Mechanics*. Cambridge University Press, 2 ed., 2017.

[11] R. Shankar, *Principles of quantum mechanics*. Springer Science & Business Media, 2012.

[12] A. Peres, *Quantum theory: concepts and methods*, vol. 57. Springer Science & Business Media, 2006.

[13] H.-P. Breuer, F. Petruccione, *et al.*, *The theory of open quantum systems*. Oxford University Press on Demand, 2002.

[14] J. Preskill, "Lecture notes for physics 229: Quantum information and computation," *California Institute of Technology*, vol. 16, 1998.

[15] U. Seifert, "Stochastic thermodynamics, fluctuation theorems and molecular machines.," *Reports on progress in physics. Physical Society (Great Britain)*, vol. 75, no. 12, p. 126001, 2012.

[16] S. Deffner and S. Campbell, *Quantum Thermodynamics*. 2053-2571, Morgan Claypool Publishers, 2019.

[17] S. Vinjanampathy and J. Anders, "Quantum thermodynamics," *Contemporary Physics*, vol. 57, no. 4, pp. 545–579, 2016.

[18] J. Goold, M. Huber, A. Riera, L. del Rio, and P. Skrzypczyk, "The role of quantum information in thermodynamics—a topical review," *Journal of Physics A: Mathematical and Theoretical*, vol. 49, no. 14, p. 143001, 2016.

[19] F. Binder, L. A. Correa, C. Gogolin, J. Anders, and G. Adesso, "Thermodynamics in the quantum regime," *Fundamental Theories of Physics (Springer, 2018)*, 2018.

[20] T. Tomé and M. C. De Oliveira, "Entropy Production in Nonequilibrium Systems at Stationary States," *Physical Review Letters*, vol. 108, p. 020601, jan 2012.

[21] L. Crochik and T. Tomé, "Entropy production in the majority-vote model," *Physical Review E - Statistical, Nonlinear, and Soft Matter Physics*, vol. 72, p. 057103, 2005.

[22] P. S. Shim, H. M. Chun, and J. D. Noh, "Macroscopic time-reversal symmetry breaking at a nonequilibrium phase transition," *Physical Review E*, vol. 93, p. 012113, 2016.

[23] Y. Zhang and A. C. Barato, "Critical behavior of entropy production and learning rate: Ising model with an oscillating field," *Journal of Statistical Mechanics: Theory and Experiment*, vol. 2016, p. 113207, 2016.

[24] T. Herpich, J. Thingna, and M. Esposito, "Collective Power: Minimal Model for Thermodynamics of Nonequilibrium Phase Transitions," *Physical Review X*, vol. 8, no. 3, p. 31056, 2018.

[25] S. Sachdev, "Quantum phase transitions," *Handbook of Magnetism and Advanced Magnetic Materials*, 2007.

[26] M. Brunelli, L. Fusco, R. Landig, W. Wieczorek, J. Hoelscher-Obermaier, G. Landi, F. L. Semião, A. Ferraro, N. Kiesel, T. Donner, G. De Chiara, and M. Paternostro, "Experimental Determination of Irreversible Entropy Production in out-of-Equilibrium Mesoscopic Quantum Systems," *Physical Review Letters*, vol. 121, no. 16, pp. 1–14, 2018.

[27] J. P. Santos, G. T. Landi, and M. Paternostro, "Wigner entropy production rate," *Phys. Rev. Lett.*, vol. 118, p. 220601, Jun 2017.

[28] B. O. Goes, C. E. Fiore, and G. T. Landi, "Quantum features of entropy production in driven-dissipative transitions," *Phys. Rev. Research*, vol. 2, p. 013136, Feb 2020.

[29] M. H. Anderson, J. R. Ensher, M. R. Matthews, C. E. Wieman, and E. A. Cornell, "Observation of bose-einstein condensation in a dilute atomic vapor," *Science*, pp. 198–201, 1995.

[30] F. Dalfovo, S. Giorgini, L. P. Pitaevskii, and S. Stringari, "Theory of bose-einstein condensation in trapped gases," *Rev. Mod. Phys.*, vol. 71, pp. 463–512, Apr 1999.

[31] M. Greiner, O. Mandel, T. Esslinger, T. W. Hänsch, and I. Bloch, "Quantum phase transition from a superfluid to a mott insulator in a gas of ultracold atoms," *Nature*, vol. 415, no. 6867, pp. 39–44, 2002.

[32] I. Bloch, "Ultracold quantum gases in optical lattices," *Nature physics*, vol. 1, no. 1, pp. 23–30, 2005.

[33] I. Rotter and J. P. Bird, "A review of progress in the physics of open quantum systems: theory and experiment," *Reports on Progress in Physics*, vol. 78, p. 114001, Oct 2015.

[34] I. de Vega and D. Alonso, "Dynamics of non-markovian open quantum systems," *Rev. Mod. Phys.*, vol. 89, p. 015001, Jan 2017.

[35] G. Lindblad, "On the generators of quantum dynamical semigroups," *Communications in Mathematical Physics*, vol. 48, no. 2, pp. 119–130, 1976.

[36] M. O. Scully and M. S. Zubairy, *Quantum Optics*. Cambridge University Press, 1997.

[37] R. Loudon, *The quantum theory of light*. OUP Oxford, 2000.

[38] R. J. Glauber, "Coherent and incoherent states of the radiation field," *Phys. Rev.*, vol. 131, pp. 2766–2788, Sep 1963.

[39] E. P. Wigner, "On the quantum correction for thermodynamic equilibrium," in *Part I: Physical Chemistry. Part II: Solid State Physics*, pp. 110–120, Springer, 1997.

[40] K. Husimi, "Some formal properties of the density matrix," *Proceedings of the Physico-Mathematical Society of Japan. 3rd Series*, vol. 22, no. 4, pp. 264–314, 1940.

[41] V. Buek, C. H. Keitel, and P. L. Knight, "Sampling entropies and operational phase-space measurement. I. General formalism," *Physical Review A*, vol. 51, no. 3, pp. 2575–2593, 1995.

[42] A. Serafini, *Quantum Continuous Variables: A Primer of Theoretical Methods*. CRC Press, Taylor & Francis Group, 2017.

[43] J. M. Keynes, *A treatise on probability*. Courier Corporation, 2013.

[44] S. M. Ross *et al.*, *A first course in probability*, vol. 7. Pearson Prentice Hall Upper Saddle River, NJ, 2006.

[45] C. E. Shannon, "A mathematical theory of communication," *Bell System Technical Journal*, vol. 27, no. 3, pp. 379–423, 1948.

[46] E. T. Jaynes, "Information theory and statistical mechanics," *Phys. Rev.*, vol. 106, pp. 620–630, May 1957.

[47] T. Tomé and M. de Oliveira, *Stochastic Dynamics and Irreversibility*. Graduate Texts in Physics, Springer International Publishing, 2014.

[48] S. Carnot, *Reflections on the motive power of fire: And other papers on the second law of thermodynamics*. Courier Corporation, 2012.

[49] R. Clausius, "Über eine veränderte form des zweiten hauptsatzes der mechanischen wärmetheorie," *Annalen der Physik*, vol. 169, no. 12, pp. 481–506, 1854.

[50] R. P. Feynman, R. B. Leighton, and M. Sands, *The Feynman lectures on physics, Vol. I: The new millennium edition: mainly mechanics, radiation, and heat*, vol. 1. Basic books, 2011.

[51] J. Schnakenberg, "Network theory of microscopic and macroscopic behavior of master equation systems," *Reviews of Modern physics*, vol. 48, no. 4, p. 571, 1976.

[52] T. Tomé and M. J. De Oliveira, "Entropy production in nonequilibrium systems at stationary states," *Physical Review Letters*, vol. 108, no. 2, pp. 1–5, 2012.

[53] T. Tomé, "Entropy production in nonequilibrium systems described by a Fokker-Planck equation," *Brazilian Journal of Physics*, vol. 36, no. 4a, pp. 1285–1289, 2006.

[54] C. Van den Broeck and M. Esposito, "Three faces of the second law. ii. fokker-planck formulation," *Physical Review E*, vol. 82, no. 1, p. 011144, 2010.

[55] R. E. Spinney and I. J. Ford, "Entropy production in full phase space for continuous stochastic dynamics," *Physical Review E*, vol. 85, no. 5, p. 051113, 2012.

[56] G. T. Landi, T. Tomé, and M. J. De Oliveira, "Entropy production in linear langevin systems," *Journal of Physics A: Mathematical and Theoretical*, vol. 46, no. 39, p. 395001, 2013.

[57] R. Landauer, "Stability and entropy production in electrical circuits," *Journal of Statistical Physics*, vol. 13, pp. 1–16, jul 1975.

[58] M. A. Nielsen and I. L. Chuang, *Quantum Computation and Quantum Information: 10th Anniversary Edition*. USA: Cambridge University Press, 10th ed., 2011.

[59] R. Uzdin and S. Rahav, "Passivity deformation approach to the thermodynamics of isolated quantum setups," *ArXiv 1912.07922*, 2019.

[60] S. Deffner, "Quantum entropy production in phase space," *EPL (Europhysics Letters)*, vol. 103, no. 3, p. 30001, 2013.

[61] J. P. Santos, L. C. Céleri, F. Brito, G. T. Landi, and M. Paternostro, "Spin-phase-space-entropy production," *Physical Review A*, vol. 97, no. 5, pp. 1–10, 2018.

[62] P. Ribeiro, J. Vidal, and R. Mosseri, "Exact spectrum of the lipkin-meshkov-glick model in the thermodynamic limit and finite-size corrections," *Phys. Rev. E*, vol. 78, p. 021106, Aug 2008.

[63] J. M. Radcliffe, "Some properties of coherent spin states," *Journal of Physics A: General Physics*, vol. 4, no. 3, pp. 313–323, 1971.

[64] G. T. Landi, E. Novais, M. J. de Oliveira, and D. Karevski, "Flux rectification in the quantum xxz chain," *Phys. Rev. E*, vol. 90, p. 042142, Oct 2014.

[65] W. Casteels, R. Fazio, and C. Ciuti, "Critical dynamical properties of a first-order dissipative phase transition," *Physical Review A*, vol. 95, no. 1, pp. 1–5, 2017.

[66] N. Bartolo, F. Minganti, W. Casteels, and C. Ciuti, "Exact steady state of a Kerr resonator with one- and two-photon driving and dissipation: Controllable Wigner-function multimodality and dissipative phase transitions," *Physical Review A*, vol. 94, p. 033841, 2016.

[67] H. J. Carmichael, "Breakdown of photon blockade: A dissipative quantum phase transition in zero dimensions," *Physical Review X*, vol. 5, no. 3, p. 031028, 2015.

[68] H. Weimer, "Variational principle for steady states of dissipative quantum many-body systems," *Physical Review Letters*, vol. 114, p. 040402, 2015.

[69] M. Benito, C. S. Munoz, and C. Navarrete-Benlloch, "Degenerate parametric oscillation in quantum membrane optomechanics," *Physical Review A*, vol. 93, no. 2, p. 023846, 2016.

[70] J. Mendoza-Arenas, S. Clark, S. Felicetti, G. Romero, E. Solano, D. Angelakis, and D. Jaksch, "Beyond mean-field bistability in driven-dissipative lattices: Bunching-antibunching transition and quantum simulation," *Physical Review A*, vol. 93, no. 2, p. 023821, 2016.

[71] W. Casteels, F. Storme, A. Le Boité, and C. Ciuti, "Power laws in the dynamic hysteresis of quantum nonlinear photonic resonators," *Phys. Rev. A*, vol. 93, p. 033824, Mar 2016.

[72] M. Foss-Feig, P. Niroula, J. T. Young, M. Hafezi, A. V. Gorshkov, R. M. Wilson, and M. F. Maghrebi, "Emergent equilibrium in many-body optical bistability," *Physical Review A*, vol. 95, p. 043826, 2017.

[73] M. Biondi, G. Blatter, H. E. Türeci, and S. Schmidt, "Nonequilibrium gas-liquid transition in the driven-dissipative photonic lattice," *Physical Review A*, vol. 96, no. 4, p. 043809, 2017.

[74] V. Savona, "Spontaneous symmetry breaking in a quadratically driven nonlinear photonic lattice," *Physical Review A*, vol. 96, p. 033826, 2017.

[75] T. E. Lee, S. Gopalakrishnan, and M. D. Lukin, "Unconventional magnetism via optical pumping of interacting spin systems," *Physical Review Letters*, vol. 110, p. 257204, 2013.

[76] J. Jin, A. Biella, O. Viyuela, L. Mazza, J. Keeling, R. Fazio, and D. Rossini, "Cluster mean-field approach to the steady-state phase diagram of dissipative spin systems," *Physical Review X*, vol. 6, p. 031011, 2016.

[77] E. M. Kessler, G. Giedke, A. Imamoglu, S. F. Yelin, M. D. Lukin, and J. I. Cirac, "Dissipative phase transition in a central spin system," *Physical Review A - Atomic, Molecular, and Optical Physics*, vol. 86, no. 1, p. 012116, 2012.

[78] T. E. Lee, H. Häffner, and M. Cross, "Antiferromagnetic phase transition in a nonequilibrium lattice of rydberg atoms," *Physical Review A*, vol. 84, no. 3, p. 031402, 2011.

[79] C. K. Chan, T. E. Lee, and S. Gopalakrishnan, "Limit-cycle phase in driven-dissipative spin systems," *Physical Review A - Atomic, Molecular, and Optical Physics*, vol. 91, p. 051601, 2015.

[80] R. Rota, F. Storme, N. Bartolo, R. Fazio, and C. Ciuti, "Critical behavior of dissipative two-dimensional spin lattices," *Physical Review B*, vol. 95, p. 134431, 2017.

[81] V. R. Overbeck, M. F. Maghrebi, A. V. Gorshkov, and H. Weimer, "Multicritical behavior in dissipative ising models," *Physical Review A*, vol. 95, no. 4, p. 042133, 2017.

[82] D. Roscher, S. Diehl, and M. Buchhold, "Phenomenology of first-order dark-state phase transitions," *Physical Review A*, vol. 98, no. 6, p. 062117, 2018.

[83] L. M. Sieberer, S. D. Huber, E. Altman, and S. Diehl, "Dynamical critical phenomena in driven-dissipative systems," *Physical Review Letters*, vol. 110, p. 195301, 2013.

[84] L. Sieberer, S. D. Huber, E. Altman, and S. Diehl, "Nonequilibrium functional renormalization for driven-dissipative bose-einstein condensation," *Physical Review B*, vol. 89, no. 13, p. 134310, 2014.

[85] E. Altman, L. M. Sieberer, L. Chen, S. Diehl, and J. Toner, "Two-dimensional superfluidity of exciton polaritons requires strong anisotropy," *Physical Review X*, vol. 5, no. 1, p. 011017, 2015.

[86] A. Wehrl, "General properties of entropy," *Reviews of Modern Physics*, vol. 50, no. 2, pp. 221–260, 1978.

[87] L. D. Landau and E. M. Lifshitz, *Mechanics, Third Edition: Volume 1 (Course of Theoretical Physics)*. Butterworth-Heinemann, 3 ed., Jan. 1976.

[88] C. W. Gardiner, *Handbook of stochastic methods for physics, chemistry and the natural sciences*, vol. 13 of *Springer Series in Synergetics*. Berlin: Springer-Verlag, third ed., 2004.

[89] H. M. Gibbs, S. L. McCall, and T. N. C. Venkatesan, "Differential gain and bistability using a sodium-filled fabry-perot interferometer," *Phys. Rev. Lett.*, vol. 36, pp. 1135–1138, May 1976.

[90] E. Gil-Santos, M. Labousse, C. Baker, A. Goetschy, W. Hease, C. Gomez, A. Lemaître, G. Leo, C. Ciuti, and I. Favero, "Light-mediated cascaded locking of multiple nano-optomechanical oscillators," *Phys. Rev. Lett.*, vol. 118, p. 063605, Feb 2017.

[91] P. Hamel, S. Haddadi, F. Raineri, P. Monnier, G. Beaudoin, I. Sagnes, A. Levenson, and A. M. Yacomotti, "Spontaneous mirror-symmetry breaking in coupled photonic-crystal nanolasers," *Nature Photonics*, vol. 9, no. 5, pp. 311–315, 2015.

[92] J. W. Fleischer, M. Segev, N. K. Efremidis, and D. N. Christodoulides, "Observation of two-dimensional discrete solitons in optically induced nonlinear photonic lattices," *Nature*, vol. 422, no. 6928, pp. 147–150, 2003.

[93] R. Vijay, M. Devoret, and I. Siddiqi, "Invited review article: The josephson bifurcation amplifier," *Review of Scientific Instruments*, vol. 80, no. 11, p. 111101, 2009.

[94] D. L. Underwood, W. E. Shanks, J. Koch, and A. A. Houck, "Low-disorder microwave cavity lattices for quantum simulation with photons," *Phys. Rev. A*, vol. 86, p. 023837, Aug 2012.

[95] M. Eichenfield, J. Chan, R. M. Camacho, K. J. Vahala, and O. Painter, "Optomechanical crystals," *Nature*, vol. 462, no. 7269, pp. 78–82, 2009.

[96] I. Carusotto and C. Ciuti, "Quantum fluids of light," *Reviews of Modern Physics*, vol. 85, no. 1, pp. 299–366, 2013.

[97] N. Y. Kim, K. Kusudo, C. Wu, N. Masumoto, A. Löffler, S. Höfling, N. Kumada, L. Worschech, A. Forchel, and Y. Yamamoto, "Dynamical d-wave condensation of exciton–polaritons in a two-dimensional square-lattice potential," *Nature Physics*, vol. 7, no. 9, pp. 681–686, 2011.

[98] F. Baboux, L. Ge, T. Jacqmin, M. Biondi, E. Galopin, A. Lemaître, L. Le Gratiet, I. Sagnes, S. Schmidt, H. E. Türeci, A. Amo, and J. Bloch, "Bosonic condensation and disorder-induced localization in a flat band," *Phys. Rev. Lett.*, vol. 116, p. 066402, Feb 2016.

[99] A. Amo, J. Lefrère, S. Pigeon, C. Adrados, C. Ciuti, I. Carusotto, R. Houdré, E. Giacobino, and A. Bramati, "Superfluidity of polaritons in semiconductor microcavities," *Nature Physics*, vol. 5, no. 11, pp. 805–810, 2009.

[100] A. Baas, J. P. Karr, H. Eleuch, and E. Giacobino, "Optical bistability in semiconductor microcavities," *Phys. Rev. A*, vol. 69, p. 023809, Feb 2004.

[101] T. Paraïso, M. Wouters, Y. Léger, F. Morier-Genoud, and B. Deveaud-Plédran, "Multistability of a coherent spin ensemble in a semiconductor microcavity," *Nature materials*, vol. 9, no. 8, pp. 655–660, 2010.

[102] S. Rodriguez, A. Amo, I. Sagnes, L. Le Gratiet, E. Galopin, A. Lemaître, and J. Bloch, "Interaction-induced hopping phase in driven-dissipative coupled photonic microcavities," *Nature communications*, vol. 7, no. 1, pp. 1–6, 2016.

[103] F. Minganti, A. Biella, N. Bartolo, and C. Ciuti, "Spectral theory of liouvillians for dissipative phase transitions," *Phys. Rev. A*, vol. 98, p. 042118, Oct 2018.

[104] D. O. Krimer and M. Pletyukhov, "Few-mode geometric description of a driven-dissipative phase transition in an open quantum system," *Phys. Rev. Lett.*, vol. 123, p. 110604, Sep 2019.

[105] S. R. K. Rodriguez, W. Casteels, F. Storme, N. Carlon Zambon, I. Sagnes, L. Le Gratiet, E. Galopin, A. Lemaître, A. Amo, C. Ciuti, and J. Bloch, "Probing a dissipative phase transition via dynamical optical hysteresis," *Phys. Rev. Lett.*, vol. 118, p. 247402, Jun 2017.

[106] K. Vogel and H. Risken, "Quasiprobability distributions in dispersive optical bistability," *Physical Review A*, vol. 39, no. 9, pp. 4675–4683, 1989.

[107] N. Bartolo, F. Minganti, W. Casteels, and C. Ciuti, "Exact steady state of a Kerr resonator with one- and two-photon driving and dissipation: Controllable Wigner-function multimodality and dissipative phase transitions," *Physical Review A*, vol. 94, no. 3, pp. 1–11, 2016.

[108] K. Stannigel, P. Rabl, and P. Zoller, "Driven-dissipative preparation of entangled states in cascaded quantum-optical networks," *New Journal of Physics*, vol. 14, p. 063014, Jun 2012.

[109] D. Roberts and A. Clerk, "Driven-dissipative quantum kerr resonators: new exact solutions, photon blockade and quantum bistability," *ArXiv 1910.00574*, 2019.

[110] R. Roy, R. Short, J. Durnin, and L. Mandel, "First-passage-time distributions under the influence of quantum fluctuations in a laser," *Phys. Rev. Lett.*, vol. 45, pp. 1486–1490, Nov 1980.

[111] F. T. Hioe and S. Singh, "Correlations, transients, bistability, and phase-transition analogy in two-mode lasers," *Phys. Rev. A*, vol. 24, pp. 2050–2074, Oct 1981.

[112] B. Kraus, H. P. Büchler, S. Diehl, A. Kantian, A. Micheli, and P. Zoller, "Preparation of entangled states by quantum markov processes," *Phys. Rev. A*, vol. 78, p. 042307, Oct 2008.

[113] I. S. Gradshteyn and I. M. Ryzhik, *Table of integrals, series, and products*. Academic press, 2014.

[114] H. Risken and K. Vogel, "Quantum tunneling rates in dispersive optical bistability for low cavity damping," *Physical review. A*, vol. 38, pp. 1349–1357, 09 1988.

[115] G. T. Landi, "Lecture notes for quantum information and quantum noise," *University of São Paulo*, 2018.

[116] L. Isserlis, "On a formula for the product-moment coefficient of any order of a normal frequency distribution in any number of variables," *Biometrika*, vol. 12, no. 1/2, pp. 134–139, 1918.

[117] G. C. Wick, "The evaluation of the collision matrix," *Phys. Rev.*, vol. 80, pp. 268–272, Oct 1950.

[118] B. O. Goes, G. T. Landi, E. Solano, M. Sanz, and L. C. Céleri, "Wehrl entropy production rate across a dynamical quantum phase transition," *ArXiv 2004.01126*, 2020.

[119] G. Strang, *Computational Science and Engineering*. Wellesley-Cambridge Press, 2007.

Quantum features of entropy production in driven-dissipative transitions

Bruno O. Goes, Carlos E. Fiore, and Gabriel T. Landi
Instituto de Física, Universidade de São Paulo, CEP 05314-970 São Paulo, São Paulo, Brazil

(Received 6 November 2019; revised manuscript received 18 December 2019; accepted 9 January 2020; published 7 February 2020)

The physics of driven-dissipative transitions is currently a topic of great interest, particularly in quantum optical systems. These transitions occur in systems kept out of equilibrium and are therefore characterized by a finite entropy production rate. However, very little is known about how the entropy production behaves around criticality and all of it is restricted to classical systems. Using quantum phase-space methods, we put forth a framework that allows for the complete characterization of the entropy production in driven-dissipative transitions. Our framework is tailored specifically to describe photon loss dissipation, which is effectively a zero-temperature process for which the standard theory of entropy production breaks down. As an application, we study the open Dicke and Kerr models, which present continuous and discontinuous transitions, respectively. We find that the entropy production naturally splits into two contributions. One matches the behavior observed in classical systems. The other diverges at the critical point.

DOI: 10.1103/PhysRevResearch.2.013136

I. INTRODUCTION

The entropy of an open system is not conserved in time, but instead evolves according to

$$\frac{dS(t)}{dt} = \Pi(t) - \Phi(t), \tag{1}$$

where $\Pi \geqslant 0$ is the irreversible entropy production rate and Φ is the entropy flow rate from the system to the environment. Thermal equilibrium is characterized by $dS/dt = \Pi = \Phi = 0$. However, if the system is connected to multiple sources, it may instead reach a nonequilibrium steady state (NESS) where $dS/dt = 0$ but $\Pi = \Phi \geqslant 0$. NESSs are therefore characterized by the continuous production of entropy, which continuously flows to the environments.

In certain systems a NESS can also undergo a phase transition. These so-called dissipative transitions [1–3] represent the open-system analog of quantum phase transitions. Similarly to the latter, they are characterized by an order parameter and may be either continuous or discontinuous [4–6]. They are also associated with the closing of a gap, although the gap in question is not of a Hamiltonian, but of the Liouvillian generating the open dynamics [7,8]. The features emerging from the competition between dissipation and quantum fluctuations have led to a burst of interest in these systems in the last few years [6–38], including several experimental realizations [39–45].

Given that the fundamental quantity characterizing the NESS is the entropy production rate Π, it becomes natural to ask how Π behaves as one crosses such a transition, such as, i.e., what are its critical exponents? Is it analytic? Does it diverge? Surprisingly, very little is known about this and almost all is restricted to classical systems.

In Ref. [46] the authors studied a continuous transition in a two-dimensional (2D) classical Ising model subject to two baths acting on even and odd sites. They showed that the entropy production rate was always finite, but had a kink at the critical point, with its derivative presenting a logarithmic divergence. A similar behavior was also observed in a Brownian system undergoing an order-disorder transition [47], the majority vote model [48], and a 2D Ising model subject to an oscillating field [49]. In the system of Ref. [49], the transition could also become discontinuous depending on the parameters. In this case they found that the entropy production has a discontinuity at the phase coexistence region. Similar results have been obtained in Ref. [50] for the dissipated work (a proxy for entropy production) in a synchronization transition.

All these results therefore indicate that the entropy production is finite across a dissipative transition, presenting either a kink or a discontinuity. This general behavior was recently shown by some of us to be universal for systems described by classical Pauli master equations and breaking a Z_2 symmetry [51]. An indication that it extends beyond Z_2 was given in Ref. [52] which studied a q-state Potts model.

Whether or not this general trend carries over to the quantum domain remains an open question. Two results, however, seem to indicate that it does not. The first refers to the driven-dissipative Dicke model, studied experimentally in Refs. [39,40]. In this system, the part of the entropy production stemming from quantum fluctuations was found to diverge at the critical point [45]. Second, in Ref. [53] the authors studied the irreversible work produced during a unitary quench evolution of the transverse field Ising model. Although being a different scenario, they also found a divergence in the limit of zero temperature (which is when the model becomes critical). Both results therefore indicate that

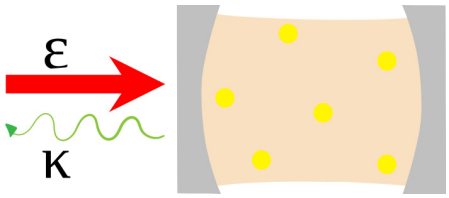

FIG. 1. Typical driven-dissipative scenario portraying an optical cavity with a nonlinear medium subject to an external pump $\mathcal{E}$ and photon losses occurring at a rate κ.

quantum fluctuations may lead to divergences of the entropy production in the quantum regime. Whether these divergences are universal, and what minimal ingredients they require, remains a fundamental open question in the field.

The reason why this issue has so far not been properly addressed is actually technical: most models explored so far fall under the category of a *driven-dissipative process*, where dissipation stems from the loss of photons in an optical cavity [54] (see Fig. 1). The problem is that photon losses are modeled effectively as a zero-temperature bath, for which the standard theory of entropy production yields unphysical results (it is infinite regardless of the state or the process) [55,56].

This "zero-temperature catastrophe" [57,58] occurs because the theory relies on the existence of fluctuations which, in classical systems, seize completely as $T \to 0$. In quantum systems, however, vacuum fluctuations remain. This was the motivation for an alternative formulation introduced by some of us in Ref. [59] and recently assessed experimentally in [45], which uses the Wigner function and its associated Shannon entropy as a starting point to formulate the entropy production problem. This has the advantage of accounting for the vacuum fluctuations, thus leading to a framework that remains useful even when $T \to 0$.

This paper builds on Ref. [59] to formulate a theory which is suited for describing driven-dissipative transitions. Since these transitions are seldom Gaussian, we use here instead the Husimi Q function and its associated Wehrl entropy [56,60]. Our focus is on defining a consistent thermodynamic limit where criticality emerges. This allow us to separate Π into a deterministic term, related to the external laser drive, plus a term related to quantum fluctuations. The latter is also additionally split into two terms, one related to the nontrivial unitary dynamics and the other to photon loss dissipation. We apply our results to the Dicke and Kerr models, two paradigmatic examples of dissipative transitions having a continuous and discontinuous transition respectively. In both cases, we find that unitary part of Π behaves exactly like in classical systems. The dissipative part, on other hand, is proportional to the variance of the order parameter and thus diverges at the critical point.

II. DRIVEN-DISSIPATIVE SYSTEMS

We consider a system described by a set of bosonic modes a_i evolving according to the Lindblad master equation

$$\partial_t \rho = -i\Big[H_0 + i\sum_i \mathcal{E}_i(a_i^\dagger - a_i),\, \rho\Big] + \sum_i 2\kappa_i\Big(a_i\rho a_i^\dagger - \frac{1}{2}\{a_i^\dagger a_i,\, \rho\}\Big), \tag{2}$$

where H_0 is the Hamiltonian, $\mathcal{E}_i$ are external pumps, and κ_i are the loss rates for each mode (see Fig. 1). The second term in Eq. (2) is the typical Lindblad dissipator describing one-photon losses of a cavity. The results below hold for arbitrary times in the dynamics, although most of our interest will be in the NESS, defined as the fixed point $d\rho/dt = 0$.

We work in phase space by defining the Husimi function $Q(\mu, \bar{\mu}) = \frac{1}{\pi}\langle\mu|\rho|\mu\rangle$, where $|\mu\rangle = \bigotimes_i |\mu_i\rangle$ are coherent states and $\bar{\mu}$ denotes complex conjugation. The master Eq. (2) is then converted into a quantum Fokker-Planck (QFP) equation [61],

$$\partial_t Q = \mathcal{U}(Q) + \sum_i \big(\partial_{\mu_i} J_i(Q) + \partial_{\bar{\mu}_i}\bar{J}_i(Q)\big), \tag{3}$$

where $\mathcal{U}(Q)$ is a differential operator related to the unitary part (see Appendixes A–C for examples) and $J_i(Q) = \kappa_i(\mu_i Q + \partial_{\bar{\mu}_i} Q)$ are irreversible quasiprobability currents associated with the photon loss dissipators.

As our basic entropic quantifier, we use the Shannon entropy of Q, known as Wehrl's entropy [60],

$$S(Q) = -\int d^2\mu\; Q \ln Q. \tag{4}$$

This quantity can be attributed an operational interpretation by viewing $Q(\mu, \bar{\mu})$ as the probability distribution for the outcomes of a heterodyne measurement. $S(Q)$ then quantifies the entropy of the system convoluted with the additional noise introduced by the heterodyning [62,63]. As a consequence, $S(Q) \geqslant S(\rho)$, with both converging in the semiclassical limit. We also mention that the Wehrl entropy has the unique advantage of being well defined for any quantum state, since $Q \geqslant 0$. This is in contrast with the Wigner entropy, which can become imaginary if the Wigner function is negative.

Next, we differentiate Eq. (4) with respect to time and use Eq. (3). Employing a standard procedure developed for classical systems [64], we can separate dS/dt as in Eq. (1), with an entropy flux rate given by

$$\Phi = \sum_i 2\kappa_i\langle a_i^\dagger a_i\rangle, \tag{5}$$

and an entropy production rate

$$\Pi = -\int d^2\mu\, \mathcal{U}(Q)\ln Q + \sum_i \frac{2}{\kappa_i}\int d^2\mu \frac{|J_i(Q)|^2}{Q}. \tag{6}$$

The entropy flux is seen to be always non-negative, which is a consequence of the fact that the dissipator is at zero temperature, so that entropy cannot flow from the bath to the system, only the other way around. As for Π in Eq. (6), the last term is the typical dissipative contribution, related to the photon loss channels and also found in [59]. The

extension to a finite temperature dissipator is straightforward and requires only a small modification of the currents J_i [59]. The new feature in Eq. (6) is the first term, which is related to the unitary contribution $\mathcal{U}(Q)$. Unlike the von Neumann entropy, the unitary dynamics can affect the Wehrl entropy. This is due to the fact that the unitary dynamics can already lead to diffusionlike terms in the Fokker-Planck Eq. (3), as discussed, e.g., in Ref. [65].

III. THERMODYNAMIC LIMIT

The results in Eqs. (5) and (6) hold for a generic master equation of the form (2), irrespective of whether or not the system is critical. We now reach the key part of our paper, which is to specialize the previous results to the scenario of driven-dissipative critical systems. The first ingredient that is needed is the notion of a thermodynamic limit. For driven-dissipative systems, criticality emerges when the pump(s) $\mathcal{E}_i$ become sufficiently large. It is therefore convenient to parametrize $\mathcal{E}_i = \epsilon_i\sqrt{N}$ and define the thermodynamic limit as $N \to \infty$, with ϵ_i finite. In driven systems $\langle a_i\rangle$ always scales proportionally to $\mathcal{E}_i$, so that we can also define $\langle a_i\rangle = \alpha_i\sqrt{N}$, where the α_i are finite and represent the order parameters of the system.

The parameter N, representing the thermodynamic limit, can therefore be thought of as being proportional to the number of photons in the pump which, in turn, is roughly the number of photons in the cavity. Thus, criticality in driven-dissipative models occur when the number of photons becomes very large. From a theoretical point of view, however, N is to be viewed as knob allowing one to tune the model towards a critical behavior.

This combination of scalings implies that at the mean-field level ($a_i \to \langle a_i\rangle$) the pump term $\mathcal{E}_i(a_i^\dagger - a_i)$ in (2) will be $O(N)$; i.e., extensive. We shall henceforth assume that the parameters in the model are such that this is also true for H_0 in Eq. (2) (see below for examples).

Introducing displaced operators $\delta a_i = a_i - \alpha_i\sqrt{N}$, the entropy flux (5) is naturally split as

$$\Phi = \Phi_{\rm ext} + \Phi_q = N\sum_i 2\kappa_i|\alpha_i|^2 + \sum_i 2\kappa_i\langle\delta a_i^\dagger\delta a_i\rangle. \quad (7)$$

The first term is extensive in N and depends solely on the mean-field values $|\alpha_i|$. It is thus independent of fluctuations. The second term, on the other hand, is intensive in N. In fact, it is proportional to the variance of the order parameter $\langle\delta a_i^\dagger\delta a_i\rangle$ (the susceptibility) and thus captures the contributions from quantum fluctuations.

We can also arrive at a similar splitting for the entropy production (6). Defining displaced phase-space variables $\nu_i = \mu_i - \alpha_i\sqrt{N}$, the currents J_i in the QFP Eq. (3) are split as $J_i = \sqrt{N}\kappa_i\alpha_i Q + J_i^\nu(Q)$, where $J_i^\nu = \kappa_i(\nu_i Q + \partial_{\bar\nu_i}Q)$. Substituting in (6) then yields

$$\Pi = \Pi_{\rm ext} + \Pi_u + \Pi_d = N\sum_i 2\kappa_i|\alpha_i|^2 - \int d^2\nu\, \mathcal{U}(Q)\ln Q + \sum_i \frac{2}{\kappa_i}\int d^2\nu\, \frac{|J_i^\nu(Q)|^2}{Q}. \quad (8)$$

This is the main result in this paper. It offers a splitting of the total entropy production rate into three contributions with distinct physical interpretations. The first, $\Pi_{\rm ext}$, is extensive and depends solely on the mean-field values α_i. It therefore corresponds to a fully deterministic contribution, independent of fluctuations. Comparing with Eq. (7), we see that

$$\Pi_{\rm ext} = \Phi_{\rm ext}, \quad (9)$$

a balance which holds irrespective of whether the system is in the NESS. Hence, this contribution does not affect the system entropy: At the mean-field level, all entropy produced flows to the environment.

The second and third terms in Eq. (8) represent, respectively, the unitary and dissipative contributions to Π. These two terms account for the contributions to the entropy production stemming from quantum fluctuations. This becomes more evident in the NESS ($dS/dt = 0$), where combining Eqs. (1) and (9) leads to

$$\Pi_u + \Pi_d = \Phi_q. \quad (10)$$

The two terms Π_u and Π_d therefore represent two sources for the quantum entropy Φ_q in Eq. (7). We also note in passing that while $\Pi_d \geqslant 0$, the same is not necessarily true for Π_u, although this turns out to be the case in the examples treated below.

IV. KERR BISTABILITY

To illustrate how the different contributions to the entropy production in Eq. (8) behave across a dissipative transition, we now apply our formalism to two prototypical models. The first is the Kerr bistability model [11,26,54], described by Eq. (2) with a the single mode a and Hamiltonian

$$H_0 = \Delta a^\dagger a + \frac{u}{2N}a^\dagger a^\dagger aa, \quad (11)$$

where Δ is the detuning and u is the nonlinearity strength. This model has a discontinuous transition.

The NESS of this model and the terms in Eq. (8) were computed using numerically exact methods. Details on the numerical calculations are provided Appendix B and the main results are shown in Fig. 2. In Figs. 2(a) and 2(b) we plot Π_u and Π_d for different sizes N. As can be seen, Π_u has a discontinuity at the critical point when $N \to \infty$. Conversely, Π_d diverges. The critical behavior in the thermodynamic limit ($N \to \infty$) can be better understood by performing a finite size analysis [Figs. 2(c) and 2(d)], where we plot Π_u and Π_d/N vs $N(\epsilon/\epsilon_c - 1)$ for multiple values of N. Surprisingly, we find that the behavior of Π_u matches exactly that of the classical entropy production in a discontinuous transition [49,51,52]. We also see from Fig. 2 that Π_u is negligible compared to Π_d. As a consequence, in view of Eq. (10) the dissipative contribution Π_d will behave like the variance of the order parameter $\langle\delta a^\dagger\delta a\rangle$, which diverges at the critical point. This is clearly visible in Fig. 2(d), which plots Π_d/N.

V. DRIVEN-DISSIPATIVE DICKE MODEL

The second model we study is the driven-dissipative Dicke model [39,40]. It is described by Eq. (2) with a mode a, subject to photon loss dissipation κ, as well as a macrospin

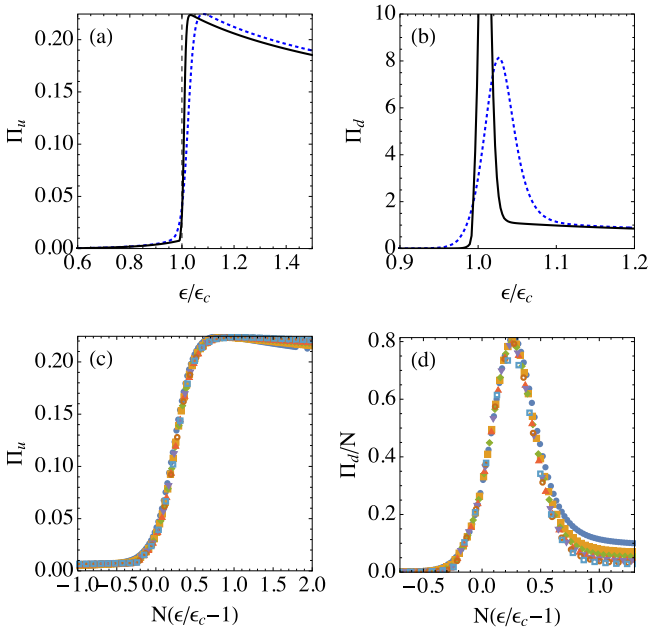

FIG. 2. Entropy production in the discontinuous transition of the Kerr bistability model [Eq. (11)]. (a), (b) Unitary and dissipative contributions Π_u and Π_d for $N = 30$ (black-solid) and 10 (blue-dashed). (c), (d) Finite-size analysis showing a data collapse of Π_u and Π_d/N vs $N(\epsilon/\epsilon_c - 1)$ for multiple values of N (from 10 to 40 in steps of 5). The critical behavior of Π_u matches that of the classical entropy production. Π_d, on the other hand, behaves similarly to $\langle \delta a^\dagger \delta a \rangle$ and thus diverges at the critical point. Other parameters were $\kappa = 1/2$, $\Delta = -2$, and $u = 1$.

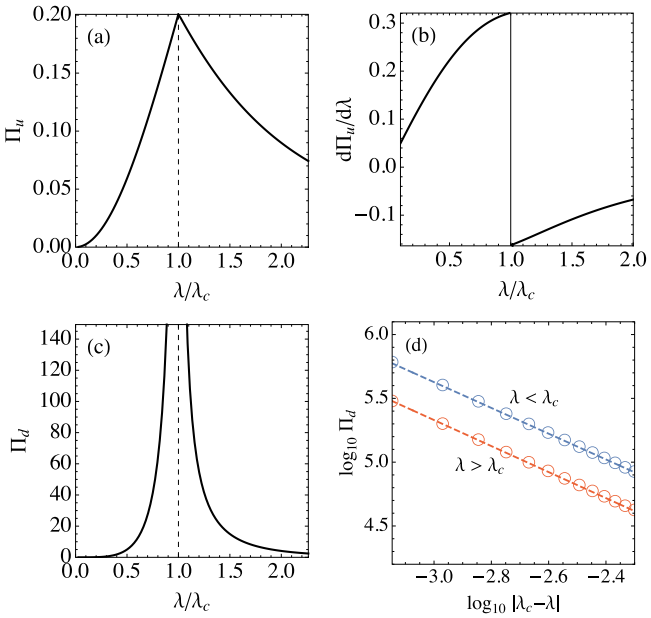

FIG. 3. Entropy production in the continuous transition of the driven-dissipative Dicke model [Eq. (12)]. (a), (b) Π_u and $d\Pi_u/d\lambda$ vs λ. This part of the entropy production is continuous, but has a kink (discontinuous first derivative) at the critical point $\lambda_c = \sqrt{\omega_0(\kappa^2+\omega^2)/\omega}$. (c) Π_d vs λ showing a divergence at λ_c. (d) $\log_{10}\Pi_d$ vs $\log_{10}|\lambda_c - \lambda|$ at the vicinity of λ_c. The points correspond to simulations, whereas the straight lines are fits with slope -1, showing that Π_d diverges as in Eq. (13). Other parameters were $\omega_0 = 0.005$, $\omega = 0.01$, and $\kappa = 1$.

of size $J = N/2$. The Hamiltonian is

$$H_0 = \omega_0 J_z + \omega a^\dagger a + \frac{2\lambda}{\sqrt{N}}(a + a^\dagger)J_x, \tag{12}$$

where J_i are macrospin operators. This model does not need a drive $\mathcal{E}$ since the last term can already be interpreted as a kind of "operator valued pump" (as it is linear in $a + a^\dagger$). In fact, this is precisely how this model was experimentally implemented in a cold-atom setup [39]. The model can also be pictured as purely bosonic by introducing an additional mode b according to the Holstein-Primakoff map $J_z = b^\dagger b - N/2$ and $J_- = \sqrt{N - b^\dagger b}\, b$. It hence falls under the category of Eq. (2), with two modes a and b.

Since this is a two-mode model, numerically exact results are more difficult. Instead, we follow Refs. [39,40,45] and consider a Gaussianization of the model valid in the limit of N large. Details are provided in Appendix C and the results are shown in Fig. 3. Once again, the unitary part Π_u of the entropy production [Figs. 3(a) and 3(b)] is found to behave like the mean-field predictions for classical transitions [46–52]. It is continuous and finite, but presents a kink (the first derivative is discontinuous) at the critical point $\lambda_c = \sqrt{\omega_0(\kappa^2+\omega^2)/\omega}$.

The dissipative part Π_d, on the other hand, diverges at λ_c. This was indeed already shown experimentally in Ref. [45]. In fact, the behavior of Π_d at the vicinity of λ_c is of the form

$$\Pi_d \sim \frac{1}{|\lambda_c - \lambda|}, \tag{13}$$

as confirmed by the analysis in Fig. 3(d). Similarly to the Kerr model, Π_u is much smaller than Π_d so that the latter essentially coincides with $2\kappa\langle \delta a^\dagger \delta a \rangle$ in the NESS [cf. Eq. (10)]. The divergence in (13) thus mimics the behavior of $\langle \delta a^\dagger \delta a \rangle$.

VI. DISCUSSION

Understanding the behavior of the entropy production across a nonequilibrium transition is both a timely and important question, specially concerning driven-dissipative quantum models, which have found renewed interest in recent years. This paper provides a framework for computing the entropy production for the zero-temperature dissipation appearing in driven-dissipative models.

We then applied our formalism to two widely used models. In both cases we found that one contribution Π_u behaved qualitatively similar to that of the entropy production in classical dissipative transitions. The other, Π_d, behaved like a susceptibility, diverging at the critical point. Why Π_u behaves in this way, remains an open question. Driven-dissipative systems have one fundamental difference when compared to classical systems. In the latter, energy input and output both take place incoherently, through the transition rates in a master equation. In driven-dissipative systems, on the other hand, the energy output is incoherent (Lindblad-like) but the input is coherent (the pump). A classical analog of this is an electrical circuit coupled to an external battery $\mathcal{E}$. For instance, the entropy production in a simple RL circuit is $\Pi_{\rm RL} = \mathcal{E}^2/RT$

[66] where R is the resistance and T is the temperature. If we consider an empty cavity with a single mode a and $H_0 = 0$, Eq. (6) predicts $\Pi_{\text{cavity}} = 2\mathcal{E}^2/\kappa$. Notwithstanding the similarity between the two results, one must bear in mind that the RL circuit still contains incoherent energy input. Indeed, Π_{RL} diverges as $T \to 0$. The cavity, on the other hand, relies solely on vacuum fluctuations. This interplay between thermal and quantum fluctuations highlights the need for extending the present analysis to additional models of driven-dissipative transitions. In particular, it would be valuable to explore models which can be tuned between classical (e.g., for large T) and quantum ($T = 0$) transitions.

ACKNOWLEDGMENTS

The authors acknowledge fruitful discussions with M. Paternostro, T. Donner, W. Nunes, and L. C. Céleri. The authors acknowledge R. Uzdin for fruitful discussion, as well as for coining the term "zero-temperature catastrophe." G.T.L. and C.E.F. acknowledge the financial support from the São Paulo Research Foundation (FAPESP) under Grants No. 2018/12813-0, No. 2017/50304-7, No. 2017/07973-5, and No. 2018/02405-1. B.O.G. acknowledges the support from the Brazilian funding agency CNPq and T. Roberta for drawing Fig. 1.

APPENDIX A: PROPERTIES OF Π_u

The entropy production rate in Eq. (6) of the main text has a term proportional to the unitary dynamics,

$$\Pi_u = -\int d^2\mu\, \mathcal{U}(Q) \ln Q, \tag{A1}$$

which depends on the differential operator $\mathcal{U}(Q)$, representing the unitary contribution to the QFP Eq. (3). Written in this way, the physics behind this term is not immediately transparent. To shed light on this, we focus here the case of a single mode. The Hamiltonian may then always be written in normal order as

$$H_0 = \sum_{r,s} H_{rs} (a^\dagger)^r a^s, \tag{A2}$$

for some coefficients H_{rs}. The thermodynamic limit hypothesis used in the main text is that H_0 should be $O(N)$ at the mean-field level ($a_i \to \langle a_i \rangle$). This implies that $H_{rs} = h_{rs} N^{1-(r+s)/2}$, where the h_{rs} are independent of N. For instance, the coefficient multiplying $a^\dagger a^\dagger a a$ should scale as $1/N$ [as in Eq. (11)]. We may thus write (A2) as

$$H_0 = N \sum_{r,s} h_{rs} \left(\frac{a^\dagger}{\sqrt{N}}\right)^r \left(\frac{a}{\sqrt{N}}\right)^s. \tag{A3}$$

The corresponding phase-space contribution $\mathcal{U}(Q)$ can be found using standard correspondence tables [61] to convert the master equation term $-i[H_0, \rho]$ into a corresponding differential operator for Q. The result is

$$\mathcal{U}(Q) = -iN \sum_{r,s} \frac{h_{rs}}{N^{(r+s)/2}} \{\bar{\mu}^r (\mu + \partial_{\bar{\mu}})^s - \mu^s (\bar{\mu} + \partial_\mu)^r\} Q. \tag{A4}$$

Normal ordering is convenient as it pushes all derivatives to the right. We now change variables to $\nu = \mu - \alpha\sqrt{N}$ and expand the result in a power series in N.

This yields, to leading order,

$$\begin{aligned}\mathcal{U}(Q) = &-i\sqrt{N} \sum_{r,s} h_{rs} \alpha^{s-1} \bar{\alpha}^{r-1} (s\bar{\alpha}\partial_{\bar{\nu}} - r\alpha\partial_\nu) Q \\ &- i \sum_{r,s} h_{rs} \frac{\alpha^{s-2}\bar{\alpha}^{r-2}}{2} \big[s(s-1)(\bar{\alpha})^2 \big(2\nu\partial_{\bar{\nu}} + \partial_{\bar{\nu}}^2\big) \\ &- r(r-1)\alpha^2 \big(2\bar{\nu}\partial_\nu + \partial_\nu^2\big) + 2rs|\alpha|^2 (\bar{\nu}\partial_{\bar{\nu}} - \nu\partial_\nu) \big] Q \\ &+ \mathcal{O}(1/\sqrt{N}).\end{aligned} \tag{A5}$$

The remaining terms in the expansion are at least $O(1/\sqrt{N})$ and thus vanish in the limit $N \to \infty$. This expression may be further simplified by introducing the constants

$$\xi_1 = -i \sum_{r,s} h_{rs}\, \alpha^{s-1} \bar{\alpha}^r s, \tag{A6}$$

$$\xi_2 = -i \sum_{r,s} h_{rs}\, \alpha^{s-2} \bar{\alpha}^r s(s-1), \tag{A7}$$

$$\xi_{11} = -i \sum_{r,s} h_{rs}\, \alpha^{s-1} \bar{\alpha}^{r-1} rs. \tag{A8}$$

Then, since $h_{rs} = h_{sr}^*$, we can write (A5) as

$$\begin{aligned}\mathcal{U}(Q) = &\sqrt{N}(\xi_1 \partial_{\bar{\nu}} + \bar{\xi}_1 \partial_\nu) Q + \tfrac{1}{2} \big[\xi_2 \big(2\nu\partial_{\bar{\nu}} + \partial_{\bar{\nu}}^2\big) \\ &+ \bar{\xi}_2 \big(2\bar{\nu}\partial_\nu + \partial_\nu^2\big) + 2\xi_{11} (\bar{\nu}\partial_{\bar{\nu}} - \nu\partial_\nu) \big] Q + O(1/\sqrt{N}).\end{aligned} \tag{A9}$$

This is the leading-order contributions of the unitary dynamics to the Fokker-Planck equation. The important point to notice is the existence of *diffusive* terms (proportional to the second derivative ∂_ν^2 and $\partial_{\bar{\nu}}^2$). This is a known feature of the Husimi function.

We now plug Eq. (A9) into Eq. (A1). Integrating by parts multiple times and using the fact that the Husimi function always vanishes at infinity, we find that the only surviving terms are

$$\Pi_u = \frac{1}{2} \int \frac{d^2\nu}{Q} [\xi_2 (\partial_{\bar{\nu}} Q)^2 + \bar{\xi}_2 (\partial_\nu Q)^2], \tag{A10}$$

which provides the leading-order contribution to Π_u. In the limit $N \to \infty$ this is the only contribution which survives.

APPENDIX B: SOLUTION OF THE KERR BISTABILITY PROBLEM

In this section we provide additional details on the solution methods used to study the entropy production in the Kerr model [Eq. (11) of the main text]. The NESS of this model can be found analytically using the generalized P function [54]. This includes all moments of the form $\langle (a^\dagger)^r a^s \rangle$, as well as the Wigner function [67]. While the Husimi function can in principle be found numerically from the Wigner function, we have found that this is quite numerically unstable due to the highly irregular nature of the latter. Instead, it is easier to simply find the steady-state density matrix ρ numerically using standard vectorization techniques (as done, e.g., in Ref. [26]).

1. Numerical procedure

The numerical calculations were performed as follows. We define the Liouvillian corresponding to the master equation (2) as

$$\mathcal{L}(\rho) = -i[H_0 + i\epsilon\sqrt{N}(a^\dagger - a), \rho] + 2\kappa\left(a\rho a^\dagger - \tfrac{1}{2}\{a^\dagger a, \rho\}\right). \tag{B1}$$

The steady-state equation,

$$\mathcal{L}(\rho) = 0, \tag{B2}$$

is then interpreted as an eigenvalue/eigenvector equation: ρ is the eigenvector of $\mathcal{L}$ with eigenvalue 0. To carry out the calculation, we decompose ρ in the Fock basis, using a sufficiently large number of states $n_{\max}$ to ensure convergence.

From ρ we then compute the Husimi function and the corresponding integrals numerically using standard integration techniques. The Husimi function is obtained by constructing approximate coherent states

$$|\mu\rangle = e^{-|\mu|^2/2}\sum_{n=0}^{n_{\max}} \frac{\mu^n}{\sqrt{n!}}|n\rangle.$$

A grid of the Husimi function $Q(\mu, \bar{\mu})$ can then be built to be subsequently integrated numerically. Derivatives of Q do not need to be computed using finite differences. Instead, one may notice that, for instance,

$$\partial_{\bar{\mu}} Q = -\mu Q + \frac{1}{\pi}\langle\mu|a\rho|\mu\rangle, \tag{B3}$$

with similar expressions for other derivatives. Finally, convergence of the numerical integration can be verified by computing moments $\langle(a^\dagger)^r a^s\rangle$ of arbitrary order from the Husimi function and comparing with the exact results of Ref. [54].

2. Bistable behavior

For fixed κ, U, and $\Delta < 0$, the NESS of Eq. (B1) presents a discontinuous transition at a certain critical value ϵ_c. This transition is related to a bistable behavior of the model at the mean-field level. For finite N the steady state of (B1) is unique [54]. However, as shown recently in Ref. [26], in the limit $N \to \infty$ the Liouvillian gap between the steady state and the first excited state closes asymptotically in the region between

$$\epsilon_\pm = \sqrt{n_\pm[\kappa^2 + (\Delta + n_\pm u)^2]} \quad \text{and} \quad n_\pm = \frac{-2\Delta \pm \sqrt{\Delta^2 - 3\kappa^2}}{3u}. \tag{B4}$$

From a numerical point of view, however, this causes no interference since all computations are done for finite N, where the NESS is unique.

3. Unitary contribution to the quantum Fokker-Planck equation

The unitary contribution $\mathcal{U}(Q)$ appearing in Eq. (4) of the main text can be obtained using standard correspondence tables [61] and reads

$$\mathcal{U}(Q) = (i\mu\Delta - \mathcal{E})\partial_\mu Q - (i\bar{\mu}\Delta + \mathcal{E})\partial_{\bar{\mu}} Q + \frac{iu}{2N}\left\{2|\mu|^2(\mu\partial_\mu Q - \bar{\mu}\partial_{\bar{\mu}} Q) + \mu^2\partial_\mu^2 Q - \bar{\mu}^2\partial_{\bar{\mu}}^2 Q\right\}. \tag{B5}$$

When plugged into Eq. (A1), the terms proportional to Δ and $\mathcal{E}$ vanish. The only surviving terms are

$$\Pi_u = \frac{iu}{2N}\int \frac{d^2\mu}{Q}[\mu^2(\partial_\mu Q)^2 - \bar{\mu}^2(\partial_{\bar{\mu}} Q)^2]. \tag{B6}$$

Substituting $\mu = \alpha\sqrt{N} + \nu$ yields a leading contribution of $O(1)$ which, of course, is the same as that which would be obtained using Eq. (A10) with $r = s = 2$.

APPENDIX C: SOLUTION OF THE DRIVEN-DISSIPATIVE DICKE MODEL

Here we describe the calculations for the driven-dissipative Dicke model [Eq. (12) of the main text]. We consider only a single source of drive and dissipation $(\mathcal{E}, \kappa)$ acting on the optical cavity mode a. The full master equation is then

$$\frac{d\rho}{dt} = -i[H, \rho] + 2\kappa\left[a\rho a^\dagger - \tfrac{1}{2}\{a^\dagger a, \rho\}\right], \tag{C1}$$

with

$$H = \omega_0 J_z + \omega a^\dagger a + \frac{2\lambda}{\sqrt{N}}(a + a^\dagger)J_x. \tag{C2}$$

Since this system involves two modes, direct solution by vectorization becomes computationally too costly. Instead, we tackle the problem using Gaussianization. The calculations are done in detail in Refs. [39,40,45]. Here we simply cite the main results and adapt the notation to our present interests.

1. Mean-field solution

We start by looking at the mean-field level by introducing $\langle a\rangle = \alpha\sqrt{N}$, $\langle J_-\rangle = \beta N$, and $\langle J_z\rangle = wN$. For large N we then get

$$\frac{d\alpha}{dt} = -(\kappa + i\omega)\alpha - i\lambda(\beta + \beta^*), \tag{C3}$$

$$\frac{d\beta}{dt} = -i\omega_0\beta + 2i\lambda(\alpha + \bar{\alpha})w, \tag{C4}$$

$$\frac{dw}{dt} = i\lambda(\alpha + \bar{\alpha})(\beta - \beta^*), \tag{C5}$$

which are independent of N, as expected. Angular momentum conservation also imposes $w^2 + |\beta|^2 = 1/4$, which leads to two choices, $w = \pm\frac{1}{2}\sqrt{1 - 4\beta^2}$.

At the steady state this implies that $\beta^* = \beta$,

$$\alpha = -\frac{2i\lambda\beta}{\kappa + i\omega}, \tag{C6}$$

and

$$-\beta\sqrt{1 - 4\beta^2} = \pm\frac{\lambda_c^2}{\lambda^2}\beta, \tag{C7}$$

where $\lambda_c = \frac{1}{2}\sqrt{\frac{\omega_0}{\omega}(\kappa^2+\omega^2)}$ is the critical interaction in the absence of any external drives. The $\pm$ sign in Eq. (C7) stems from the two choices $w = \pm\frac{1}{2}\sqrt{1-4\beta^2}$ respectively. The minus solution in Eq. (C7) always yields the trivial result $\beta = 0$. The plus solution, on the other hand, can be nontrivial when $\lambda > \lambda_c$. For this reason, we henceforth focus on the solution of

$$\beta\sqrt{1-4\beta^2} = \frac{\lambda_c^2}{\lambda^2}\beta, \tag{C8}$$

which yields either $\beta = 0$ or $\beta \in [0, 1/2]$. Moreover, this solution corresponds to $w = -\frac{1}{2}\sqrt{1-4\beta^2}$, so that the spin is pointing downwards.

2. Holstein-Primakoff expansion

Next we introduce a Holstein-Primakoff expansion

$$J_z = b^\dagger b - \frac{N}{2}, \tag{C9}$$

$$J_- = \sqrt{N - b^\dagger b}\, b \tag{C10}$$

and expand

$$a = \alpha\sqrt{N} + \delta a, \quad b = \tilde{\beta}\sqrt{N} + \delta b, \tag{C11}$$

for α and $\tilde{\beta}$ independent of N. The constant $\tilde{\beta}$ can be related with $\beta = \langle J_-\rangle/N$ by expanding Eq. (C10) in a power series in $1/N$, resulting in

$$\tilde{\beta}\sqrt{1-\tilde{\beta}^2} = \beta, \tag{C12}$$

which has two solutions

$$\tilde{\beta}_\pm = \sqrt{\frac{1\pm\sqrt{1-4\beta^2}}{2}}. \tag{C13}$$

Which solution to choose is fixed by imposing that Eq. (C9) should also comply with $\langle J_z\rangle = w\sqrt{N}$ and $w = -\frac{1}{2}\sqrt{1-4\beta^2}$. This fixes $\tilde{\beta}_-$ as the appropriate choice. It is also useful to note that $\tilde{\beta}_+^2 + \tilde{\beta}_-^2 = 1$ and $\tilde{\beta}_-\tilde{\beta}_+ = \beta$.

In terms of the expansion (C11) the operator J_z in Eq. (C9) becomes

$$J_z = \frac{N}{2}\sqrt{1-4\beta^2} + \sqrt{N}\tilde{\beta}_-(\delta b + \delta b^\dagger) + \delta b^\dagger \delta b. \tag{C14}$$

We similarly expand J_- in Eq. (C10), leading to

$$\begin{aligned} J_- = {} & N\beta + \sqrt{N}\tilde{\beta}_+\left[\delta b - \frac{1}{2}\frac{\tilde{\beta}_-^2}{\tilde{\beta}_+^2}(\delta b + \delta b^\dagger)\right] \\ & - \frac{\tilde{\beta}_-}{2\tilde{\beta}_+}\left[\delta b^\dagger\delta b + (\delta b + \delta b^\dagger)\delta b + \frac{\tilde{\beta}_-^2}{4\tilde{\beta}_+^2}(\delta b + \delta b^\dagger)^2\right] \\ & + \mathcal{O}(1/\sqrt{N}). \end{aligned} \tag{C15}$$

Substituting Eqs. (C14) and (C15) into Eq. (C2) we find, to leading order, the quadratic Hamiltonian

$$\begin{aligned} H = {} & \tilde{\omega}_0\delta b^\dagger\delta b + \omega\delta a^\dagger\delta a + \tilde{\lambda}(\delta a + \delta a^\dagger)(\delta b + \delta b^\dagger) \\ & - \zeta(\delta b + \delta b^\dagger)^2, \end{aligned} \tag{C16}$$

where

$$\tilde{\omega}_0 = \omega_0 - \lambda(\alpha + \bar{\alpha})\frac{\tilde{\beta}_-}{\tilde{\beta}_+}, \tag{C17}$$

$$\tilde{\lambda} = \lambda\tilde{\beta}_+\left(1 - \frac{\tilde{\beta}_-^2}{\tilde{\beta}_+^2}\right), \tag{C18}$$

$$\zeta = \frac{\lambda(\alpha+\bar{\alpha})}{2}\frac{\tilde{\beta}_-}{\tilde{\beta}_+}\left(1 + \frac{\tilde{\beta}_-^2}{2\tilde{\beta}_+^2}\right). \tag{C19}$$

3. Stabilization of the solution

The Gaussianization procedure above explicitly already takes the limit $N \to \infty$. Because of this, it turns out that on order to obtain a stable steady state, it is also necessary to add a small dissipation to δb. Here we do so in the simplest way possible, as a zero-temperature dissipator. We therefore consider the evolution of the Gaussianized master equation

$$\frac{d\rho}{dt} = -i[H,\rho] + 2\kappa\mathcal{D}[\delta a] + 2\gamma\mathcal{D}[\delta b], \tag{C20}$$

where $D[L] = L\rho L^\dagger - \frac{1}{2}\{L^\dagger L, \rho\}$. The value of γ was actually determined experimentally in [45] and is more than six orders of magnitude smaller than κ. One must therefore use a nonzero value, but the value itself can be arbitrarily small. In Fig. 3 of the main text, we have used $\gamma = 10^{-3}\kappa$ simply to ensure numerical stability.

4. Lyapunov equation

Once Gaussianized, we can study the steady state by solving for the second moments of δa and δb. Define quadrature operators

$$\delta q_b = \frac{\delta b + \delta b^\dagger}{\sqrt{2}} \quad \delta p_b = \frac{i}{\sqrt{2}}(\delta b^\dagger - \delta b), \tag{C21}$$

with identical definitions for δq_a and δp_a. The Hamiltonian (C16) then transforms to

$$H_2 = \frac{\tilde{\omega}_0}{2}\left(\delta q_b^2 + \delta p_b^2\right) + \frac{\omega}{2}\left(\delta q_a^2 + \delta p_a^2\right) + 2\tilde{\lambda}\delta q_a\delta q_b - 2\zeta\delta q_b^2. \tag{C22}$$

Next define the covariance matrix (CM)

$$\sigma_{ij} = \tfrac{1}{2}\langle\{R_i, R_j\}\rangle, \quad \boldsymbol{R} = (\delta q_b, \delta p_b, \delta q_a, \delta p_a). \tag{C23}$$

Since both the Hamiltonian and the dissipator are Gaussian preserving, the dynamics of σ is closed and described by a Lyapunov equation,

$$\frac{d\sigma}{dt} = A\sigma + \sigma A^{\mathrm{T}} + \mathcal{D}, \tag{C24}$$

where

$$A = \begin{pmatrix} -\gamma & \tilde{\omega}_0 & 0 & 0 \\ 4\zeta - \tilde{\omega}_0 & -\gamma & -2\tilde{\lambda} & 0 \\ 0 & 0 & -\kappa & \omega \\ -2\tilde{\lambda} & 0 & -\omega & -\kappa \end{pmatrix} \tag{C25}$$

and $\mathcal{D} = \mathrm{diag}(\gamma, \gamma, \kappa, \kappa)$.

The assumption that the state of the system can be Gaussianized allows us to write down the Husimi function of the NESS, which has the form

$$Q = \frac{1}{\pi\sqrt{|\sigma + \mathbb{I}_4/2|}} \exp\left\{-\tfrac{1}{2}\boldsymbol{r}^{\mathrm{T}}(\sigma + \mathbb{I}_4/2)^{-1}\boldsymbol{r}\right\}, \tag{C26}$$

where $\boldsymbol{r} = (x_b, y_b, x_a, y_a)$ are the phase-space variables corresponding to the quadrature operators $\boldsymbol{R}$ in Eq. (C23) and $\mathbb{I}_4$ is the identity matrix of dimension 4. All integrals appearing in Eq. (8) will then be Gaussian and can thus be trivially computed.

[1] M. J. Hartmann, F. G. S. L. Brandão, and M. B. Plenio, Nat. Phys. **2**, 849 (2006).
[2] S. Diehl, A. Micheli, A. Kantian, B. Kraus, H. P. Büchler, and P. Zoller, Nat. Phys. **4**, 878 (2008).
[3] F. Verstraete, M. M. Wolf, and J. I. Cirac, Nat. Phys. **5**, 633 (2009).
[4] J. Marro and R. Dickman, *Nonequilibrium Phase Transitions in Lattice Models*, 1st ed. (Cambridge University Press, Cambridge, UK, 1999).
[5] A. Tomadin, S. Diehl, and P. Zoller, Phys. Rev. A **83**, 013611 (2011).
[6] H. J. Carmichael, Phys. Rev. X **5**, 031028 (2015).
[7] E. M. Kessler, G. Giedke, A. Imamoglu, S. F. Yelin, M. D. Lukin, and J. I. Cirac, Phys. Rev. A **86**, 012116 (2012).
[8] F. Minganti, A. Biella, N. Bartolo, and C. Ciuti, Phys. Rev. A **98**, 042118 (2018).
[9] T. E. Lee, S. Gopalakrishnan, and M. D. Lukin, Phys. Rev. Lett. **110**, 257204 (2013).
[10] E. G. Torre, S. Diehl, M. D. Lukin, S. Sachdev, and P. Strack, Phys. Rev. A **87**, 023831 (2013).
[11] I. Carusotto and C. Ciuti, Rev. Mod. Phys. **85**, 299 (2013).
[12] L. M. Sieberer, S. D. Huber, E. Altman, and S. Diehl, Phys. Rev. Lett. **110**, 195301 (2013).
[13] C. K. Chan, T. E. Lee, and S. Gopalakrishnan, Phys. Rev. A **91**, 051601 (2015).
[14] E. Mascarenhas, H. Flayac, and V. Savona, Phys. Rev. A **92**, 022116 (2015).
[15] L. M. Sieberer, S. D. Huber, E. Altman, and S. Diehl, Phys. Rev. B **89**, 134310 (2014).
[16] T. E. Lee, C. K. Chan, and S. F. Yelin, Phys. Rev. A **90**, 052109 (2014).
[17] H. Weimer, Phys. Rev. Lett. **114**, 040402 (2015).
[18] W. Casteels, F. Storme, A. Le Boité, and C. Ciuti, Phys. Rev. A **93**, 033824 (2016).
[19] J. J. Mendoza-Arenas, S. R. Clark, S. Felicetti, G. Romero, E. Solano, D. G. Angelakis, and D. Jaksch, Phys. Rev. A **93**, 023821 (2016).
[20] J. Jin, A. Biella, O. Viyuela, L. Mazza, J. Keeling, R. Fazio, and D. Rossini, Phys. Rev. X **6**, 031011 (2016).
[21] N. Bartolo, F. Minganti, W. Casteels, and C. Ciuti, Phys. Rev. A **94**, 033841 (2016).
[22] W. Casteels and C. Ciuti, Phys. Rev. A **95**, 013812 (2017).
[23] V. Savona, Phys. Rev. A **96**, 033826 (2017).
[24] R. Rota, F. Storme, N. Bartolo, R. Fazio, and C. Ciuti, Phys. Rev. B **95**, 134431 (2017).
[25] M. Biondi, G. Blatter, H. E. Türeci, and S. Schmidt, Phys. Rev. A **96**, 043809 (2017).
[26] W. Casteels, R. Fazio, and C. Ciuti, Phys. Rev. A **95**, 012128 (2017).
[27] M. Raghunandan, J. Wrachtrup, and H. Weimer, Phys. Rev. Lett. **120**, 150501 (2018).
[28] J. Gelhausen and M. Buchhold, Phys. Rev. A **97**, 023807 (2018).
[29] M. Foss-Feig, P. Niroula, J. T. Young, M. Hafezi, A. V. Gorshkov, R. M. Wilson, and M. F. Maghrebi, Phys. Rev. A **95**, 043826 (2017).
[30] F. A. S. Barbosa, A. S. Coelho, L. F. Muñoz-Martínez, L. Ortiz-Gutiérrez, A. S. Villar, P. Nussenzveig, and M. Martinelli, Phys. Rev. Lett. **121**, 073601 (2018).
[31] T. E. Lee, H. Häffner, and M. C. Cross, Phys. Rev. A **84**, 031402(R) (2011).
[32] J. Hannukainen and J. Larson, Phys. Rev. A **98**, 042113 (2018).
[33] R. Gutiérrez-Jáuregui and H. J. Carmichael, Phys. Rev. A **98**, 023804 (2018).
[34] F. Vicentini, F. Minganti, R. Rota, G. Orso, and C. Ciuti, Phys. Rev. A **97**, 013853 (2018).
[35] M.-J. Hwang, P. Rabl, and M. B. Plenio, Phys. Rev. A **97**, 013825 (2018).
[36] A. Vukics, A. Dombi, J. M. Fink, and P. Domokos, Quantum **3**, 150 (2019).
[37] A. Patra, B. L. Altshuler, and E. A. Yuzbashyan, Phys. Rev. A **99**, 033802 (2019).
[38] J. Tangpanitanon, S. R. Clark, V. M. Bastidas, R. Fazio, D. Jaksch, and D. G. Angelakis, Phys. Rev. A **99**, 043808 (2019).
[39] K. Baumann, C. Guerlin, F. Brennecke, and T. Esslinger, Nature (London) **464**, 1301 (2010).
[40] R. Landig, F. Brennecke, R. Mottl, T. Donner, and T. Esslinger, Nat. Commun. **6**, 7046 (2015).
[41] J. M. Fink, A. Dombi, A. Vukics, A. Wallraff, and P. Domokos, Phys. Rev. X **7**, 011012 (2017).
[42] M. Fitzpatrick, N. M. Sundaresan, A. C. Y. Li, J. Koch, and A. A. Houck, Phys. Rev. X **7**, 011016 (2017).
[43] T. Fink, A. Schade, S. Hofling, C. Schneider, and A. Imamoglu, Nat. Phys. **14**, 365 (2018).
[44] S. R. K. Rodriguez, W. Casteels, F. Storme, N. Carlon Zambon, I. Sagnes, L. Le Gratiet, E. Galopin, A. Lemaître, A. Amo, C. Ciuti, and J. Bloch, Phys. Rev. Lett. **118**, 247402 (2017).
[45] M. Brunelli, L. Fusco, R. Landig, W. Wieczorek, J. Hoelscher-Obermaier, G. Landi, F. L. Semião, A. Ferraro, N. Kiesel, T. Donner, G. De Chiara, and M. Paternostro, Phys. Rev. Lett. **121**, 160604 (2018).
[46] T. Tomé and M. J. de Oliveira, Phys. Rev. Lett. **108**, 020601 (2012).
[47] P. S. Shim, H. M. Chun, and J. D. Noh, Phys. Rev. E **93**, 012113 (2016).
[48] L. Crochik and T. Tomé, Phys. Rev. E **72**, 057103 (2005).
[49] Y. Zhang and A. C. Barato, J. Stat. Mech. (2016) 113207.
[50] T. Herpich, J. Thingna, and M. Esposito, Phys. Rev. X **8**, 031056 (2018).
[51] C. E. Fernandez Noa, P. E. Harunari, M. J. de Oliveira, and C. E. Fiore, Phys. Rev. E **100**, 012104 (2019).
[52] T. Herpich and M. Esposito, Phys. Rev. E **99**, 022135 (2019).

[53] R. Dorner, J. Goold, C. Cormick, M. Paternostro, and V. Vedral, Phys. Rev. Lett. **109**, 160601 (2012).
[54] P. Drummond and D. Walls, J. Phys. A: Math. Gen. **13**, 725 (1980).
[55] J. P. Santos, A. L. De Paula, R. Drumond, G. T. Landi, and M. Paternostro, Phys. Rev. A **97**, 050101 (2018).
[56] J. P. Santos, L. C. Céleri, F. Brito, G. T. Landi, and M. Paternostro, Phys. Rev. A **97**, 052123 (2018).
[57] R. Uzdin, in *Thermodynamics in the Quantum Regime—Fundamental Aspects and New Directions* (Springer International Publishing, Cham, Switzerland, 2018), pp. 681–712.
[58] R. Uzdin and S. Rahav, arXiv:1912.07922.
[59] J. P. Santos, G. T. Landi, and M. Paternostro, Phys. Rev. Lett. **118**, 220601 (2017).
[60] A. Wehrl, Rev. Mod. Phys. **50**, 221 (1978).
[61] C. Gardiner and P. Zoller, *Quantum Noise: A Handbook of Markovian and Non-Markovian Quantum Stochastic Methods with Applications to Quantum Optics* (Springer, New York, 2004), Vol. 56.
[62] K. Wódkiewicz, Phys. Rev. Lett. **52**, 1064 (1984).
[63] V. Buzek, C. H. Keitel, and P. L. Knight, Phys. Rev. A **51**, 2575 (1995).
[64] U. Seifert, Rep. Prog. Phys. **75**, 126001 (2012).
[65] A. Altland and F. Haake, Phys. Rev. Lett. **108**, 073601 (2012).
[66] R. Landauer, J. Stat. Phys. **13**, 1 (1975).
[67] K. V. Kheruntsyan, J. Opt. B: Quantum Semiclass. Opt. **1**, 225 (1999).